

Coplanar Waveguide to Double-Sided Parallel-Strip Line Transitions and Their Applications

Thesis submitted by

NELSON K. J.

in partial fulfillment of the requirements for the award of the degree of

DOCTOR OF PHILOSOPHY

Under the guidance of

Dr. K. VASUDEVAN



Department of Electronics
Faculty of Technology
Cochin University of Science and Technology
Cochin - 682 022, Kerala, India.

December 2019

Coplanar Waveguide to Double-Sided Parallel-Strip Line Transitions and Their Applications

Ph.D. Thesis under the Faculty of Technology

Author:

Nelson K. J.

(University Registration Number: 3720)

Centre for Research in Electromagnetics and Antennas

Department of Electronics

Cochin University of Science and Technology

Cochin - 682 022, Kerala, India.

Email: nelsonkj@gmail.com

Supervisor:

Dr. K. Vasudevan

Emeritus Professor

Department of Electronics

Cochin University of Science and Technology

Cochin - 682 022, Kerala, India.

Email: vasudevankdr@gmail.com

Department of Electronics

Cochin University of Science and Technology

Cochin - 682 022, Kerala, India.

December 2019

Dedicated to All.....



Dr. K. Vasudevan
Emeritus Professor
Department of Electronics
Cochin University of Science and Technology
Cochin - 682 022.

Certificate

This is to certify that this thesis entitled **Coplanar Waveguide to Double-Sided Parallel-Strip Line Transitions and Their Applications** is a bonafide record of the research work carried out by **Mr. Nelson K. J.** under my supervision in the **Department of Electronics, Cochin University of Science and Technology**. The results embodied in this thesis or parts of it have not been presented for the award of any other degree.

I further certify that the corrections and modifications suggested by the audience during the pre-synopsis seminar and recommended by the doctoral committee of **Mr. Nelson K. J.** are incorporated in the thesis.

Cochin - 22
30th December 2019

Dr. K. Vasudevan

Declaration

I hereby declare that the work presented in this thesis entitled “**Coplanar Waveguide to Double-Sided Parallel-Strip Line Transitions and Their Applications**” is based on the original research work carried out by me under the supervision and guidance of **Dr. K. Vasudevan, Emeritus Professor, Department of Electronics, Cochin University of Science and Technology, Cochin-22**, and has not been included in any other thesis submitted previously for the award of any degree.

Cochin - 22
30th December 2019

Nelson K. J.
Department of Electronics.

Acknowledgments

I would like to express my sincere gratitude to my supervising guide Dr. K. Vasudevan for his valuable guidance given throughout my research work. I also express gratitude to Dr. P. Mohanan and Dr. C. K. Aanandan for thier inspiration and advice given throughout my research period.

I am thankful to Prof. James Kurian, Head of the Department and all former Heads during the period of my research for providing the necessary facilities. Also, I am grateful to all the faculty and staff of Department of Electronics for all their help.

I sincerely thank all the faculty, staff and students of Government Engineering Colleges at Thrissur, Idukki and Sreekrishnapuram for their support.

I am indebted to family and friends for their unconditional love and support.

Finally, I would like to thank everybody who was important to the successful realization of the thesis, as well as expressing my apology that I could not mention personally one by one.

Nelson K. J.

Investigations on Coplanar Waveguide to Double-Sided Parallel-Strip Line Transitions and its Applications

Coplanar Waveguide (CPW) probe pads used for rapid measurement and characterization of packaged microwave integrated circuits (MICs), require the coplanar waveguides at the end points of device under test (DUT). Therefore, wideband, non dispersive transitions between CPW and other transmission lines are a necessity. DSPSL, a differential transmission line, is having wide range of easily realizable characteristic impedances . The differential signalling in the high frequency circuits results in better signal integrity and a higher signal-to-noise ratio (SNR) due to lower electromagnetic interference (EMI) and higher immunity to electromagnetic noise and crosstalk. With recent technological advances, differential circuits are increasingly used in the RF domain apart from the low-frequency analog and digital systems. Differential systems need balanced circuits and interconnects, which increases layout complexity.

From the above scenario, we can understand that transitions between CPW to DSPSL is a primary requirement at present. No vertical transitions between CPW and DSPSL have been introduced upto this point. These transitions are useful in feeding differentially fed antennas like antipodal vivaldi. Eventhough normal transitions between CPW and CPW is reported, Phase inverted vertical transitions between CPW structures are not yet reported. Finally geometrically optimized, vertical or normal and with via or via-less broadbanded transitions between CPW and DSPSL are a requirement for converting the single ended signals to the differentail one.

Outcomes of the work presented in the thesis: The vertical broadband transitions between DSPSL and CPW have been designed, optimized and measured for the first time. The proposed transitions (Types A and B)

are based on a single via connection and connected CPW grounds. An approximate equivalent circuit, which is a Π shaped LC low pass filter, is discussed. Transitions are fabricated on Rogers RO4003C and FR4 substrates, using the standard photolithography process. A via-less transition is designed, prototyped in Rogers RT Duroid 5870, and measured, in the second part of the chapter and its equivalent circuit is discussed.

Ultra-wideband CPW to CPW, vertical transitions with phase inverting nature have been designed, optimized and prototyped for the first time. The proposed transitions utilize two types of CPW to DSPSL transitions. These are also fabricated on Rogers RO4003C and FR4 substrates, using the standard photolithography process. A compact CPW Fed Ultra-wideband (UWB) Antipodal Vivaldi Antenna (AVA) has been designed and prototyped on the cost effective substrate (FR4). The CPW fed AVA structures are very rare in literature . The gain and radiation pattern of the antenna are measured. The proposed antenna utilizes the CPW to DSPSL transition as feeding structure and elliptically tapered flares as radiators.

List of Figures

1.1	Amplitude measurements of high frequency voltage signal at the beginning (location A) and somewhere along a wire connecting load to source [1].	4
1.2	Segmentation of two-wire transmission line into Δz long sections suitable for lumped parameter analysis.	5
1.3	Equivalent circuit of a two-conductor transmission line of differential length Δz	5
1.4	Stripline.	8
1.5	Microstrip.	8
1.6	Coplanar Waveguide	8
1.7	Slotline	8
1.8	Substrate Integrated Waveguide	8
1.9	Coplanar waveguide [2].	11
1.10	Conductor Backed Coplanar Waveguide [2].	11
1.11	Double-sided parallel-strip line, (a) three dimensional view, (b) cross sectional view.	12
1.12	Cross sectional view of the double-sided parallel-strip transmission line and electric field distributions [4].	13
1.13	Characteristic impedance and normalized guided wavelength of a microstrip line and double-sided parallel-strip line [4].	13
1.14	Configurations of Typical AVA. [8]	15
1.15	Configurations of the BAVA. [8]	15
2.1	Different DSPSL Transitions	21
2.2	Different CPW to DSPSL Transitions	22
2.3	Different CBCPW to Microstrip Transitions	23
2.4	Different CPW to Microstrip Transitions	24
2.5	Different CPW to Microstrip Transitions	25
2.6	Different CPW to Microstrip Transitions	26
2.7	Different CPW to Microstrip Transitions	27
2.8	Different CPW to CPW Transitions	28

2.9	Different CPW to Slotline Transitions	29
2.10	Different CPW to Slotline Transitions	30
2.11	Different CPW to Slotline Transitions	31
2.12	Different CPW to CPS Transitions	32
2.13	Different CPW to CPS Transitions	33
2.14	Different Antipodal Vivaldi Antennas.	34
2.15	Different Antipodal Vivaldi Antennas.	35
2.16	Different Antipodal Vivaldi Antennas.	36
3.1	Design Flow for the Transition Fabrication.	46
3.2	Reflection/Transmission parameters used for for high-frequency device characterization using lightwave analogy [3].	49
3.3	Measurement of scattering parameters [3].	50
3.4	Group delay calculation [3].	51
3.5	VNA block diagram [4].	52
3.6	Agilent Technologies E8362B VNA (10 MHz to 20 GHz)	52
3.7	Keysight Fieldfox N9927A handheld VNA (30 kHz to 20 GHz)	53
3.8	Anechoic chamber and turn table assembly.	54
4.1	Double-sided parallel-strip line, (a) three dimensional view, (b) cross sectional view	59
4.2	Configuration of the proposed Type A transition: (a) schematic layout, (b) top view, (c) bottom view. ($W_1=5$ mm, $W_2=4$ mm, $W_3=4.4$ mm, $G_1=0.35$ mm, $L_1=1$ mm, $L_2=2.4$ mm, $L_3=7.4$ mm, $R_1=0.75$ mm, $R_2=2$ mm)	61
4.3	Cross-sectional views of proposed transition (Type A) and electric field distributions: (a) AA' - CPW mode, (b) EE' - DSPSL mode, (c) BB',CC',DD' - Transition modes.	62
4.4	Configuration of the proposed Type B transition: (a) schematic layout, (b) top view, (c) bottom view. ($W_1=5$ mm, $W_2=4$ mm, $W_3=4.4$ mm, $G_2=0.35$ mm, $L_4=7.35$ mm, $R_1=0.75$ mm, $R_2=2$ mm, $R_3=2.35$ mm, $R_4=7.35$ mm)	63
4.5	Cross-sectional views of proposed transition (Type B) and electric field distributions: (a) AA' - CPW mode, (b) EE' - DSPSL mode, (c) BB',CC',DD' - Transition modes.	63

4.6	Coplanar waveguide open circuit with connected grounds. [18]	64
4.7	Configuration of the back-to-back transitions (Type A): (a) schematic layout, (b) top view and (c) bottom view.	67
4.8	Simulated scattering parameters of the back-to-back transitions (Type A) against frequency with different Y-junction thicknesses (L_3).	68
4.9	Simulated scattering parameters of the back-to-back transitions (Type A) against frequency with different CPW length offset distances (L_1).	68
4.10	Simulated scattering parameters of the back-to-back transitions (Type A) against frequency with different layer interconnecting via radii (R_1).	69
4.11	Simulated scattering parameters of the back-to-back transitions (Type A) against frequency with different CPW ground widths (W_1).	69
4.12	Configuration of the back-to-back transitions (Type B): (a) schematic layout, (b) top view and (c) bottom view.	70
4.13	Simulated scattering parameters of the back-to-back transitions (Type B) against frequency with different CPW ground widths (W_1).	71
4.14	Simulated scattering parameters of the back-to-back transitions (Type B) against frequency with different layer interconnecting via radii (R_1).	71
4.15	Simplified equivalent circuit of CPW with connected grounds.	72
4.16	Simplified equivalent circuit of via (Lumped).	73
4.17	Simplified equivalent circuit of a single transition (Type A and Type B).	74
4.18	Simplified equivalent circuit of the back to back configuration of the transition (Type A and Type B).	74
4.19	Simulated and measured scattering parameters of the back-to-back transitions- Type A (Rogers RO4003C)	76
4.20	Actual photograph of the back-to-back transitions - Type A (Rogers RO4003C)	76

4.21	Simulated and measured scattering parameters of the back-to-back transitions - Type A (FR4)	77
4.22	Actual photograph of the back-to-back transitions - Type A (FR4)	77
4.23	Measured scattering parameter S_{21} phase (in degrees) of the back-to-back transitions - Type A (Rogers RO4003C).	78
4.24	Measured scattering parameter S_{21} phase (in degrees) of the back-to-back transitions - Type A (FR4).	78
4.25	Measured group delays of the back-to-back transitions - Type A	79
4.26	Simulated and measured scattering parameters of the back-to-back transitions - Type B (Rogers RO4003C)	80
4.27	Measured scattering parameter S_{21} phase (in degrees) of the back-to-back transitions - Type B (Rogers RO4003C).	81
4.28	Actual photograph of the back-to-back transitions - Type B (Rogers RO4003C)	81
4.29	Simulated and measured scattering parameters of the back-to-back transitions - Type B (FR4)	82
4.30	Actual photograph of the back-to-back transitions - Type B (FR4).	82
4.31	Measured scattering parameter S_{21} phase (in degrees) of the back-to-back transitions - Type B (FR4).	83
4.32	Measured group delays of the back-to-back transitions (a). Type A; (b). Type B.	83
4.33	Configuration of the via-less transition: (a) schematic layout, (b) top view, (c) bottom view. ($W_1=5$ mm, $W_2=3.5$ mm, $W_3=5$ mm, $W_4=4$ mm, $W_5=6$ mm, $G_1=0.2$ mm, $\theta^\circ=70^\circ$, $L_1=8$ mm, $L_2=20$ mm, $L_3=6$ mm)	84
4.34	Cross-sectional views of proposed transition (Type B) and electric field distributions: (a) AA' - CPW mode, (b) EE' - DSPSL mode, (c) BB',CC',DD' - Transition modes.	86
4.36	Simulated scattering parameters of the back-to-back via-less transitions against frequency with different transition lengths (L_2).	87

4.35	Configuration of the back to back via-less transitions: (a) schematic layout, (b) top view, (c) bottom view. ($W_1=5$ mm, $W_2=3.5$ mm, $W_3=5$ mm, $W_4=4$ mm, $W_5=6$ mm, $G_1=0.2$ mm, $\theta^\circ=70^\circ$, $L_1=8$ mm, $L_2=20$ mm, $L_3=6$ mm)	88
4.37	Simulated scattering parameters of the back-to-back via-less transitions against frequency with different radial stub lengths (W_5).	89
4.38	Simulated scattering parameters of the back-to-back via-less transitions against frequency with different radial stub angles (θ°).	89
4.39	Simulated scattering parameters of the back-to-back via-less transitions against frequency with different CPW ground widths (W_1).	90
4.40	Simplified equivalent circuit of a single via-less transition. . .	90
4.41	Simplified equivalent circuit of the back to back configuration of the via-less transitions.	91
4.42	Simulated and measured scattering parameters of the back-to-back via-less transitions.	93
4.43	Actual photograph of the back-to-back via-less transitions. . .	93
4.44	Measured scattering parameter S_{21} phase (in degrees) of the back-to-back via-less transitions.	94
4.45	Measured group delays of the back-to-back via-less transitions.	94
5.1	Configuration of the CPW to CPW transitions (Type A): (a) schematic layout, (b) top view and (c) bottom view.	101
5.2	Configuration of the CPW to CPW transitions (Type B): (a) schematic layout, (b) top view and (c) bottom view.	102
5.3	Cross-sectional views of both transitions (Type A and B) and electric field distributions: (a) AA', II' - CPW modes, (b) EE' - DSPSL mode, (c) BB', CC', DD', FF', GG', HH' - Transition modes.	103
5.4	Simplified equivalent circuit: (a) equivalent circuit of CPW with connected grounds, (b) equivalent circuit of via (Lumped), (c) complete equivalent circuit of the transitions (Type A & Type B)	105

5.5	Simulated and measured scattering parameters of the CPW to CPW transition - Type A (Rogers RO4003C)	106
5.6	Actual photograph of the CPW to CPW transition transitions - Type A (Rogers RO4003C).	107
5.7	Measured scattering parameter S_{21} phase (in degrees) of the CPW to CPW transition - Type A (Rogers RO4003C).	107
5.8	Simulated and measured scattering parameters of the CPW to CPW transition - Type A (FR4).	108
5.9	Actual photograph of the CPW to CPW transition transitions - Type A (FR4).	108
5.10	Measured scattering parameter S_{21} phase (in degrees) of the CPW to CPW transitions - Type A (FR4).	109
5.11	Measured group delays of the CPW to CPW transitions - Type A	109
5.12	Simulated and measured scattering parameters of the CPW to CPW transition - Type B (Rogers RO4003C).	111
5.13	Actual photograph of the CPW to CPW transition transitions - Type B (Rogers RO4003C).	111
5.14	Simulated and measured scattering parameters of the CPW to CPW transition - Type B (FR4).	112
5.15	Actual photograph of the CPW to CPW transition transitions - Type B (FR4).	112
5.16	Measured scattering parameter S_{21} phase (in degrees) of the CPW to CPW transitions - Type B (Rogers RO4003C).	113
5.17	Measured scattering parameter S_{21} phase (in degrees) of the CPW to CPW transitions - Type B (FR4).	113
5.18	Measured group delays of the CPW to CPW transitions - Type B	114
5.19	Configuration of the Antipodal Vivaldi Antenna: (a) top view, (b) bottom view. ; Configuration of the proposed Type B transition: (c) top view, (d) bottom view.	115
5.20	Schematic layout of the proposed Antenna: (a) top view, (b) bottom view.	116
5.21	Configuration of the proposed Antenna.	117
5.22	Simulated return losses of the proposed Antenna against frequency with different values of L_3	119

5.23	Simulated return losses of the proposed Antenna against frequency with different values of L_4	119
5.24	Simulated radiation pattern of the proposed Antenna at 4 GHz.	120
5.25	Simulated radiation pattern of the proposed Antenna at 6 GHz.	120
5.26	Simulated radiation pattern of the proposed Antenna at 9 GHz.	120
5.27	Simulated and Measured return loss (dB) of the proposed Antenna against frequency.	121
5.28	Measured radiation pattern of the proposed Antenna at 4 GHz.	122
5.29	Measured radiation pattern of the proposed Antenna at 6 GHz.	123
5.30	Measured radiation pattern of the proposed Antenna at 9 GHz.	124
5.31	Actual photograph of the proposed Antenna.	125
5.32	Measured peak gain of the proposed Antenna against frequency.	125

List of Tables

1.1	Origin of Transmission Line Parameters	6
1.2	Comparison of Different Transmission Lines in Terms of Characteristic Impedance (Z_0) [5]	14
2.1	Different CPW to DSPSL Transitions	22
4.1	Geometrical parameters of the proposed transition (Type A) (in mm).	66
4.2	Geometrical parameters of the proposed transition (Type B) (in mm).	72
4.3	Measured losses of the back-to-back transitions (Type A).	75
4.4	Measured losses of the back-to-back transitions (Type B).	80
4.5	Geometrical parameters of the proposed transition (in mm).	87
4.6	Measured losses of the back-to-back via-less transitions.	92
5.1	Geometrical parameters of the proposed transition (Type A) (in mm).	101
5.2	Geometrical parameters of the proposed transition (Type B) (in mm).	102
5.3	Measured losses of the transitions (Type A).	106
5.4	Measured losses of the transitions (Type B).	110
5.5	Geometrical parameters of the proposed Antenna (in mm).	118

List of Abbreviations

Z_0	Characteristic Impedance
CPW	Coplanar Waveguide
FGCPW	Finite Ground Coplanar Waveguide
FWCPW	Finite Width Coplanar Waveguide
CBCPW	Conductor Backed Coplanar Waveguide
DSPSL	Double-Sided Parallel-Strip Line
BCS	Broadside Coupled Strip Line
CPS	Coplanar Strip Line
DUT	Device Under Test
EM	Electromagnetic
RF	Radio Frequency
AVA	Antipodal Vivaldi Antenna
BAVA	Balanced Antipodal Vivaldi Antenna
MIC	Microwave Integrated Circuit
MMIC	Monolithic Microwave Integrated Circuit
MoM	Method of Moments
FEM	Finite Element Method
FDTD	Finite-Difference Time-Domain
EMI	Electromagnetic Interference
VNA	Vector Network Analyzer
SMA	SubMiniature version A

Contents

List of Figures	xii
List of Tables	xiii
1 Introduction	1
1.1 Introduction	2
1.2 History	2
1.3 Transmission Lines	4
1.4 Transitions	9
1.5 Coplanar Waveguide (CPW)	10
1.6 Double-Sided Parallel-Strip Line (DSPSL)	12
1.7 Antipodal Vivaldi Antenna (AVA)	14
1.8 Motivation of Research	15
1.9 Thesis Organization	16
References	17
2 Literature Survey	20
2.1 DSPSL Transitions	20
2.2 CPW Transitions	23
2.3 Antipodal Vivaldi Antennas	34
2.4 Chapter Summary	36
References	37
3 Methodology	45
3.1 Guidelines for the Transition Design	45
3.2 Simulation	47
3.3 Prototyping	48
3.4 Measurements	49
3.5 Chapter Summary	56
References	56

4	CPW to DSPSL Transitions	57
4.1	CPW to DSPSL Vertical Transitions with Via	58
4.1.1	Transition Geometry and its Design	58
4.1.2	Simulation Studies	66
4.1.3	Equivalent Circuit	72
4.1.4	Measured Results	75
4.2	CPW to DSPSL Transition without Via	84
4.2.1	Transition Geometry and its Design	84
4.2.2	Simulation Studies	86
4.2.3	Equivalent Circuit	90
4.2.4	Measured Results	92
4.3	Chapter Summary	95
	References	95
5	Applications of CPW to DSPSL Transitions	98
5.1	CPW to CPW Phase Inverted Vertical Transitions	99
5.1.1	Transition Geometry and its Design	99
5.1.2	Equivalent Circuit	104
5.1.3	Measured Results	104
5.2	CPW Fed UWB Antipodal Vivaldi Antenna	114
5.2.1	Antenna Geometry and its Design	115
5.2.2	Simulation Studies	118
5.2.3	Measured Results	121
5.3	Chapter Summary	126
	References	126
6	Conclusion and Future Prospects	129
6.1	Conclusions	129
6.2	Major Contributions	130
6.3	Suggestions for Future Work	131
	List of Publications	132
	Resume	133

Chapter 1

Introduction

Contents

1.1	Introduction	2
1.2	History	2
1.3	Transmission Lines	4
1.4	Transitions	9
1.5	Coplanar Waveguide (CPW)	10
1.6	Double-Sided Parallel-Strip Line (DSPSL)	12
1.7	Antipodal Vivaldi Antenna (AVA)	14
1.8	Motivation of Research	15
1.9	Thesis Organization	16
	References	17

This chapter reviews the fundamentals and history in the first section and explains the need of the transmission line theory. It further discusses the different varieties of planar transmission lines. Then the transitions are explained and different techniques for achieving it are discussed. The basics of two planar transmission line types (Coplanar Waveguide and Double-Sided Parallel-Strip Line) and the Antipodal Vivaldi Antenna are discussed next. The motivation of research is also furnished. This chapter concludes with a description about the organization of the thesis.

1.1 Introduction

Analog and digital design engineers are continuously refining their systems for higher frequencies to match with the ever increasing clock speeds. In the wireless communication scenario, more compact active and passive devices like amplifier, filter, oscillator and mixer are needed at higher frequencies to catch up with the generation networks. This trend will result in new design challenges that are not familiar at lower frequencies.

At higher frequencies the wavelengths become comparable to the dimensions of discrete lumped elements, such as resistors, capacitors and inductors, which will deviate from their ideal electrical response at that frequency. As a result, the voltages and currents no longer remain spatially uniform when compared to the geometric size of the discrete lumped circuit elements. The conventional conservation laws in circuit theory, the Kirchhoff's voltage and current laws, do not account for these spatial variations. So a new theory, known as transmission line theory, where signals are treated as propagating waves is introduced. Transmission lines are mainly used for connecting radio transceivers with their antennas and for connecting different distributed elements.

In a high frequency system, different transmission line structures are utilized at different places. Therefore interconnections between them are absolutely needed and they are called transitions. Transitions can be between balanced to balanced, unbalanced to unbalanced and balanced to unbalanced transmission lines.

1.2 History

- In 1885 Oliver Heaviside, who published his analysis of propagation of signals in cables using his distributed-element modelling of transmission lines, found a correct description of the behaviour of signals on the dispersive transatlantic telegraph cable and suggested methods for overcoming it.

- In 1927 first coaxial filter using distributed element circuits is patented by Warren P. Mason
- In 1939 R. D. Richtmeyer introduced dielectric resonator.
- In 1940 Cavity Magnetron oscillator is invented.
- In 1947 W. A. Tyrrell introduced Hybrid Ring.
- In 1948 Paul I. Richards' commensurate line theory published.
- In 1948 MIT Radiation Lab Publications - Word War II - Major advancements.
- In 1951 Robert M. Barrett invents stripline.
- In 1951 stripline power divider by Rumsey and Jamieson
- In 1952 microstrip is introduced by Grieg and Engelmann.
- In 1952 the first planar slab dielectric line, imageline by King.
- In 1955 Kuroda's identities, a set of transforms which overcame some practical limitations of Richards theory.
- In 1964 George Matthaei described interdigital filter and the combline filter.
- In 1968 Slotline is introduced by Cohn.
- In 1969 Coplanar Waveguide is invented by Wen.
- In 1972 Finline invented by Meier.
- In 1972 the first MMIC, an X band amplifier, is introduced by Pengelly and Turner of Plessey.
- In 1979 Vivaldi Ariel by Gibson.
- In 1988 Antipodal Vivaldi Antenna by Gazit.
- In 1993 Balanced Antipodal Vivaldi Antenna by Langley.
- In 1998 SIW was first described by Hirokawa and Ando.

1.3 Transmission Lines

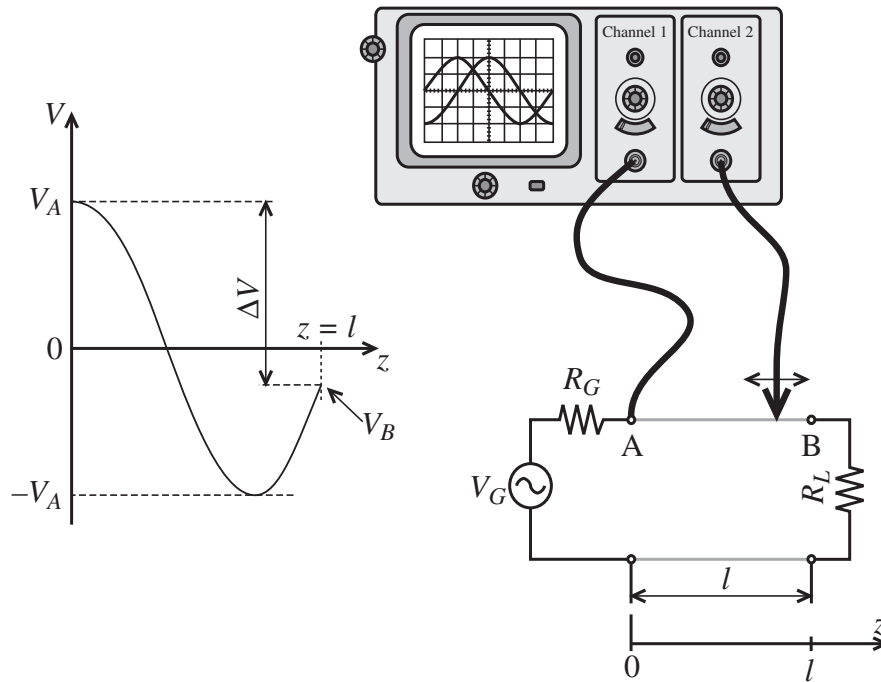


Figure 1.1: Amplitude measurements of high frequency voltage signal at the beginning (location A) and somewhere along a wire connecting load to source [1].

The basic elements in a circuit, such as resistors, capacitors, inductors, and the connections between them, are considered lumped elements if the time delay in traversing the elements is negligible. The fundamental rule is that one must consider elements as distributed if the propagation delay across the element dimension is of the order of the shortest time interval of interest. This means that their resistive, capacitive, and inductive characteristics must be evaluated on a per-unit-distance basis. Amplitude measurements of high frequency voltage signal at the beginning location A and somewhere along a wire connecting load to source is shown in Figure 1.1. It clearly shows the spatial variation of voltage along the line. This leads to the Heaviside's analysis of transmission lines.

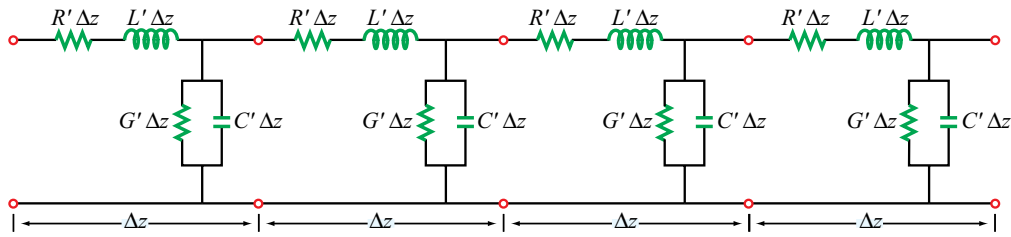


Figure 1.2: Segmentation of two-wire transmission line into Δz long sections suitable for lumped parameter analysis.

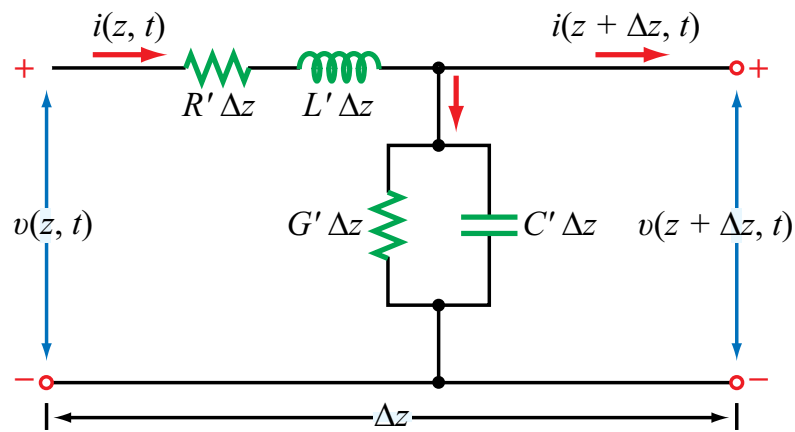


Figure 1.3: Equivalent circuit of a two-conductor transmission line of differential length Δz .

A transverse electromagnetic (TEM) transmission line will be represented by a parallel-wire configuration, regardless of its specific shape or constitutive parameters as shown in Figures 1.2 and 1.3.

R' : The combined resistance of both conductors per unit length, in Ω/m ,

L' : The combined inductance of both conductors per unit length, in H/m ,

G' : The conductance of the insulation medium between the two conductors per unit length, in S/m , and

C' : The capacitance of the two conductors per unit length, in F/m .

The linear first-order partial differential equations given below are the time-domain forms of the transmission-line equations, describe the spatial

Table 1.1: Origin of Transmission Line Parameters

Model Parameter	Origin	Comment
R'	Conductance	atomic property of metal used
	Geometry	larger cross section = lower R ; longer = higher R
	Radiation	fields not contained are losses
	Skin Effect	current flows in smaller cross-section as frequency increases
	Proximity Affect	adjacent conductor's field forces current into smaller cross-section
L'	Permeability	property of metal used
	Geometry	larger cross section = lower L ; longer = higher L
	Skin Effect	currents at different depths in conductor have different phases, net effect is inductive
	Proximity	adjacent conductor's field forces current into smaller cross-section
	Radiation	
C'	Geometry	larger area = higher C ; closer conductors = higher C
	Permittivity	higher ϵ_r = higher C
G'	Loss Tangent	higher loss tan = higher losses in dielectric
	Conductance	semiconductor dielectrics
	Geometry	

distribution of voltage and current on an transmission line with time. Otherwise known as the telegrapher's equations (or telegraph equations).

$$-\frac{\partial v(z, t)}{\partial z} = R'i(z, t) + L'\frac{\partial i(z, t)}{\partial t} \quad (1.1)$$

$$-\frac{\partial i(z, t)}{\partial z} = G'v(z, t) + C'\frac{\partial v(z, t)}{\partial t} \quad (1.2)$$

This model introduced by Oliver Heaviside demonstrates that the electromagnetic waves can be reflected on the wire, and that wave patterns can form along the line. The telegrapher's equations in phasor form is given below

$$-\frac{d\tilde{V}(z)}{dz} = (R' + j\omega L')\tilde{I}(z) \quad (1.3)$$

$$-\frac{d\tilde{I}(z)}{dz} = (G' + j\omega C')\tilde{V}(z) \quad (1.4)$$

The Heaviside condition (distortionless condition), which an electrical transmission line must meet in order for there to be no distortion of a transmitted signal is given below

$$\frac{G}{C} = \frac{R}{L} \quad (1.5)$$

Eventhough the general transmission line theory is developed for telegraph lines, it can be applied to all frequencies from direct current (DC) to high frequency. The origin of different transmission line parameters is given in Table 1.1.

Planar Transmission Lines

Planar transmission lines are flat or ribbon shaped transmission lines made of conductors or dielectrics, used as interconnects and constructing elements of different distributed type of components. Different types of the planar transmission lines and their derived varieties are shown in Figures 1.4 to 1.8.

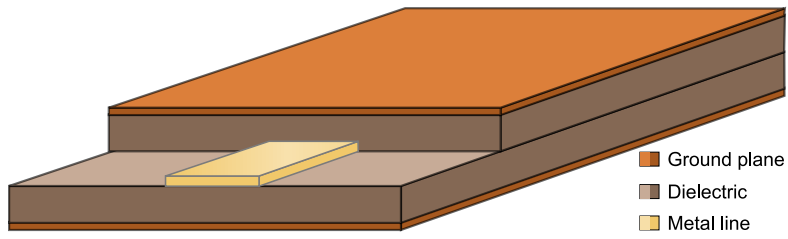


Figure 1.4: Stripline.

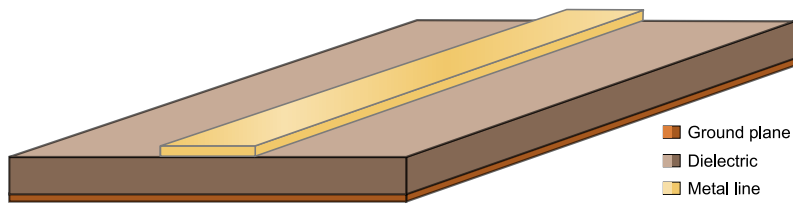


Figure 1.5: Microstrip.

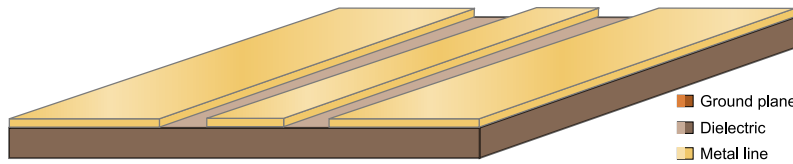


Figure 1.6: Coplanar Waveguide

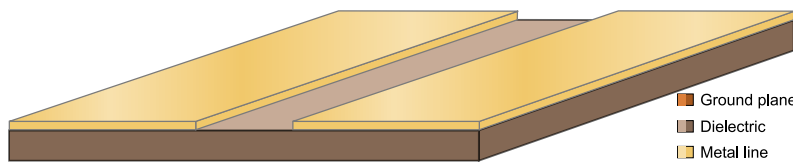


Figure 1.7: Slotline

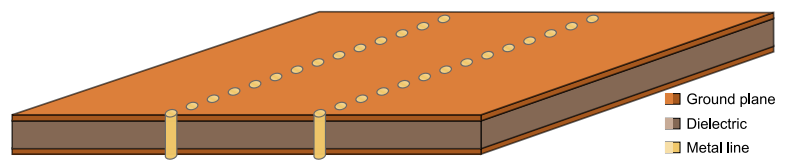


Figure 1.8: Substrate Integrated Waveguide

In the four most popular types (stripline, microstrip, suspended stripline, and coplanar waveguide), the field pattern of the electromagnetic wave (mode) is almost identical to a pair of wires. On the other hand, slotline and substrate integrated waveguide, transmit along a strip of dielectric have different mode of propagation.

The modes describes the electromagnetic field patterns inside the geometry of the transmission line structure. The transverse electromagnetic mode is the dominant mode in ordinary conductive cables and in some planar transmission lines and can be used upto to zero frequency.

1.4 Transitions

Distributed elements, interconnects and feeding lines of a RF system are best implemented using multiple transmission line types. The interconnecting structures between various transmission line types, otherwise known as transitions, are therefore required. Transitions can filter the signals, connect different signal layers in a three dimensional module, cancel or provide the DC coupling, etc. Vertical transitions provide layer changing of signals in a multilayer environment. The quasi-planar transitions are the ones which connect the signal lines on one layer but employing the matching elements placed on both sides of the substrate. They can provide more degree of freedom, less radiation loss and wide-band performance.

The interconnecting transition structures between balanced lines and unbalanced lines are known as balun. Transitions introduce mode discontinuities as the electric and magnetic field orientations are changing. Mode discontinuities results in purely reactive impedance, thereby storage of electric and magnetic energy. This introduces frequency dependence and limits bandwidth, primarily setting the upper frequency limit of the transitions. Other related point is that, transitions can excite higher order modes in transmission lines.

A good transition structure must provide field matching and impedance matching between transmission lines. Transitions structures can be between different impedances values other than 50Ω lines, in that cases impedance

matching is a requirement. Eventhough impedance is matched, the electromagnetic field pattern must be changed to the new mode smoothly by minimizing the mode discontinuities. The problem is to design the reflectionless transitions for different lines, and no well-developed theory is known and this problem is difficult to formalize analytically. Detailed description of two major techniques used for the transition structures are (electrical contacts and electromagnetic field coupling) are given below.

1. Electrical Contact

- Via holes, Ribbon, Air bridge, Bonding wires and abrupt steps in the conductor
- Compact size and Wide bandwidth
- Some degree of mechanical complexity

2. Electromagnetic Coupling

- No wired bonds or via holes
- Surface to surface, Single substrate, Radial stub, Cavity/Slot
- Narrow bandwidth and Larger size
- Recently wider bandwidth transition

1.5 Coplanar Waveguide (CPW)

A coplanar waveguide fabricated on a dielectric substrate was first demonstrated by C. P. Wen in 1969. The characteristic impedance is determined by the ratio of a/b , so size reduction is possible without limit as shown in Figure 1.9, with higher losses. Due to the ground planes, cross talk effects between adjacent lines are very low, so high packing density possible.

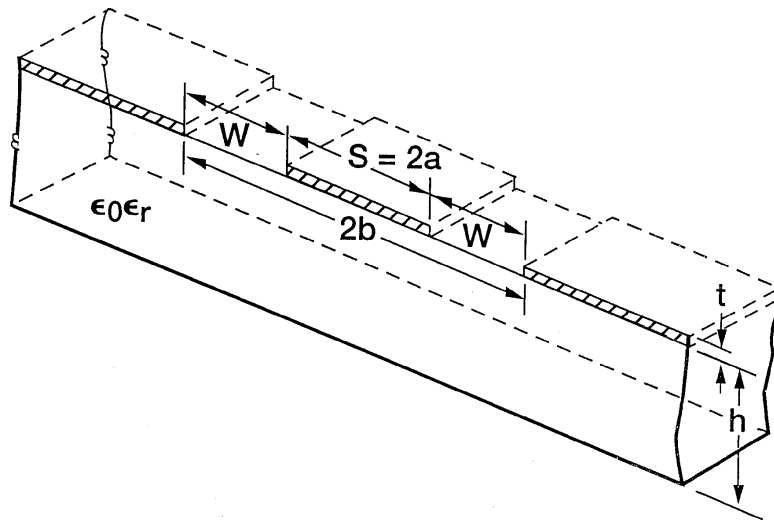


Figure 1.9: Coplanar waveguide [2].

In a conventional CPW, the ground planes are of semi-infinite extent on either side. However, in a practical circuit the ground planes are made of finite extent (FGCPW/FWCPW). The conductor-backed CPW has a lower ground plane, which not only provides mechanical support to the substrate, but also acts as a heat sink as shown in Figure 1.10.

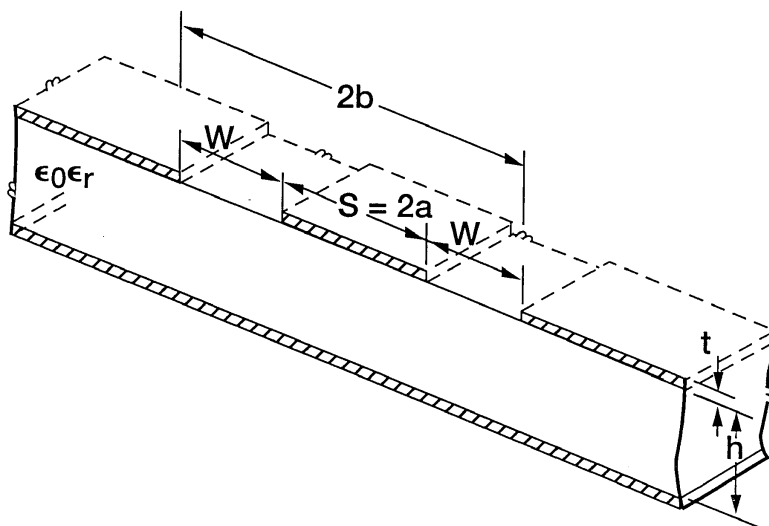


Figure 1.10: Conductor Backed Coplanar Waveguide [2].

1.6 Double-Sided Parallel-Strip Line (DSPSL)

Differential structure of DSPSL with quasi-TEM mode propagation is shown in Figure 1.11(a). It was initially proposed and analyzed by H. Wheeler in 1964 [3]. The field distribution remains unchanged if an infinite sized ground plane is inserted at the middle of the dielectric and parallel to the strip lines. Cross sectional view of the double-sided parallel-strip transmission line and electric field distributions is shown in Figure 1.12. Placing infinite sized perfect electric conductor at a distance $h/2$ from either strip will convert the DSPSL to two similar microstrips placed together as shown in Figure 1.11(b).

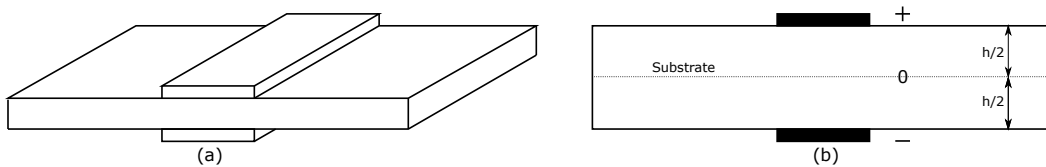


Figure 1.11: Double-sided parallel-strip line, (a) three dimensional view, (b) cross sectional view.

For the same line width, the $(Z_0)_{dspsl}$ with substrate thickness h is double the $(Z_0)_{microstrip}$ with substrate thickness $t = h/2$.

$$(Z_0)_{dspsl} = 2 * (Z_0)_{microstrip}$$

The effective dielectric constant remains the same in this situation. Off-setted DSPSL and edges-even DSPSL are the versions of double-sided parallel-strip line with a shift in the stripline position. The most important dimensional parameters are the microstrip width, w , and the height, h (equal to the thickness of the substrate). Eventhough double-sided structure is a short coming, simple wideband transition structures to other popular lines and easy realization of wide range of characteristic impedances are the advantages of this line.

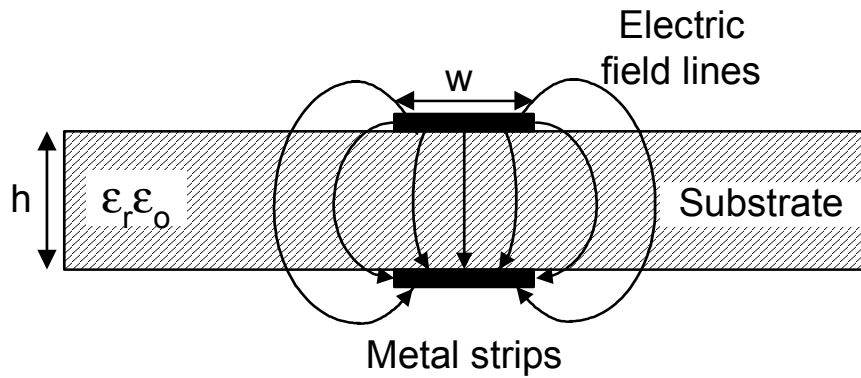


Figure 1.12: Cross sectional view of the double-sided parallel-strip transmission line and electric field distributions [4].

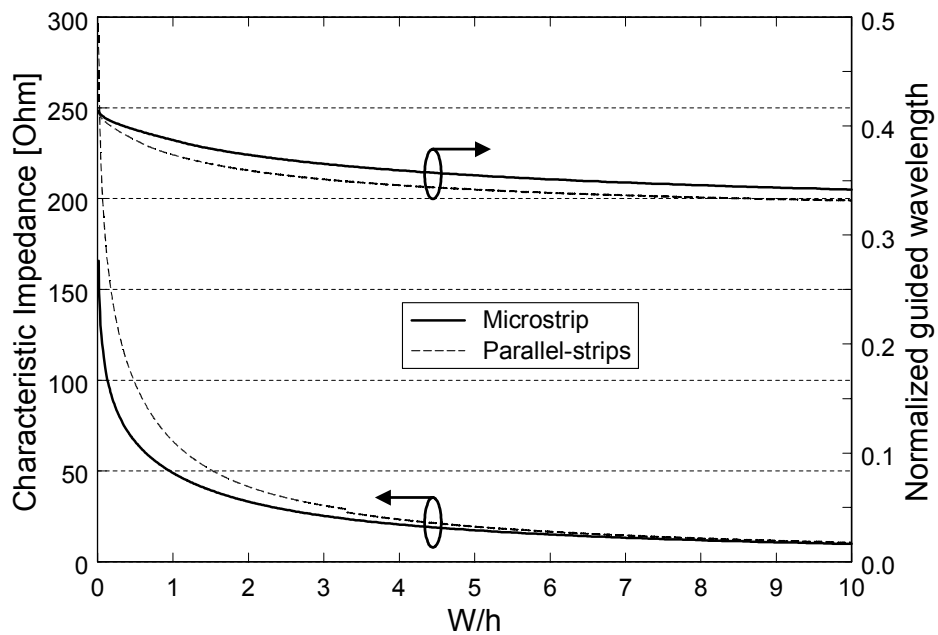


Figure 1.13: Characteristic impedance and normalized guided wavelength of a microstrip line and double-sided parallel-strip line [4].

Table 1.2: Comparison of Different Transmission Lines in Terms of Characteristic Impedance (Z_0) [5]

Type/ Z_0	Unbalanced Transmission Line		Balanced Transmission Line		
	Microstrip	CPW	Coplanar Strip Line	Slot Line	DSPSL
Low Z_0	×	×			×
High Z_0			×	×	×

Figure 1.13 shows the characteristic impedances and the normalized guided wavelengths (the ratio of the guided wavelength λ_g to the free-space wavelength λ_o) of microstrip and double-sided parallel-strip lines on the substrate with a dielectric constant of 10. Comparison of different transmission lines in terms of characteristic impedance (Z_0) is shown in Table 1.2.

1.7 Antipodal Vivaldi Antenna (AVA)

An antipodal Vivaldi antenna (AVA) was first proposed in 1988 by Gazit [6], for bandwidth enhancement of the Vivaldi antenna by Gibson in 1979 [7] and has applications such as in wireless monitoring, imaging and communication systems. Unique tapering structure makes the antenna operates over a wide frequency band.

Vivaldi antenna is traditionally fed from a slot line and transition structures to slot line limits its bandwidth. The antipodal vivaldi antenna (AVA) overcomes the problem of bandwidth limiting transitions. In addition, the AVA has wider bandwidth because of broadband transitions, without any change in beam width and gain.

Electric field vectors in the tapered slots are angled, and this angle is small at low frequencies, as the frequency increases, it increases to 90° , which is the cause of the cross polarisation. To improve the polarization purity the balanced antipodal vivaldi antenna (BAVA) is introduced [9]. The BAVA uses

a three layer arrangement shown in Figure 1.15. The larger cross-polarization rejection is done by the mirrored grounds, which are costly and complicated.

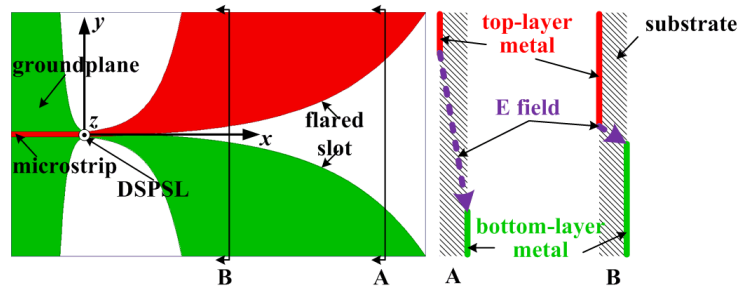


Figure 1.14: Configurations of Typical AVA. [8]

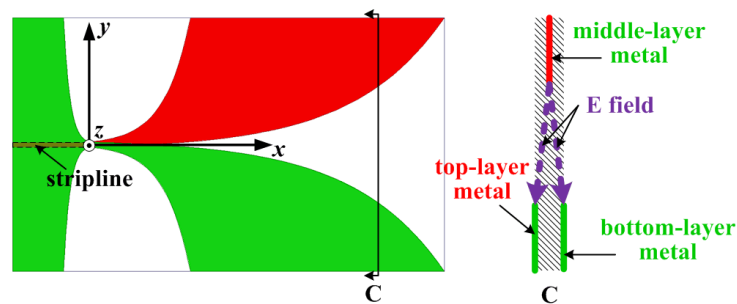


Figure 1.15: Configurations of the BAVA. [8]

1.8 Motivation of Research

In the current communication networks, in spite of significant improvement, there is an underlying strong demand for higher data rate systems. An increasing system complexity leads to new challenges in circuit design. In order to cope with the new demand, the combined use of different types of transmission lines are necessary to achieve optimum performance. Different planar transmission lines bring interesting, simple, and original circuits and interconnects. Transition structures are mainly used not only to transform electromagnetic energy between two types of transmission lines, but also for filtering, phase inverting, layer switching, impedance matching and power dividing applications.

RF probe pads used for rapid measurement and characterization of packaged microwave integrated circuits (MICs), require the coplanar waveguides at the end points of device under test (DUT). Therefore, wideband, non dispersive transitions between CPW and other transmission lines are a necessity. DSPSL, a differential transmission line, is having wide range of easily realizable characteristic impedances . The differential signalling in the high frequency circuits results in better signal integrity and a higher signal-to-noise ratio (SNR) due to lower electromagnetic interference (EMI) and higher immunity to electromagnetic noise and crosstalk. With recent technological advances, differential circuits are increasingly used in the RF domain apart from the low-frequency analog and digital systems. Differential systems need balanced circuits and interconnects, which increases layout complexity.

From the above scenario, we can understand that transitions between CPW to DSPSL is a primary requirement at present. No vertical transitions between CPW and DSPSL have been introduced upto this point [4, 10–17]. These transitions are useful in feeding differentially fed antennas like antipodal vivaldi. Eventhough normal transitions between CPW and CPW is reported, Phase inverted vertical transitions between CPW structures are not yet reported. Finally geometrically optimized, vertical or normal and with via or via-less broadbanded transitions between CPW and DSPSL are a requirement for converting the single ended signals to the differential one.

1.9 Thesis Organization

The thesis presents the simulation and experimental studies of CPW to DSPSL transitions and their applications.

Chapter 1: Reviews the need and fundamentals of general transmission line theory. All the major planar transmission line types are reviewed with special emphasis on CPW and DSPSL. Finally the basics of AVAs are also briefly mentioned.

Chapter 2: Literature review on the topics like CPW transitions, DSPSL transitions and AVAs are done in this chapter.

Chapter 3: The design flow of planar waveguide transitions is provided here. The simulation using three dimensional EM analysis package (CST Microwave Studio[®] (MWS)) and the fabrication techniques are explained. The measurement of scattering parameters and group delay of the transitions and the measurement of gain and farfield radiation patterns of the antenna are also explained.

Chapter 4: Two (Type A & B) single via vertical transitions, and a via-less transition, between CPW and DSPSL also are proposed, simulated, prototyped and measured.

Chapter 5: Applications of the designed transitions, like CPW to CPW phase inverted vertical transitions and CPW fed UWB AVA are proposed, simulated, prototyped and measured.

Chapter 6: Conclusions drawn from the research work in this thesis are provided. Major contributions of the thesis are summarized and suggestions for further works are also proposed.

References

- [1] R. Ludwig and P. Bretchko, *RF Circuit Design: Theory and Applications*. Pearson, 2000.
- [2] R. N. Simons, *Coplanar Waveguide Circuits, Components and Systems*. Wiley-IEEE Press, 2004.
- [3] H. A. Wheeler, "Transmission-line properties of parallel strips separated by a dielectric sheet," *IEEE Transactions on Microwave Theory and Techniques*, vol. 13, pp. 172–185, March 1965.

- [4] Sang-Gyu Kim and Kai Chang, “Ultrawide-band transitions and new microwave components using double-sided parallel-strip lines,” *IEEE Transactions on Microwave Theory and Techniques*, vol. 52, pp. 2148–2152, Sep. 2004.
- [5] J. X. Chen, *Double-sided parallel-strip line circuit analysis and applications to microwave component designs*. PhD thesis, City University of Hong Kong, 2008.
- [6] E. Gazit, “Improved design of the vivaldi antenna,” *IEE Proceedings H - Microwaves, Antennas and Propagation*, vol. 135, pp. 89–92, April 1988.
- [7] P. J. Gibson, “The vivaldi aerial,” in *1979 9th European Microwave Conference*, pp. 101–105, Sep. 1979.
- [8] Y. Wang and Z. Yu, “A novel symmetric double-slot structure for antipodal vivaldi antenna to lower cross-polarization level,” *IEEE Transactions on Antennas and Propagation*, vol. 65, pp. 5599–5604, Oct 2017.
- [9] J. D. S. Langley, P. S. Hall, and P. Newham, “Novel ultrawide-bandwidth vivaldi antenna with low crosspolarisation,” *Electronics Letters*, vol. 29, pp. 2004–2005, Nov 1993.
- [10] J.-X. Chen, J.-L. Li, and Q. Xue, “Novel via-less double-sided parallel strip line to coplanar waveguide transition,” *Microwave and Optical Technology Letters*, vol. 48, no. 9, pp. 1717–1718, 2006.
- [11] X. Y. Zhang, J. Chen, and Q. Xue, “Broadband transition between double-sided parallel-strip line and coplanar waveguide,” *IEEE Microwave and Wireless Components Letters*, vol. 17, pp. 103–105, Feb 2007.
- [12] C. H. Ahn and K. Chang, “Wideband coplanar stripline to double-sided parallel-strip line transition,” *Electronics Letters*, vol. 45, pp. 748–749, July 2009.

- [13] P. L. Carro and J. de Mingo, “Analysis and synthesis of double-sided parallel-strip transitions,” *IEEE Transactions on Microwave Theory and Techniques*, vol. 58, pp. 372–380, Feb 2010.
- [14] T. W. Eubanks and K. Chang, “Low-loss ultra-wideband double-sided parallel-strip line transition and power divider,” *Electronics Letters*, vol. 46, pp. 93–94, January 2010.
- [15] W. . Lu, C. Cheng, and H. . Zhu, “Wideband coplanar waveguide to edges-even broadside-coupled stripline transition,” *Electronics Letters*, vol. 47, pp. 1286–1287, November 2011.
- [16] W. Lu, Y. Bo, and H. Zhu, “A broadband transition design for a conductor-backed coplanar waveguide and a broadside coupled stripline,” *IEEE Microwave and Wireless Components Letters*, vol. 22, pp. 10–12, Jan 2012.
- [17] W. Lu, H. Tong, Y. Bo, and H. Zhu, “Design and study of enhanced wideband transition between coplanar waveguide and broadside coupled stripline,” *IET Microwaves, Antennas Propagation*, vol. 7, pp. 715–721, June 2013.

Chapter 2

Literature Survey

Contents

2.1 DSPSL Transitions	20
2.2 CPW Transitions	23
2.3 Antipodal Vivaldi Antennas	34
2.4 Chapter Summary	36
References	37

This chapter surveys the transitions between CPW and other popular transmission lines, such as microstrip, coplanar stripline(CPS), slotline etc. in the first section. In the second section, all the DSPSL transitions are reviewed. The final section reviews all major recent developments in the area of antipodal vivaldi antennas. The geometry of the transitions and antennas are also provided here.

2.1 DSPSL Transitions

In [1], as shown in Figures 2.1a, 2.1b and 2.1c, tapered transitions from microstrip line to DSPSL are designed and a return loss better than 10 dB for a bandwidth of 1 to 30 GHz is reported.

[2] reports first CPS to DSPSL transition in Figure 2.1d with return loss of better than 10 dB, and an insertion loss of 2.5 dB has been obtained from 2.4 to 10.7 GHz.

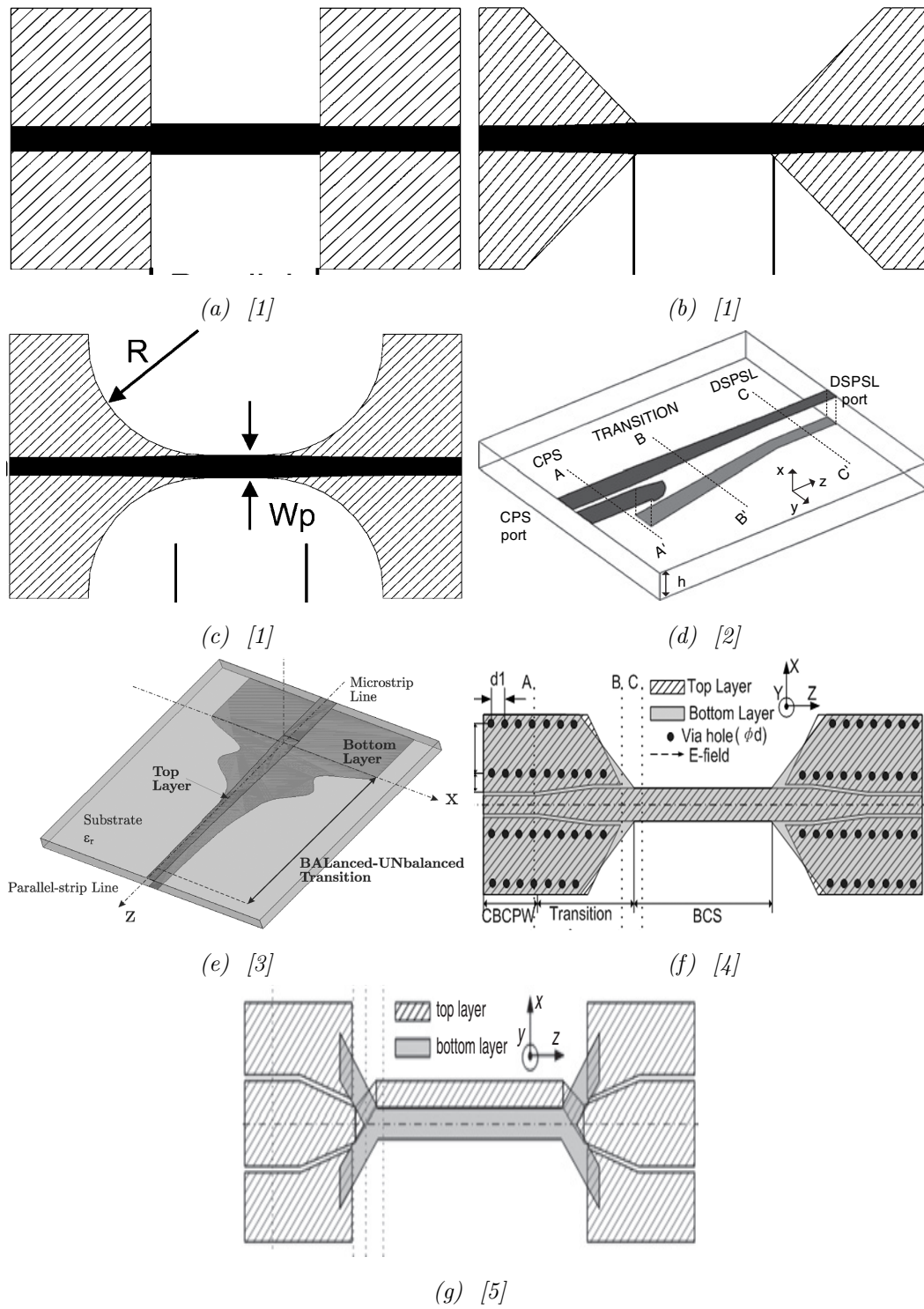


Figure 2.1: Different DSPSL Transitions

Table 2.1: Different CPW to DSPSL Transitions

Transition	Bandwidth (GHz)	Insertion Loss (dB)	Return Loss (dB)	Substrate
[6]	1.1 - 6.45	≤ 1.8	≥ 10.0	$\epsilon_r=9.6$ Thickness = 0.8 mm
[7]	1.3 - 9.0	≤ 1.4	≥ 10.0	$\epsilon_r=6.15$ Thickness = 0.635 mm
[8]	1.16 - 12.01	≤ 1.41	≥ 10.0	$\epsilon_r=3.38$ Thickness = 0.5 mm
[9]	0.04 - 27.0	≤ 1.2	≥ 10.0	$\epsilon_r=3.38$ Thickness = 0.2 mm

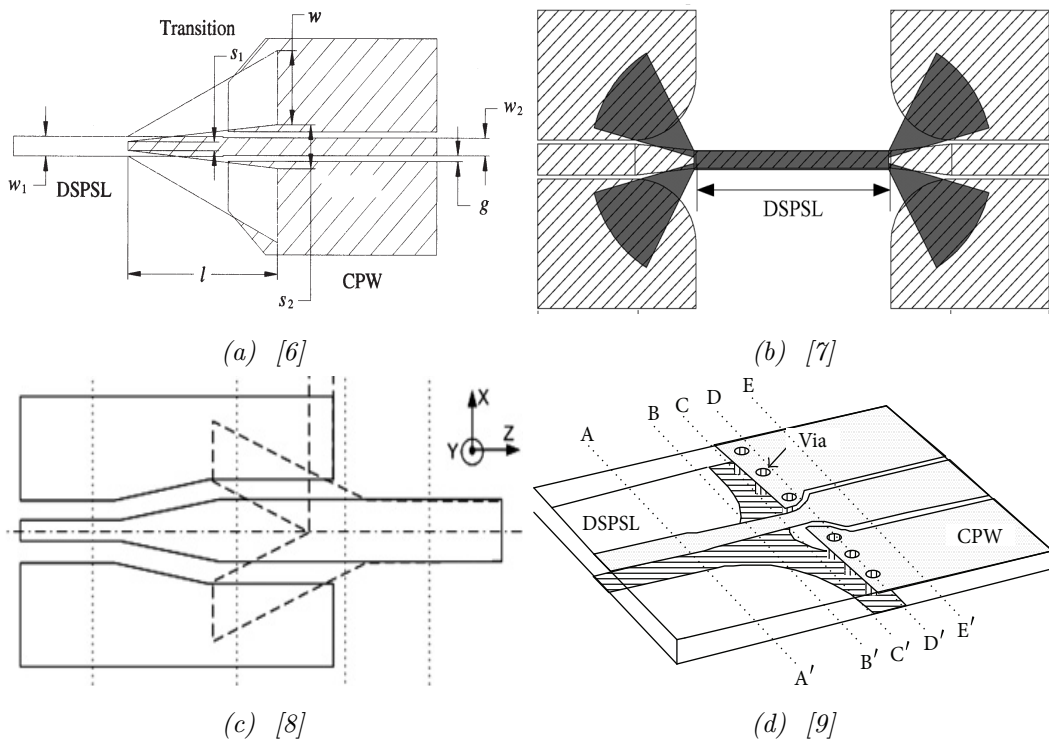


Figure 2.2: Different CPW to DSPSL Transitions

As shown in Figure 2.1e, [3] reports a new method based on conformal mapping to evaluate and optimize the return losses of a tapered microstrip to DSPSL with impedance matching capabilities.

Figure 2.1f shows a Conductor Backed CPW (CBCPW) to DSPSL transition, reported in [4], with maximum insertion loss of 2.3 dB and return loss of higher than 10 dB is obtained from 50 MHz to 20 GHz.

[5] reports transition from edges even DSPSL to CPW as in Figure 2.1g. It shows maximum insertion loss of 2.4 dB and a return loss of better than 10 dB for 1.1 to 11.2 GHz band.

Table 2.1 and Figure 2.2 shows different CPW to DSPSL transitions [6–9].

2.2 CPW Transitions

This section reviews the geometries of the transitions between CPW to other popular transmission lines such as microstrip, CPW, slotline and CPS [10].

Conductor Backed CPW - Microstrip Transitions

Figure 2.3, shows two CBCPW to microstrip transitions utilizing direct coupling via multiple metal posts [11, 12].

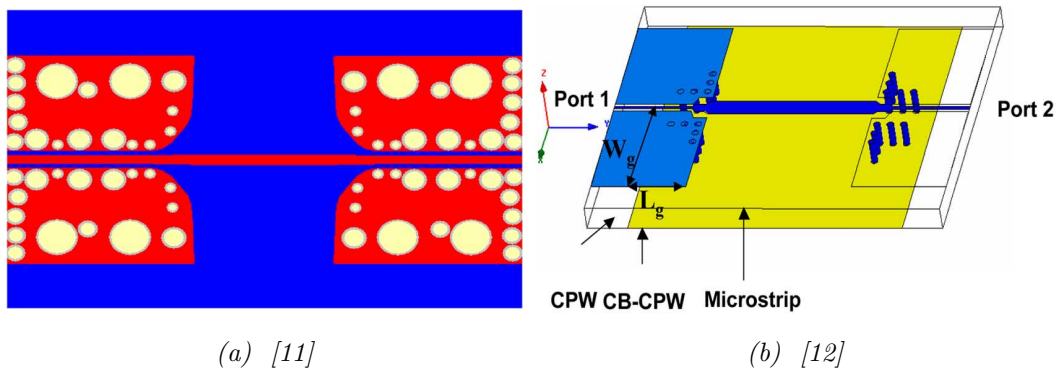


Figure 2.3: Different CBCPW to Microstrip Transitions

CPW - Microstrip Transitions

Broadly electromagnetic and direct coupling techniques are used for creating CPW to microstrip transitions. Figure 2.4a, shows a common ground arrangement with signal continuity ensured using a gold ribbon or a bond wire [13].

Electromagnetic coupling between strip conductors [14] and between ground conductors [15] are also used for transitions as in Figures 2.4b and 2.4c. Figure 2.4d shows transition via phase shifting network [16].

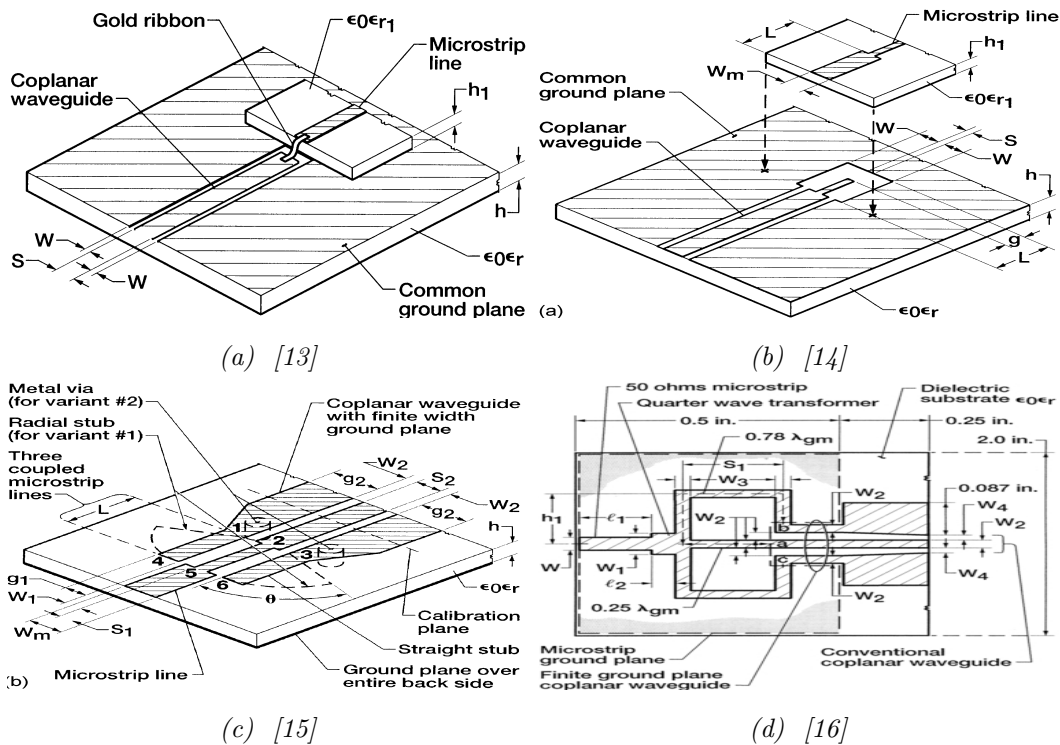


Figure 2.4: Different CPW to Microstrip Transitions

Transitions using metal posts or via-hole interconnects [17, 18] are shown in Figures 2.5a and 2.5b. Figure 2.5c shows orthogonal transition via direct contact [19].

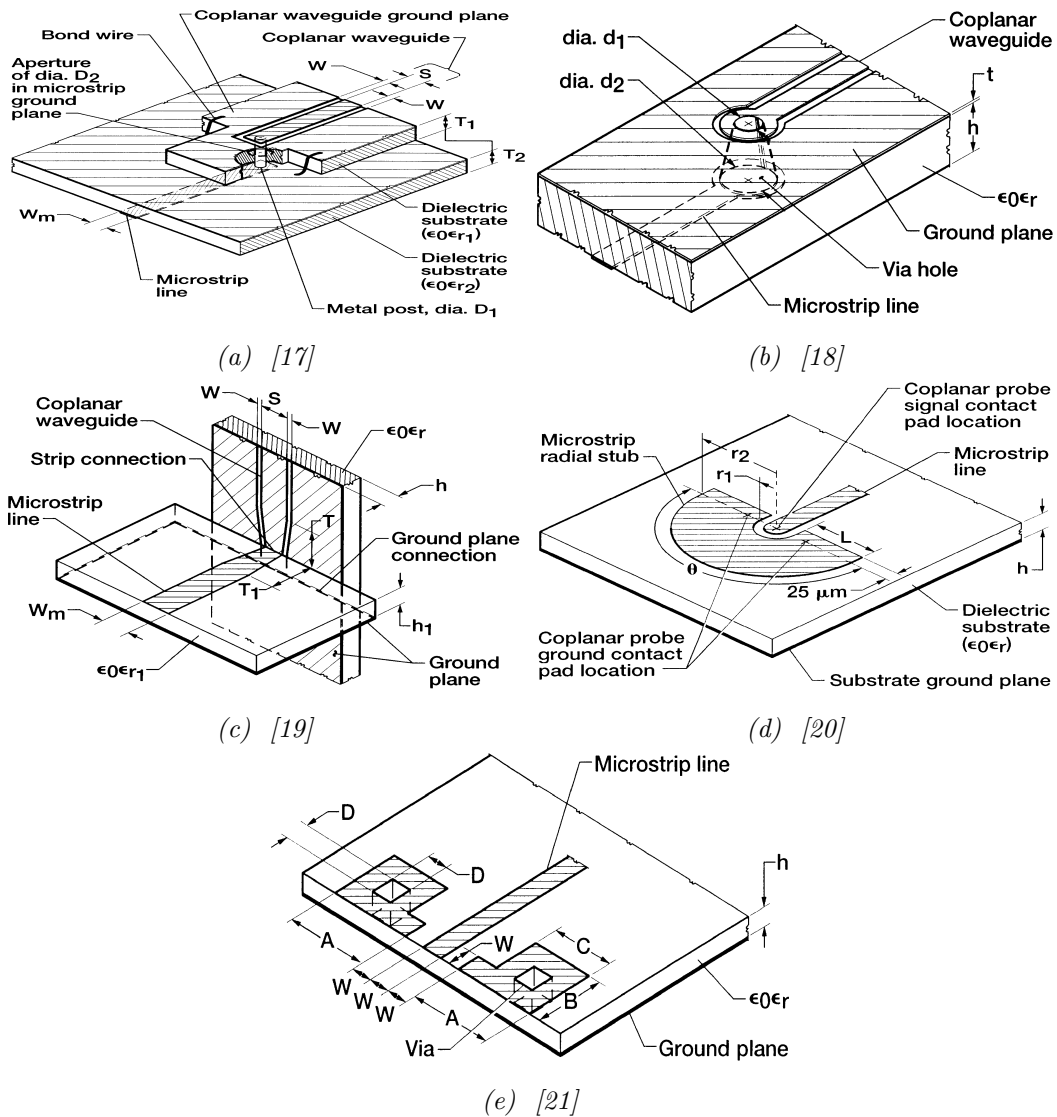


Figure 2.5: Different CPW to Microstrip Transitions

For facilitating input/output ports in monolithic microwave integrated circuits (MMICs) CPW probe pads are used. Figures 2.5e and 2.5d are the transitions from microstrip to these pads [20, 21].

Recent developments [22–33] in the CPW to microstrip transitions are shown in Figures 2.6 and 2.7. It also utilizes the same techniques mentioned above for achieving transitions.

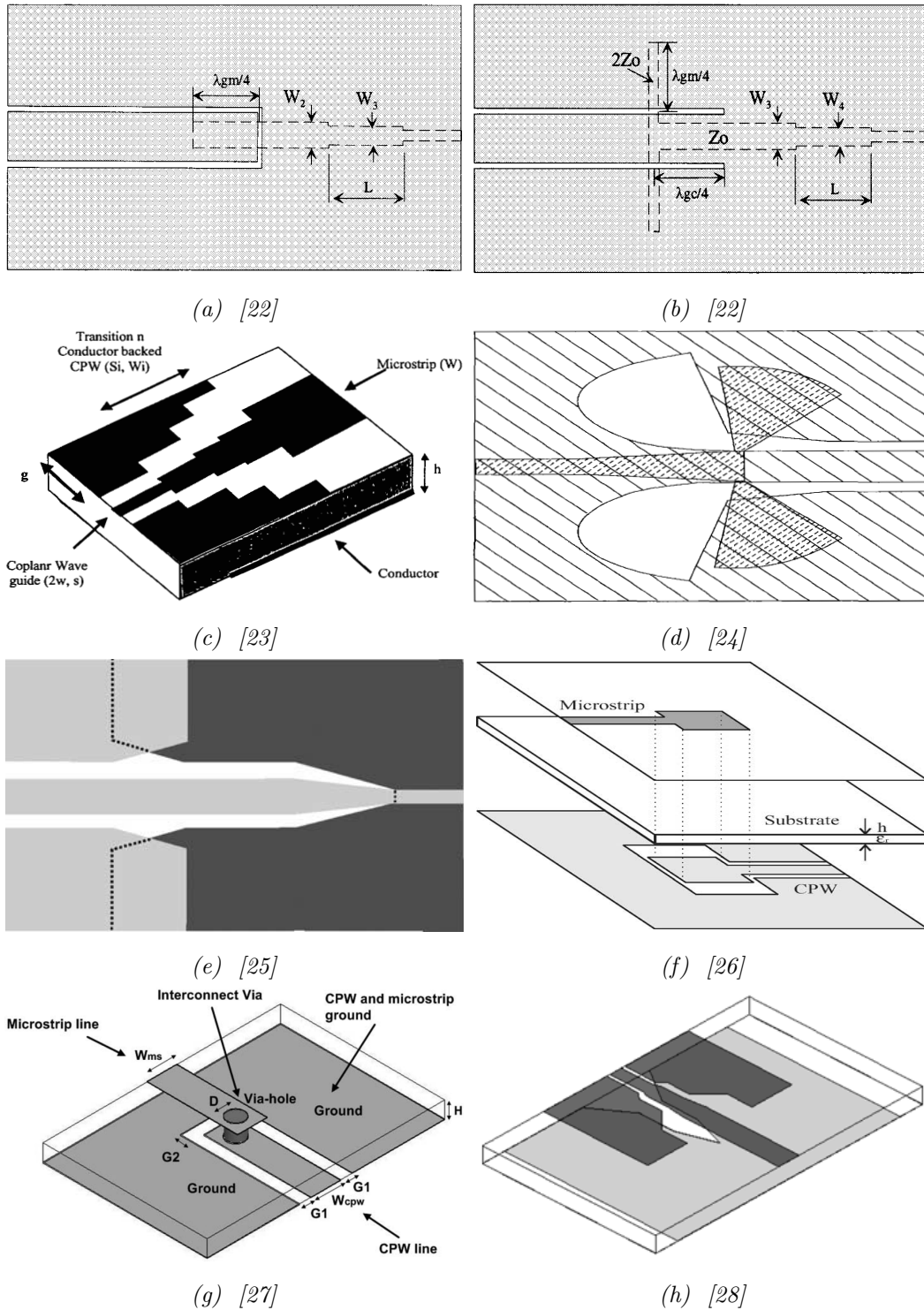


Figure 2.6: Different CPW to Microstrip Transitions

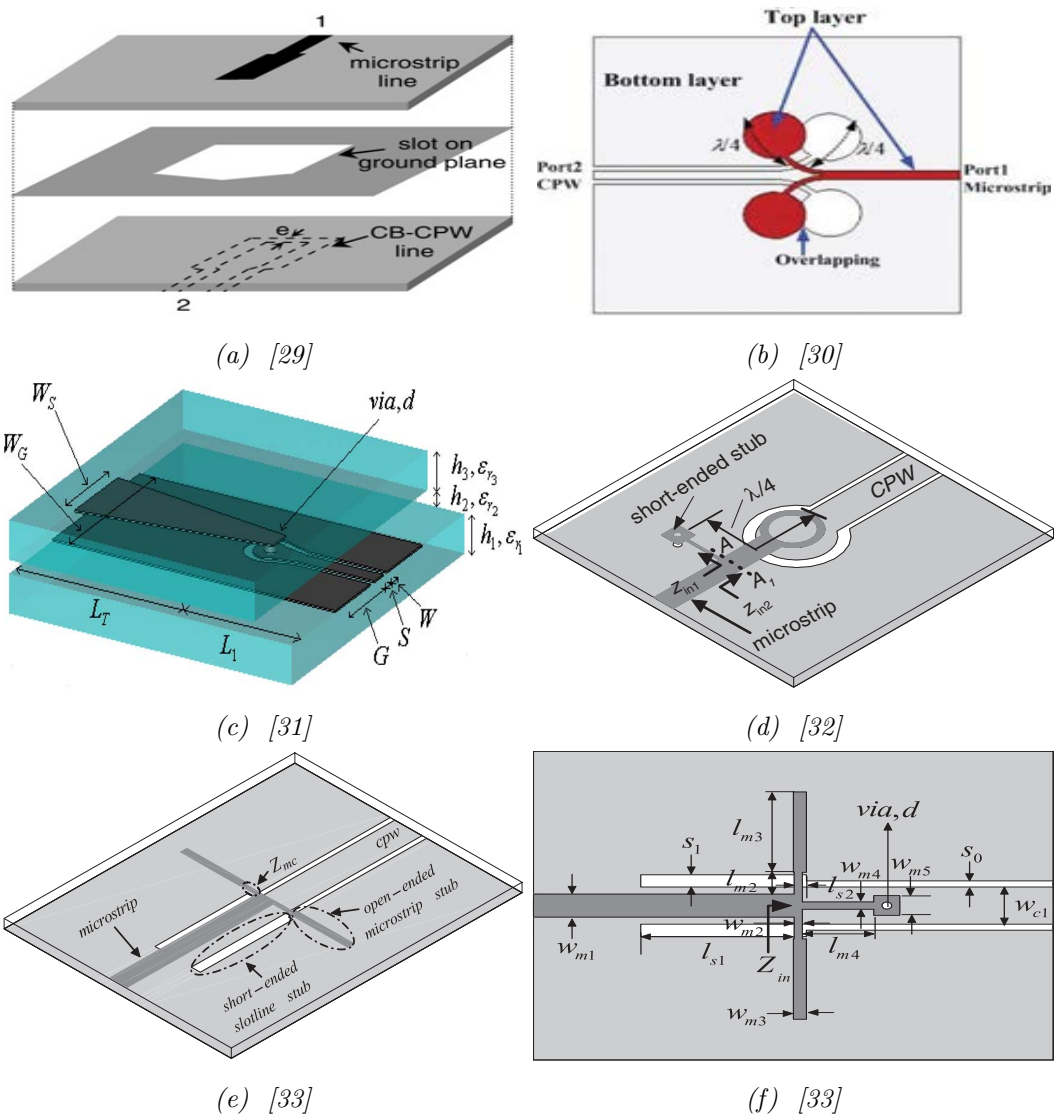


Figure 2.7: Different CPW to Microstrip Transitions

CPW - CPW Transitions

Different techniques like vertical fed-through interconnects between finite ground coplanar waveguides (FGCPWs) [34], orthogonal transitions [35, 37], electromagnetically coupled transitions [36] and using bond wires [38] are shown in Figure 2.8.

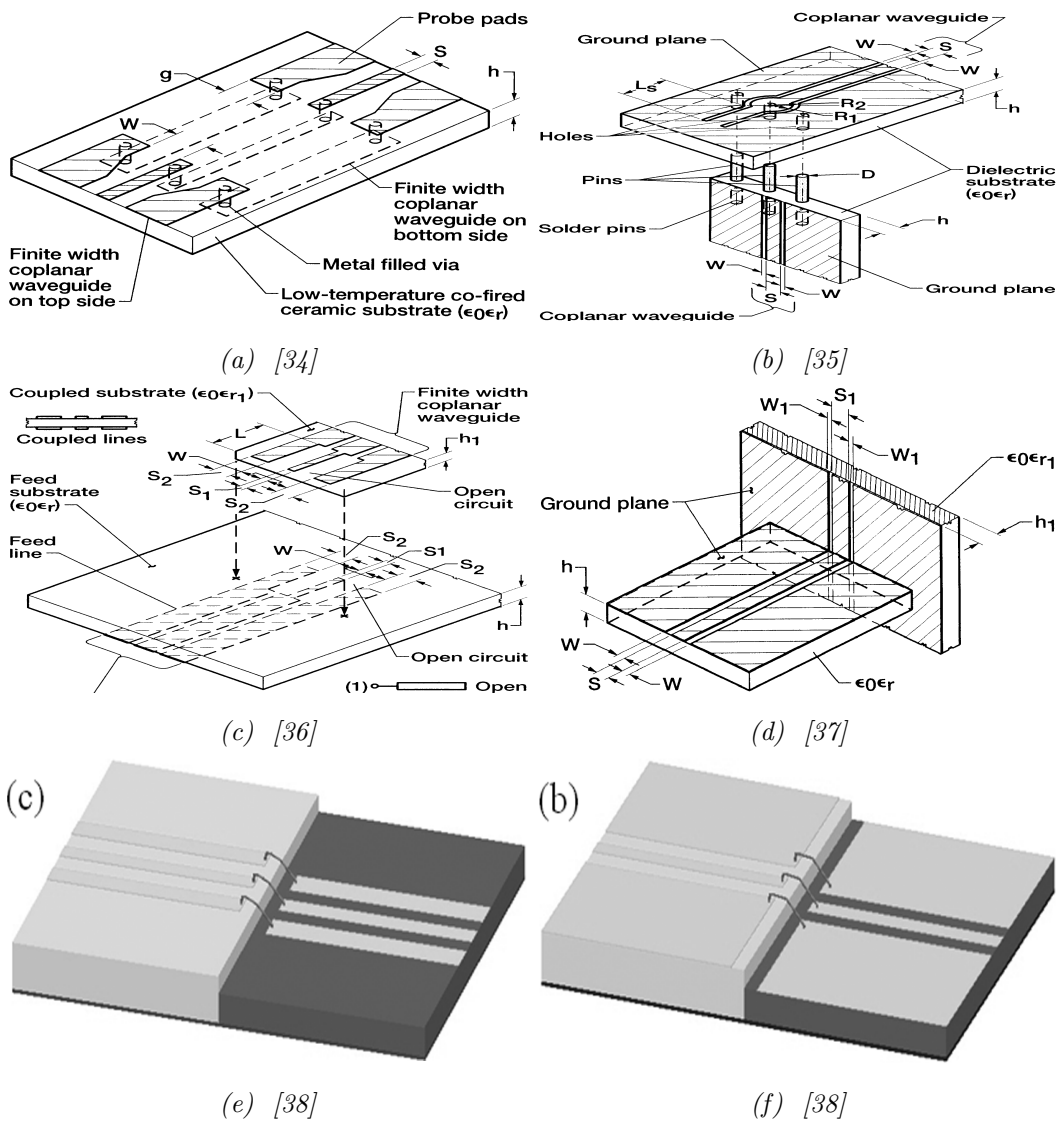


Figure 2.8: Different CPW to CPW Transitions

CPW - Slotline Transitions

Transitions between unbalanced CPW and balanced slotline is presented in this section. Transitions of these type are commonly referred as baluns. In Figure 2.9, [13] proposes compensated Marchand transition, [39] is the transition with radial stub termination and DC isolating slot, [40] introduces circular stub termination and [39] shows double-Y transition.

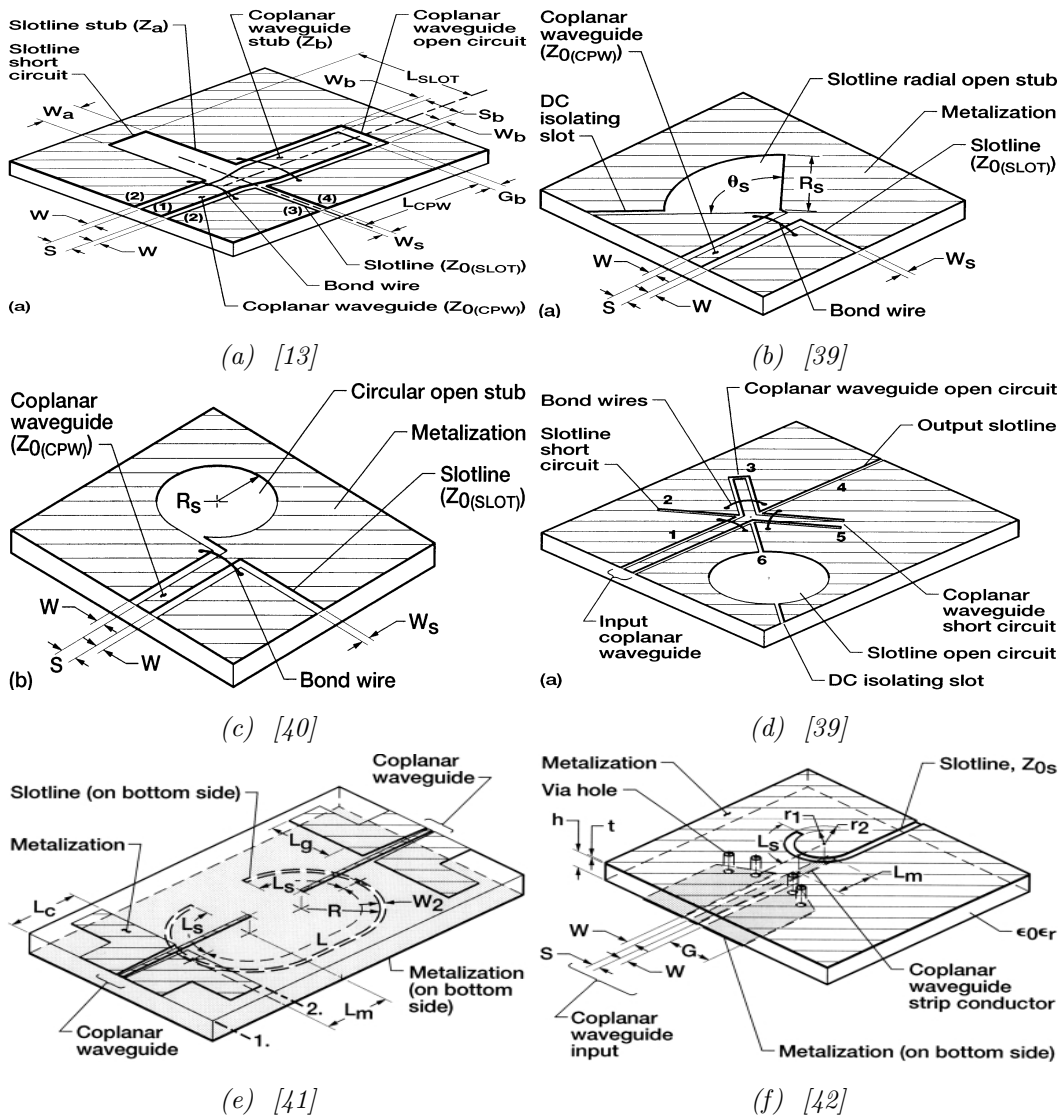


Figure 2.9: Different CPW to Slotline Transitions

[41, 42] are electromagnetically coupled transitions with latter using metal filled vias for connecting ground planes as shown in Figures 2.9e and 2.9f, and [41, 43] shows air-bridge coupled transitions as in Figures 2.10a and 2.10b. [44] utilizes phase shifter and air bridge to achieve transition as shown in Figure 2.10c. Figures 2.10e, 2.10f and 2.11 are lumped element uniplanar transitions [45–47], with the second one [46], bridgeless.

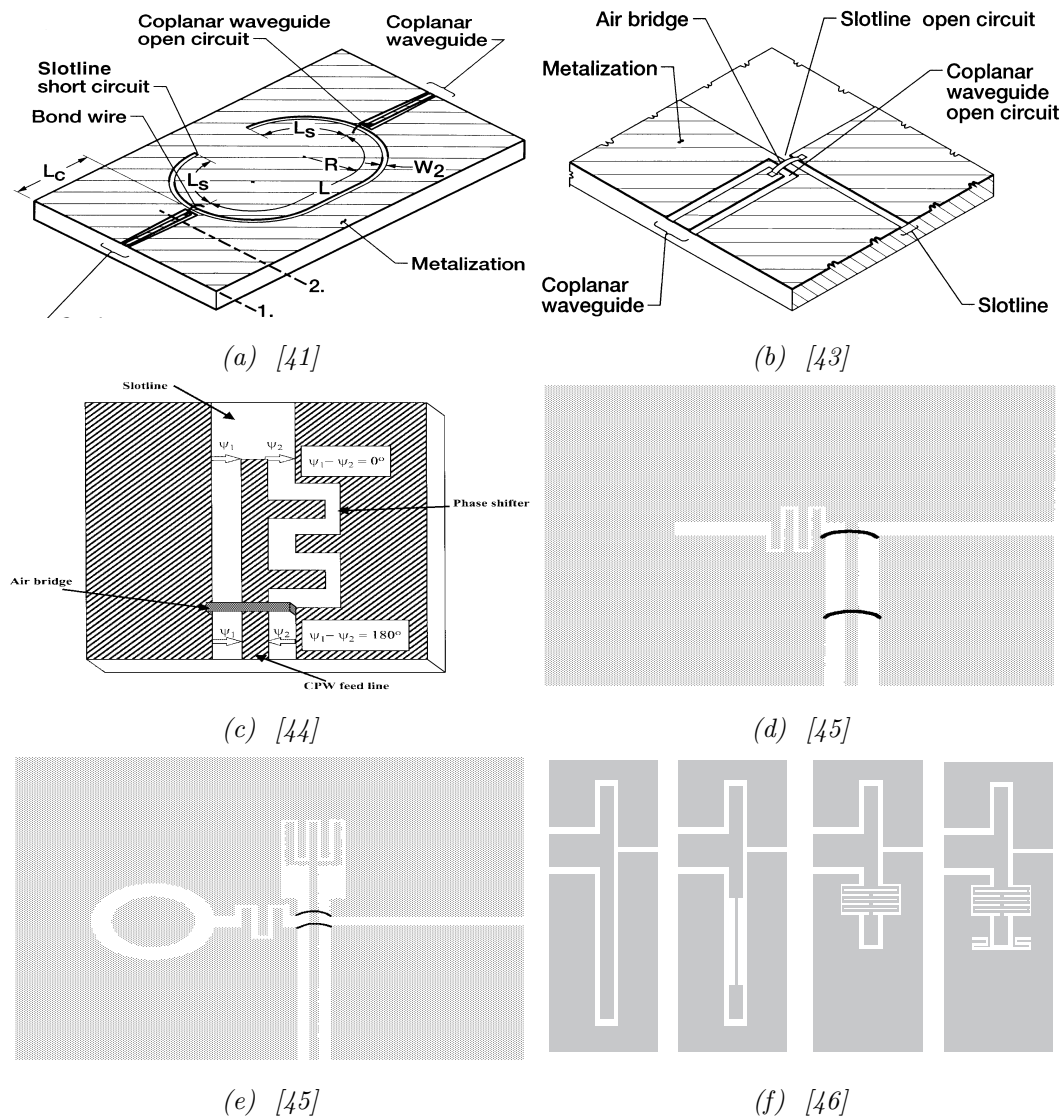


Figure 2.10: Different CPW to Slotline Transitions

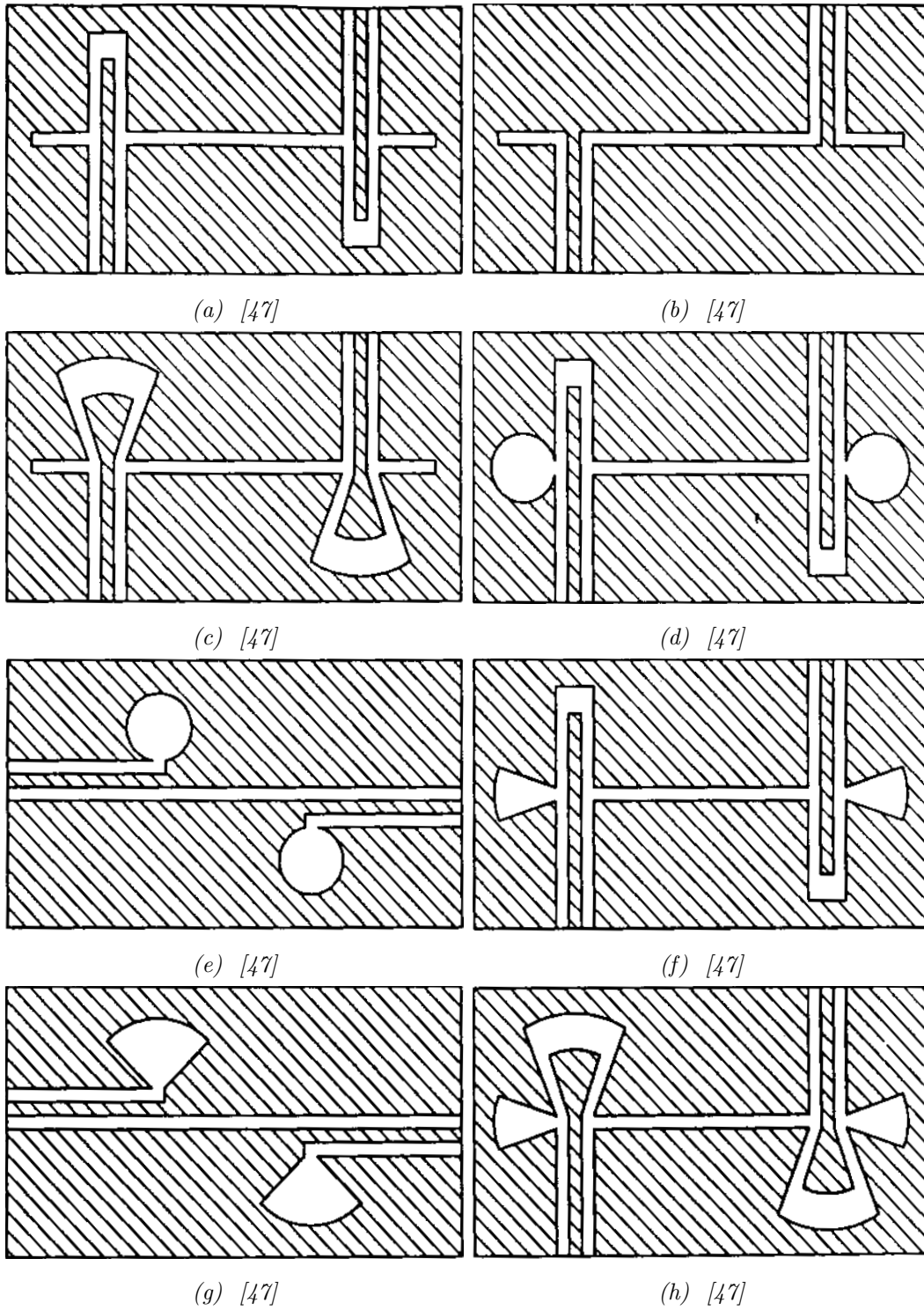


Figure 2.11: Different CPW to Slotline Transitions

CPW - Coplanar Stripline (CPS) Transitions

CPW and CPS are uniplanar transmission lines, and the transition between them is also a balun. Figure 2.12a is a transition with three strip transmission lines [48]. [49] and [50] utilizes radial slotline stub and double-Y structure for achieving transition as in Figures 2.12b and 2.12c. Figures 2.12d, 2.12e and 2.12f shows lumped uniplanar transitions [45].

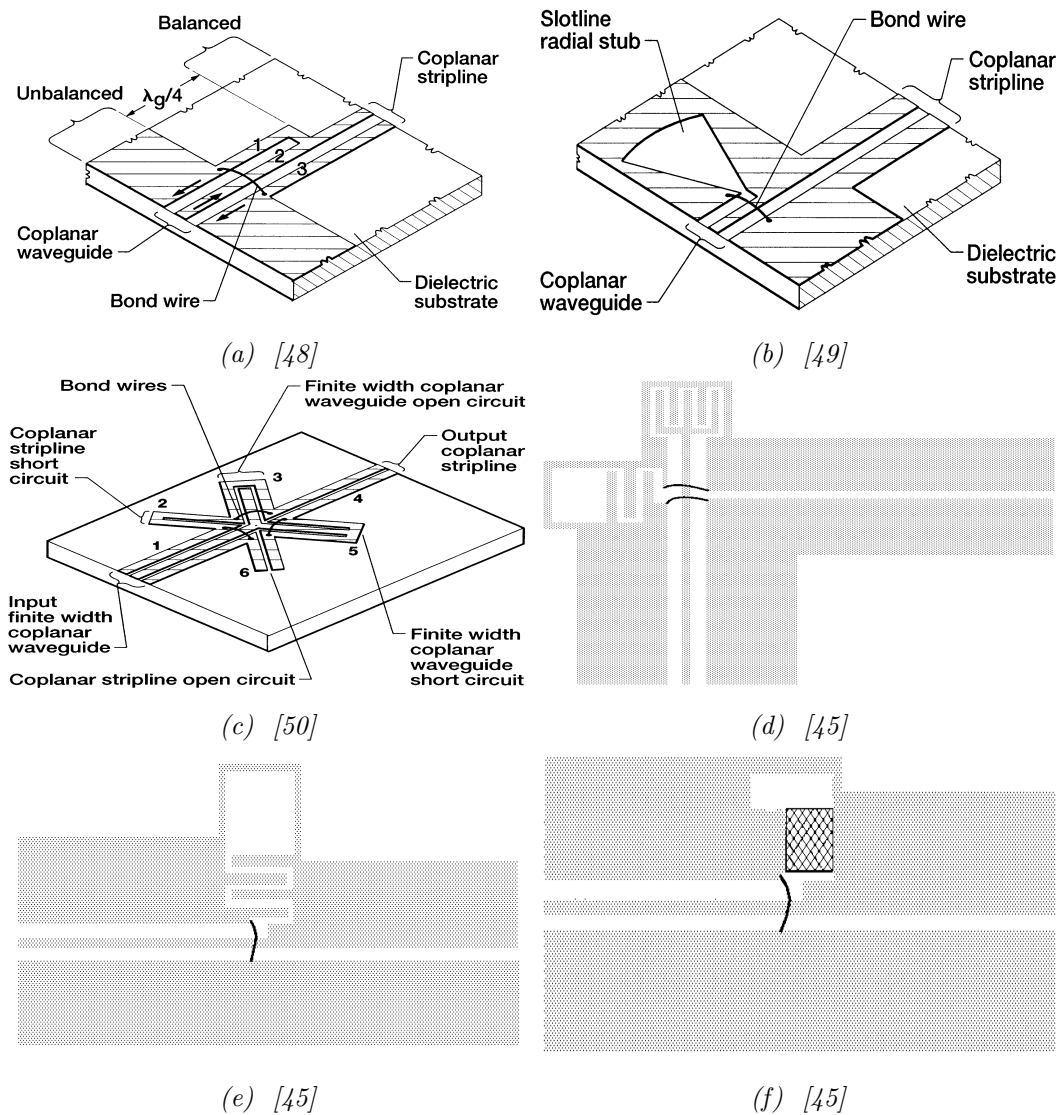


Figure 2.12: Different CPW to CPS Transitions

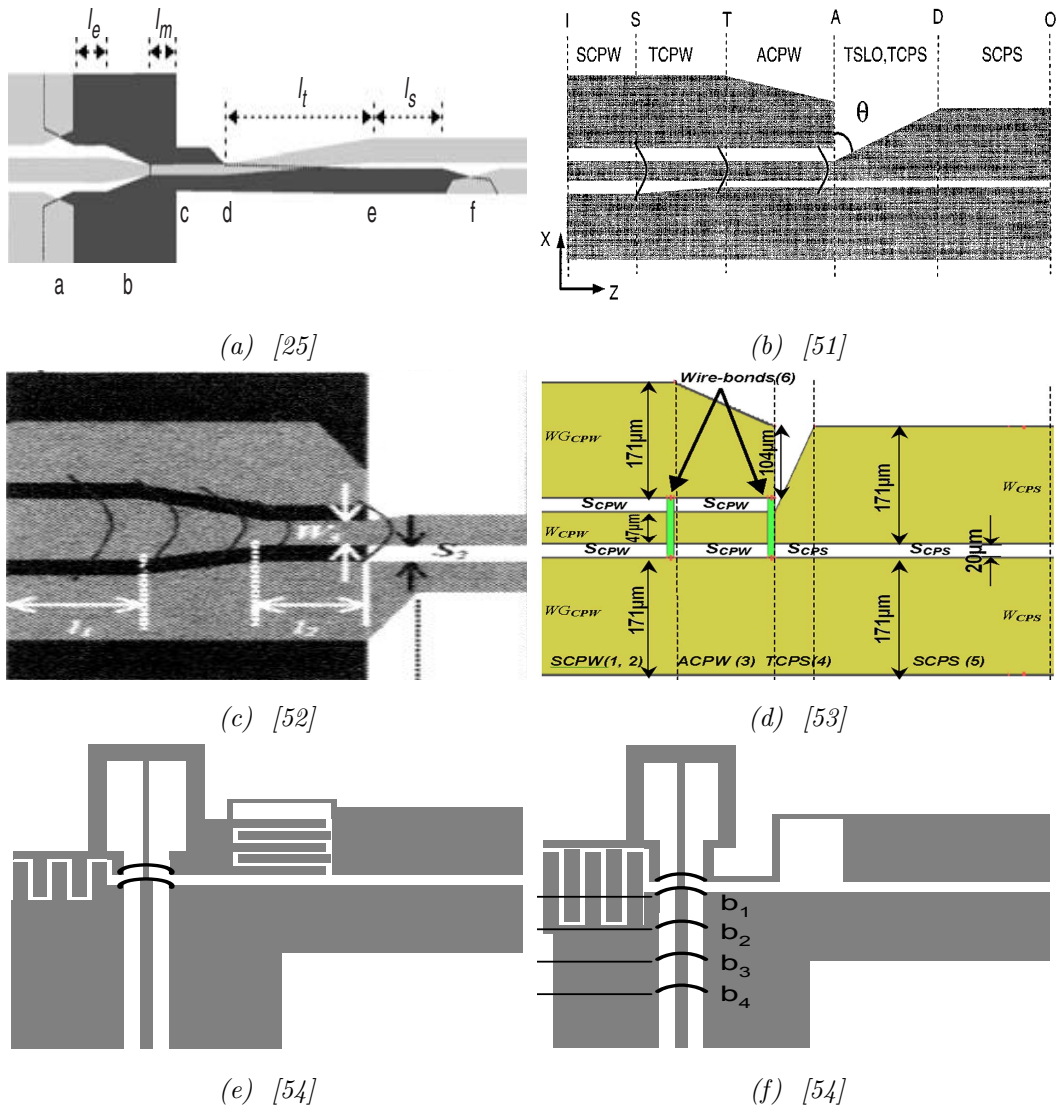


Figure 2.13: Different CPW to CPS Transitions

Figure 2.13 shows CPW to CPS transitions found in literature.

2.3 Antipodal Vivaldi Antennas

The vivaldi antenna is a tapered slot antenna which is wideband in nature, introduced by Gibson in 1979 [55]. As shown by Gazit in 1988 [56], the bandwidth enhancement can be achieved for vivaldi by making it antipodal in nature (antipodal vivaldi antennas (AVA)). The bandwidth constraints in different vivaldi antennas are limited by the feeding transitions. The feeding structure of AVA is the DSPSL structure. Therefore transitions to the DSPSL structure is extremely important. AVAs have skewed electric field components which result in the poor cross polarization and at higher frequencies this skew results in serious beam tilt also. These problems can be avoided to some extent by using thin substrates with limited range of application. The balanced AVA (BAVA) introduced by Langley in 1993 [57], with three layered structure, reduces this problem at the expense of increased manufacturing cost and difficulty.

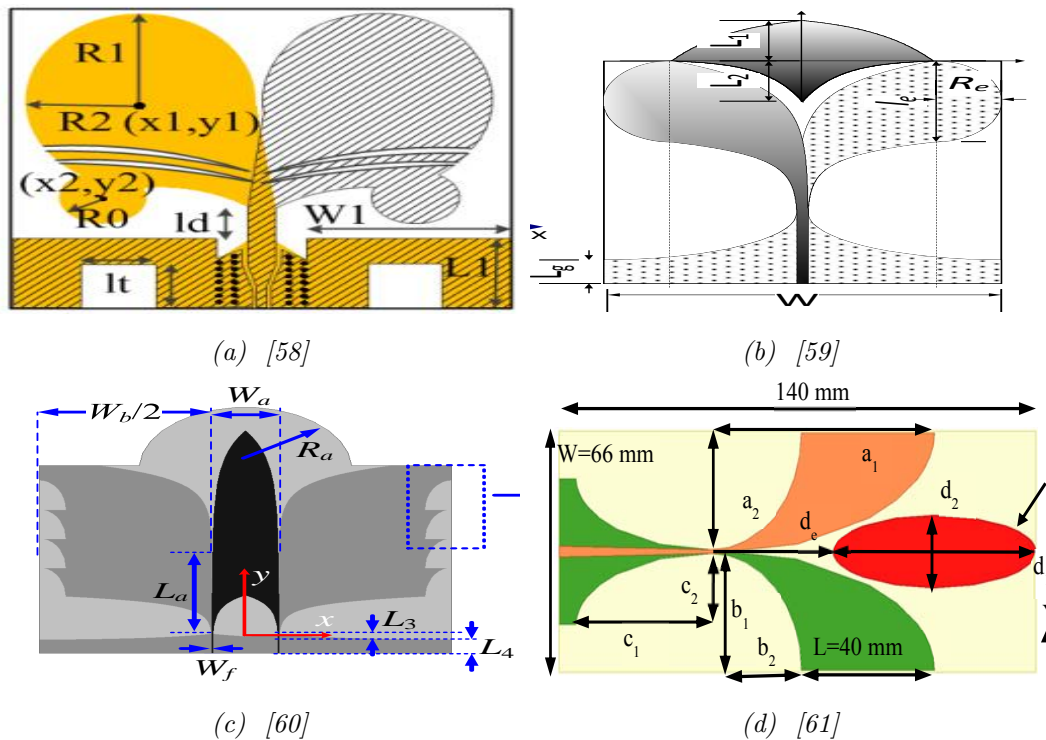


Figure 2.14: Different Antipodal Vivaldi Antennas.

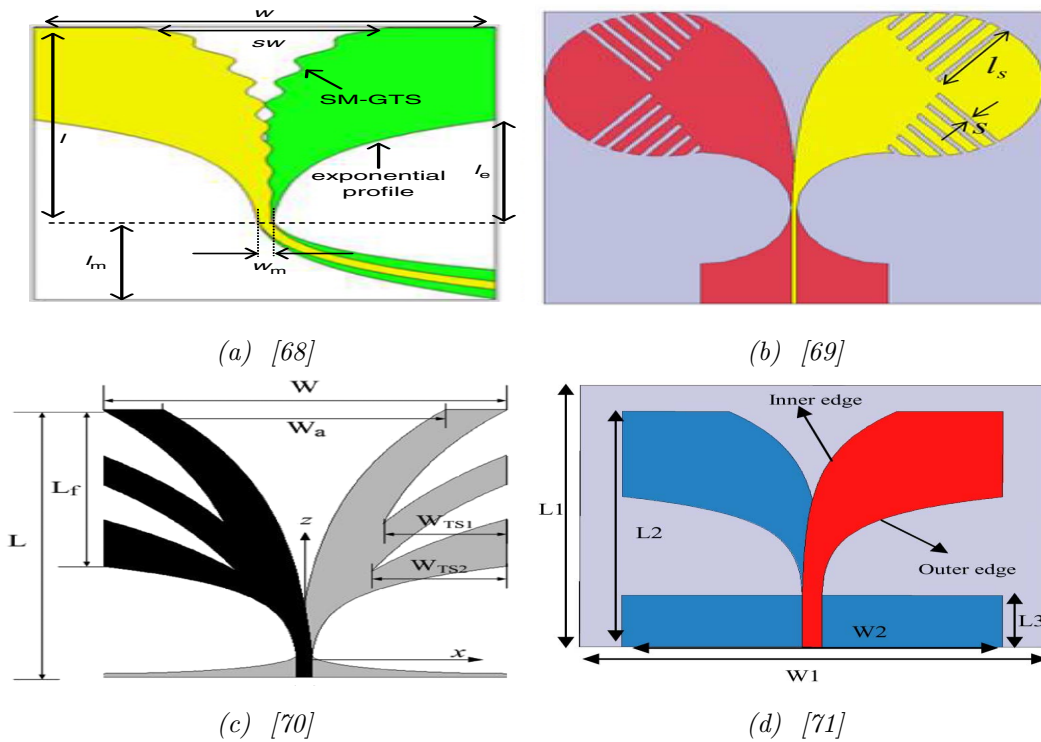


Figure 2.16: Different Antipodal Vivaldi Antennas.

2.4 Chapter Summary

This chapter reviews the transitions of CPW and DSPSL with other popular transmission lines, such as microstrip, coplanar stripline(CPS), slotline etc. in the first two sections. In the final part, all major recent developments in the area of antipodal vivaldi antennas are given. The geometry of the transitions and antennas are provided briefly in this chapter.

References

- [1] Sang-Gyu Kim and Kai Chang, “Ultrawide-band transitions and new microwave components using double-sided parallel-strip lines,” *IEEE Transactions on Microwave Theory and Techniques*, vol. 52, pp. 2148–2152, Sep. 2004.
- [2] C. H. Ahn and K. Chang, “Wideband coplanar stripline to double-sided parallel-strip line transition,” *Electronics Letters*, vol. 45, pp. 748–749, July 2009.
- [3] P. L. Carro and J. de Mingo, “Analysis and synthesis of double-sided parallel-strip transitions,” *IEEE Transactions on Microwave Theory and Techniques*, vol. 58, pp. 372–380, Feb 2010.
- [4] W. Lu, Y. Bo, and H. Zhu, “A broadband transition design for a conductor-backed coplanar waveguide and a broadside coupled stripline,” *IEEE Microwave and Wireless Components Letters*, vol. 22, pp. 10–12, Jan 2012.
- [5] W. . Lu, C. Cheng, and H. . Zhu, “Wideband coplanar waveguide to edges-even broadside-coupled stripline transition,” *Electronics Letters*, vol. 47, pp. 1286–1287, November 2011.
- [6] J.-X. Chen, J.-L. Li, and Q. Xue, “Novel via-less double-sided parallel strip line to coplanar waveguide transition,” *Microwave and Optical Technology Letters*, vol. 48, no. 9, pp. 1717–1718, 2006.
- [7] X. Y. Zhang, J. Chen, and Q. Xue, “Broadband transition between double-sided parallel-strip line and coplanar waveguide,” *IEEE Microwave and Wireless Components Letters*, vol. 17, pp. 103–105, Feb 2007.
- [8] W. Lu, H. Tong, Y. Bo, and H. Zhu, “Design and study of enhanced wideband transition between coplanar waveguide and broadside coupled stripline,” *IET Microwaves, Antennas Propagation*, vol. 7, pp. 715–721, June 2013.

- [9] Y.-G. Kim and K. W. Kim, “Design and study of enhanced wideband transition between coplanar waveguide and broadside coupled stripline,” *Design of an Ultra-Wideband Transition from Double-Sided Parallel Stripline to Coplanar Waveguide*, p. 8, 2013.
- [10] R. N. Simons, *Coplanar Waveguide Circuits, Components and Systems*. Wiley-IEEE Press, 2004.
- [11] Q. Jiang, C. Domier, and N. C. Luhmann, “A ultra wideband low loss cbcpw-to-microstrip transition with multiple via holes,” *IEEE Microwave and Wireless Components Letters*, vol. 24, pp. 751–753, Nov 2014.
- [12] Z. Zhou and K. L. Melde, “Development of a broadband coplanar waveguide-to-microstrip transition with vias,” *IEEE Transactions on Advanced Packaging*, vol. 31, pp. 861–872, Nov 2008.
- [13] M. Houdart and C. Aury, “Various excitation of coplanar waveguide,” in *1979 IEEE MTT-S International Microwave Symposium Digest*, pp. 116–118, April 1979.
- [14] J. J. Burke and R. W. Jackson, “Surface-to-surface transition via electromagnetic coupling of microstrip and coplanar waveguide,” *IEEE Transactions on Microwave Theory and Techniques*, vol. 37, pp. 519–525, March 1989.
- [15] G. P. Gauthier, L. P. Katehi, and G. M. Rebeiz, “W-band finite ground coplanar waveguide (fggpw) to microstrip line transition,” in *1998 IEEE MTT-S International Microwave Symposium Digest (Cat. No.98CH36192)*, vol. 1, pp. 107–109 vol.1, June 1998.
- [16] N. I. Dib, R. N. Simons, and L. P. B. Katehi, “New uniplanar transitions for circuit and antenna applications,” *IEEE Transactions on Microwave Theory and Techniques*, vol. 43, pp. 2868–2873, Dec 1995.
- [17] R. N. Simons and R. Q. Lee, “Coplanar-waveguide/microstrip probe coupler and applications to antennas,” *Electronics Letters*, vol. 26, pp. 1998–2000, Nov 1990.

- [18] B. Golja, H. B. Sequeira, S. Duncan, G. Mendenilla, and N. E. Byer, "A coplanar-to-microstrip transition for w-band circuit fabrication with 100- μ m-thick GaAs wafers," *IEEE Microwave and Guided Wave Letters*, vol. 3, pp. 29–31, Feb 1993.
- [19] L. Hyden, S. Hagelin, P. Starski, and K. Yhland, "Analysis and design of a vertical CPW transition between microstrip planes," in *1997 IEEE MTT-S International Microwave Symposium Digest*, vol. 2, pp. 727–730 vol.2, June 1997.
- [20] D. F. Williams and T. H. Miers, "A coplanar probe to microstrip transition," *IEEE Transactions on Microwave Theory and Techniques*, vol. 36, pp. 1219–1223, July 1988.
- [21] D. Harvey, "A lumped coplanar to microstrip transition model for de-embedding S-parameters measured on GaAs wafers," in *29th ARFTG Conference Digest*, vol. 11, pp. 204–217, June 1987.
- [22] T. Girard, R. Staraj, E. Cambiaggio, and F. Muller, "Microstrip-CPW transitions for antenna array applications," *Microwave and Optical Technology Letters*, vol. 23, no. 3, pp. 131–133, 1999.
- [23] A. M. E. Safwata, K. A. Zaki, W. Johnson, and C. H. Lee, "Novel design for coplanar waveguide to microstrip transition," in *2001 IEEE MTT-S International Microwave Symposium Digest (Cat. No.01CH37157)*, vol. 2, pp. 607–610 vol.2, May 2001.
- [24] T. . Lin, "Via-free broadband microstrip to CPW transition," *Electronics Letters*, vol. 37, pp. 960–961, July 2001.
- [25] T. Chiu, "A building-block design scheme for planar transmission-line transitions," *IEE Proceedings - Microwaves, Antennas and Propagation*, vol. 150, pp. 405–410, Dec 2003.
- [26] Lei Zhu and W. Menzel, "Broad-band microstrip-to-CPW transition via frequency-dependent electromagnetic coupling," *IEEE Transactions on Microwave Theory and Techniques*, vol. 52, pp. 1517–1522, May 2004.

- [27] Jui-Chieh Chiu, Jih-Ming Lin, Mau-Phon Houng, and Yeong-Her Wang, “A pcb-compatible 3-db coupler using microstrip-to-cpw via-hole transitions,” *IEEE Microwave and Wireless Components Letters*, vol. 16, pp. 369–371, June 2006.
- [28] Lin Zhu and K. L. Melde, “On-wafer measurement of microstrip-based circuits with a broadband vialess transition,” *IEEE Transactions on Advanced Packaging*, vol. 29, pp. 654–659, Aug 2006.
- [29] M. Nedil, T. A. Denidni, and A. Djaiz, “Ultra-wideband microstrip to cb-cpw transition applied to broadband filter,” *Electronics Letters*, vol. 43, pp. 464–466, April 2007.
- [30] A. M. Abbosh, “Multioctave microstrip-to-coplanar waveguide vertical transition,” *Microwave and Optical Technology Letters*, vol. 53, no. 1, pp. 187–189, 2011.
- [31] S. Bulja and D. Mirshekar-Syahkal, “Novel wideband transition between coplanar waveguide and microstrip line,” *IEEE Transactions on Microwave Theory and Techniques*, vol. 58, pp. 1851–1857, July 2010.
- [32] Z. Tao, J. Wang, and Y. Dou, “Design of broadband microstrip-to-cpw transition,” *Electronics Letters*, vol. 50, pp. 35–37, January 2014.
- [33] Z. Tao, “Broadband transition design from microstrip to cpw,” *IEEE Microwave and Wireless Components Letters*, vol. 25, pp. 712–714, Nov 2015.
- [34] R. N. Simons, R. A. Lee, K. A. Shalkhausere, J. Owens, J. Demarco, J. Leen, and D. Sturzebecher, “Finite width coplanar waveguide patch antenna with vertical fed through interconnect,” in *IEEE Antennas and Propagation Society International Symposium. 1996 Digest*, vol. 2, pp. 1338–1341 vol.2, July 1996.
- [35] R. N. Simons, T. D. Perl, and R. Q. Lee, “New coplanar waveguide feed network for 2×2 linearly tapered slot antenna subarray,” *Microwave and Optical Technology Letters*, vol. 5, no. 9, pp. 420–423, 1992.

- [36] R. W. Jackson and D. W. Matolak, "Surface-to-surface transition via electromagnetic coupling of coplanar waveguides," *IEEE Transactions on Microwave Theory and Techniques*, vol. 35, pp. 1027–1032, Nov 1987.
- [37] R. Q. Lee and R. N. Simons, "Electromagnetically coupled feed network for an array module of four microstrip elements," in *1988 IEEE AP-S. International Symposium, Antennas and Propagation*, pp. 1018–1021 vol.3, June 1988.
- [38] JuHwan Lim, DaeHan Kwon, Jae-Sung Rieh, Soo-Won Kim, and SungWoo Hwang, "Rf characterization and modeling of various wire bond transitions," *IEEE Transactions on Advanced Packaging*, vol. 28, pp. 772–778, Nov 2005.
- [39] W. Grammer and K. S. Yngvesson, "Coplanar waveguide transitions to slotline: design and microprobe characterization," *IEEE Transactions on Microwave Theory and Techniques*, vol. 41, pp. 1653–1658, Sep. 1993.
- [40] T. Q. Ho and S. M. Hart, "A broad-band coplanar waveguide to slotline transition," *IEEE Microwave and Guided Wave Letters*, vol. 2, pp. 415–416, Oct 1992.
- [41] R. N. Simons, S. R. Taub, and P. G. Young, "Novel coplanar waveguide to slotline transition on high resistivity silicon," *Electronics Letters*, vol. 28, pp. 2209–2210, Nov 1992.
- [42] R. N. Simons, R. Q. Lee, T. D. Perl, and J. Silvestro, "Effect of a dielectric overlay on a linearly tapered slot antenna excited by a coplanar waveguide," *Microwave and Optical Technology Letters*, vol. 6, no. 4, pp. 225–228, 1993.
- [43] T. Hirota, Y. Tarusawa, and H. Ogawa, "Uniplanar mmic hybrids - a proposed new mmic structure," *IEEE Transactions on Microwave Theory and Techniques*, vol. 35, pp. 576–581, June 1987.
- [44] K. . Ma, Y. Qian, and T. Itoh, "Analysis and applications of a new cpw-slotline transition," *IEEE Transactions on Microwave Theory and Techniques*, vol. 47, pp. 426–432, April 1999.

- [45] Yo-Shen Lin and Chun Hsiung Chen, “Novel lumped-element uniplanar transitions,” *IEEE Transactions on Microwave Theory and Techniques*, vol. 49, pp. 2322–2330, Dec 2001.
- [46] A. A. Ibrahim, A. M. E. Safwat, and H. El-Hennawy, “Uniplanar bridgeless cpw-to-slotline transition and its application to cpw balun,” *Electronics Letters*, vol. 48, pp. 443–444, April 2012.
- [47] C. . Ho, L. Fan, and K. Chang, “Experimental investigations of cpw-slotline transitions for uniplanar microwave integrated circuits,” in *1993 IEEE MTT-S International Microwave Symposium Digest*, pp. 877–880 vol.2, June 1993.
- [48] R. E. Dabrecht, “Coplanar balun circuits for gaas fet high-power push-pull amplifiers,” in *1973 IEEE G-MTT International Microwave Symposium*, pp. 309–312, June 1973.
- [49] Chien-Hsun Ho, Lu Fan, and Kai Chang, “Broad-band uniplanar hybrid-ring and branch-line couplers,” *IEEE Transactions on Microwave Theory and Techniques*, vol. 41, pp. 2116–2125, Dec 1993.
- [50] V. Trifunovic and B. Jokanovic, “Four decade bandwidth uniplanar balun,” *Electronics Letters*, vol. 28, pp. 534–535, March 1992.
- [51] Shau-Gang Mao, Chieh-Tsao Hwang, Ruey-Beei Wu, and Chun Hsiung Chen, “Analysis of coplanar waveguide-to-coplanar stripline transitions,” *IEEE Transactions on Microwave Theory and Techniques*, vol. 48, pp. 23–29, Jan 2000.
- [52] Shau-Gang Mao and Shiou-Li Chen, “Broadband series-fed printed dipole arrays with conductor-backed coplanar waveguide-to-coplanar stripline transitions,” in *2005 IEEE Antennas and Propagation Society International Symposium*, vol. 3A, pp. 565–568 vol. 3A, July 2005.
- [53] D. E. Anagnostou, M. Morton, J. Papapolymerou, and C. G. Christodoulou, “A 0–55-ghz coplanar waveguide to coplanar strip transition,” *IEEE Transactions on Microwave Theory and Techniques*, vol. 56, pp. 1–6, Jan 2008.

- [54] Yo-Shen Lin and Chun Hsiung Chen, “Lowpass lumped-element coplanar waveguide-tocoplanar stripline transitions,” in *Proceedings of the XXVI-Ith URSI General Assembly in New Delhi (October 2005)*, 2001.
- [55] P. J. Gibson, “The vivaldi aerial,” in *1979 9th European Microwave Conference*, pp. 101–105, Sep. 1979.
- [56] E. Gazit, “Improved design of the vivaldi antenna,” *IEE Proceedings H (Microwaves, Antennas and Propagation)*, vol. 135, pp. 89–92(3), April 1988.
- [57] J. D. S. Langley, P. S. Hall, and P. Newham, “Novel ultrawide-bandwidth vivaldi antenna with low crosspolarisation,” *Electronics Letters*, vol. 29, pp. 2004–2005, Nov 1993.
- [58] Z. Wang, Y. Yin, J. Wu, and R. Lian, “A miniaturized cpw-fed antipodal vivaldi antenna with enhanced radiation performance for wideband applications,” *IEEE Antennas and Wireless Propagation Letters*, vol. 15, pp. 16–19, 2016.
- [59] M. Amiri, F. Tofigh, A. Ghafoorzadeh-Yazdi, and M. Abolhasan, “Exponential antipodal vivaldi antenna with exponential dielectric lens,” *IEEE Antennas and Wireless Propagation Letters*, vol. 16, pp. 1792–1795, 2017.
- [60] S. Malakooti, M. Moosazadeh, D. C. Ranasinghe, and C. Fumeaux, “Antipodal vivaldi antenna for sum and difference radiation patterns with reduced grating lobes,” *IEEE Antennas and Wireless Propagation Letters*, vol. 16, pp. 3139–3142, 2017.
- [61] I. T. Nassar and T. M. Weller, “A novel method for improving antipodal vivaldi antenna performance,” *IEEE Transactions on Antennas and Propagation*, vol. 63, pp. 3321–3324, July 2015.
- [62] Y. Wang and Z. Yu, “A novel symmetric double-slot structure for antipodal vivaldi antenna to lower cross-polarization level,” *IEEE Transactions on Antennas and Propagation*, vol. 65, pp. 5599–5604, Oct 2017.

- [63] B. Biswas, R. Ghatak, and D. R. Poddar, “A fern fractal leaf inspired wideband antipodal vivaldi antenna for microwave imaging system,” *IEEE Transactions on Antennas and Propagation*, vol. 65, pp. 6126–6129, Nov 2017.
- [64] R. Natarajan, J. V. George, M. Kanagasabai, L. Lawrance, B. Moorthy, D. B. Rajendran, and M. G. Nabi Alsath, “Modified antipodal vivaldi antenna for ultra-wideband communications,” *IET Microwaves, Antennas Propagation*, vol. 10, no. 4, pp. 401–405, 2016.
- [65] R. Natarajan, M. Kanagasabai, and M. Gulam Nabi Alsath, “Dual mode antipodal vivaldi antenna,” *IET Microwaves, Antennas Propagation*, vol. 10, no. 15, pp. 1643–1647, 2016.
- [66] A. M. De Oliveira, M. B. Perotoni, S. T. Kofuji, and J. F. Justo, “A palm tree antipodal vivaldi antenna with exponential slot edge for improved radiation pattern,” *IEEE Antennas and Wireless Propagation Letters*, vol. 14, pp. 1334–1337, 2015.
- [67] R. Natarajan, J. V. George, M. Kanagasabai, and A. Kumar Shrivastav, “A compact antipodal vivaldi antenna for uwb applications,” *IEEE Antennas and Wireless Propagation Letters*, vol. 14, pp. 1557–1560, 2015.
- [68] G. K. Pandey, H. Verma, and M. K. Meshram, “Compact antipodal vivaldi antenna for uwb applications,” *Electronics Letters*, vol. 51, no. 4, pp. 308–310, 2015.
- [69] J. Bai, S. Shi, and D. W. Prather, “Modified compact antipodal vivaldi antenna for 4–50-ghz uwb application,” *IEEE Transactions on Microwave Theory and Techniques*, vol. 59, pp. 1051–1057, April 2011.
- [70] P. Fei, Y. Jiao, W. Hu, and F. Zhang, “A miniaturized antipodal vivaldi antenna with improved radiation characteristics,” *IEEE Antennas and Wireless Propagation Letters*, vol. 10, pp. 127–130, 2011.
- [71] A. Z. Hood, T. Karacolak, and E. Topsakal, “A small antipodal vivaldi antenna for ultrawide-band applications,” *IEEE Antennas and Wireless Propagation Letters*, vol. 7, pp. 656–660, 2008.

Chapter 3

Methodology

Contents

3.1	Guidelines for the Transition Design	45
3.2	Simulation	47
3.3	Prototyping	48
3.4	Measurements	49
3.5	Chapter Summary	56
	References	56

This chapter explains various aspects of planar waveguide transition design. It further explains the simulation, measurement and fabrication techniques of the transitions and its applications. CST Microwave Studio is used for all the simulations in the thesis. The measurement of scattering parameters, group delay of the transitions, measurement of gain and farfield radiation patterns of the antenna are also explained in this chapter.

3.1 Guidelines for the Transition Design

The transition design flow is given in Figure 3.1 [1, 2].

The transition design flow can be summarized as, first choosing a configuration (which ensures smooth electromagnetic (EM) field transition), method (EM coupling/via) and dielectric (substrate) according to the requirements. In the second stage line lengths and port impedances are calculated using

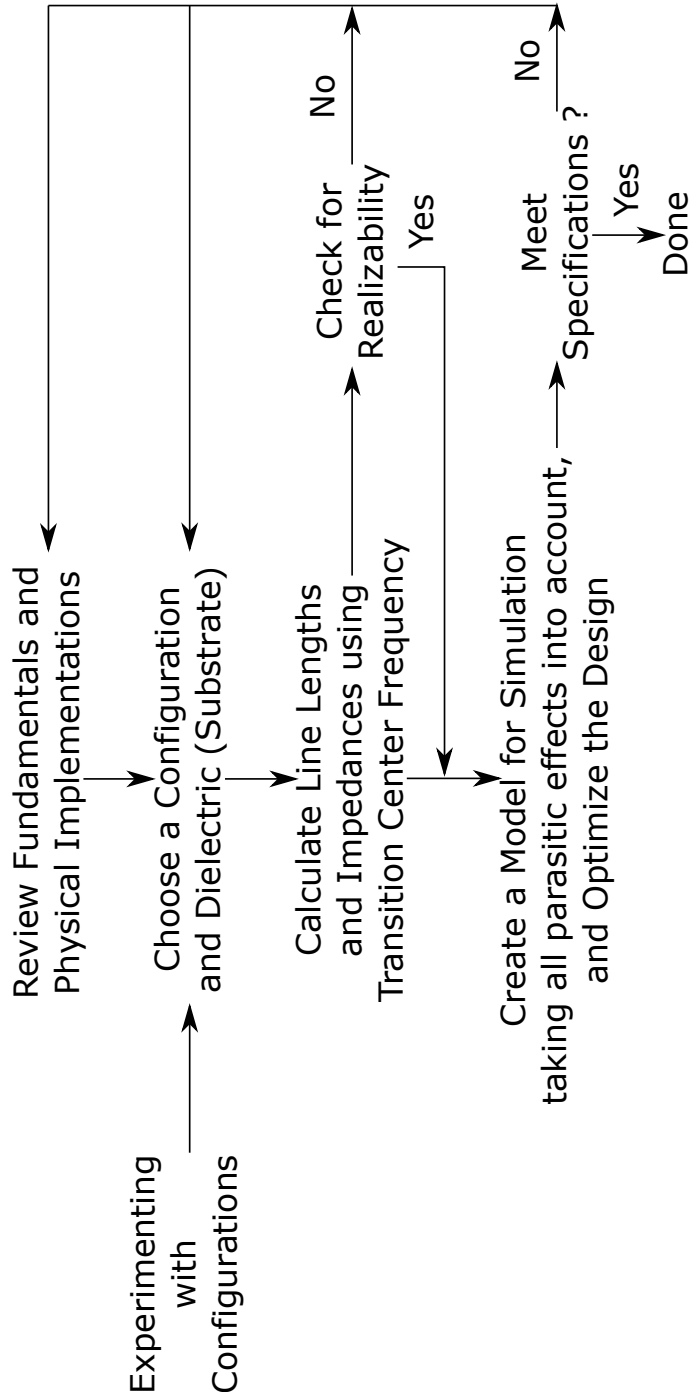


Figure 3.1: Design Flow for the Transition Fabrication.

approximate transition center frequency ensuring impedance matching and physical realizability. In final step a model for simulation taking all parasitic effects into account is created and parametrically optimized to meet the required specifications.

3.2 Simulation

EM simulator gives us an approximate solution to Maxwell's equations for a particular set of boundary conditions and initial conditions. Experimenting with virtual prototypes at the earliest stages of the design process, comparing the performances of different configurations and substrates, and optimization, all can be done using a three dimensional EM simulator.

The steps involved in the EM simulation is given below.

1. **Physical Model (Layout Geometry):** The layout geometry of the structure is drawn in this part. All materials are assigned properties from the standard library of material manufacturer's or from the custom made set.
2. **Simulation Environment:** Background and boundary conditions, port assignments, frequency range and solver preference is given in this stage. In solver settings, meshing accuracy, port impedances, parametric variations and sensitivity analysis can be controlled.
3. **Performing Simulation:** Meshing of the structure layout is done according to the settings in this section. The cells formed from meshing, are analyzed for field/current using different basis functions, whose weights are adjusted to meet the given boundary conditions.
4. **Post Processing:** The scattering parameters (magnitude and phase), group delay, return/insertion loss and radiation parameters like farfield radiation patterns, gain etc. are calculated in this part. Visualization and exporting of different parametrically varied results can also be done here.

CST Studio Suite[®]

CST Microwave Studio[®] (MWS) is a three dimensional EM analysis software package in CST Studio Suite[®]. It offers three most popular EM simulation solvers: method-of-moments (MoM) in the multilayer solver, finite element method (FEM) in frequency domain solver and finite difference time domain (FDTD) in time domain solver. The time domain solver could be best for wideband or planar antennas, the frequency domain solver may be more suitable for electrically small and narrowband antennas, while the multilayer solver can efficiently simulate 3D planar structures (stacked structures) with vertical geometry features like vias. Almost all parameters of the antenna including 3D and 2D radiation pattern, antenna gain, efficiency, scattering parameters and surface currents can be simulated using CST Microwave Studio[®]. CST MWS comprises of six different, high frequency solvers and for our studies, a multilayer (for transitions) and time-domain (antennas) solvers are used.

3.3 Prototyping

Photolithographic techniques were used to fabricate the transitions and antenna configurations on the selected substrate. Initially the substrates are chemically cleaned and a very thin film of photoresist is applied. Photoresists are of two types, positive and negative. For positive ones, exposure to the UV light changes the chemical structure of the resist so that it becomes more soluble in the developer solution, leaving windows of the bare underlying metallic region. But, the negative resist does the opposite, so that masks used for negative photo resist, must contain the inverse of the pattern to be metallized. After developing, the unwanted metallic portions are cleared using Ferric Chloride solution.

3.4 Measurements

In this thesis two kind of device measurements are done, transitions and antenna. Transitions are characterized by reflection and transmission parameters obtained from the scattering parameters. For antenna farfield radiation pattern and gain are measured.

Scattering Parameters

Scattering parameters as shown in Figure 3.2 and 3.3, are vector representation that show reflection and transmission characteristics (both amplitude and phase) in frequency domain.

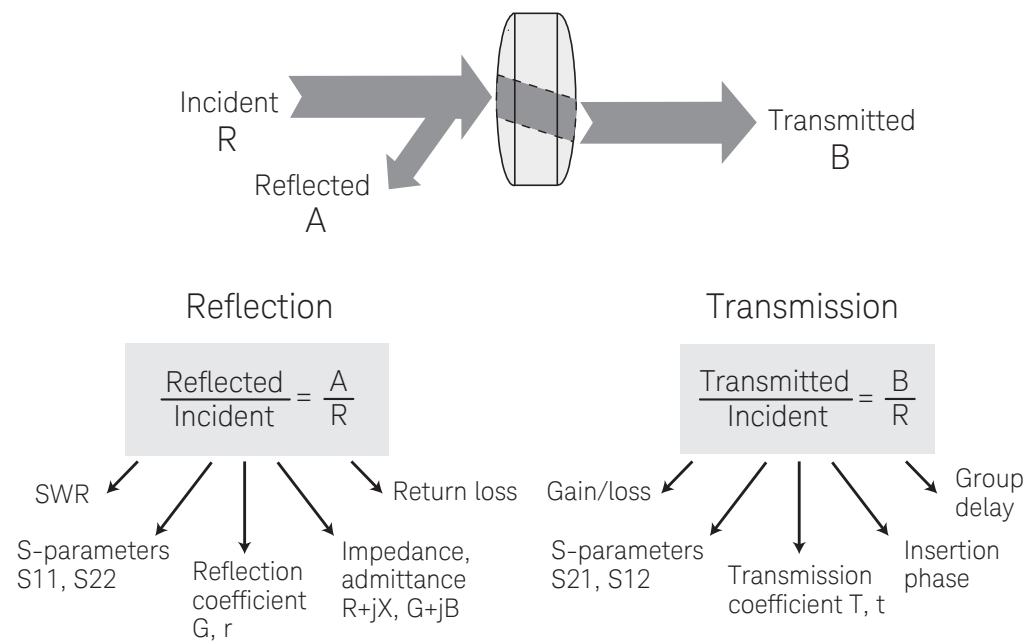


Figure 3.2: Reflection/Transmission parameters used for for high-frequency device characterization using lightwave analogy [3].

$$\begin{aligned} \text{Reflection/Input} &= \text{Reflection coefficient} \rightarrow S_{11}, S_{22} \\ \text{Transmission/Input} &= \text{Transmission coefficient} \rightarrow S_{21}, S_{12} \end{aligned}$$

Reflection parameters are

$$\text{Reflection coefficient} = \Gamma = \frac{V_{\text{reflected}}}{V_{\text{incident}}} = r \angle \Phi = \frac{Z_L - Z_0}{Z_L + Z_0}$$

$$\text{Return loss(dB)} = -20 \log(|\Gamma|).$$

Transmission parameters are

$$\text{Transmission coefficient} = T = \frac{V_{\text{Transmitted}}}{V_{\text{Incident}}} = \tau \angle \phi$$

$$\text{Insertion loss(dB)} = -20 \log \left| \frac{V_{\text{Trans}}}{V_{\text{Inc}}} \right| = -20 \log \tau.$$

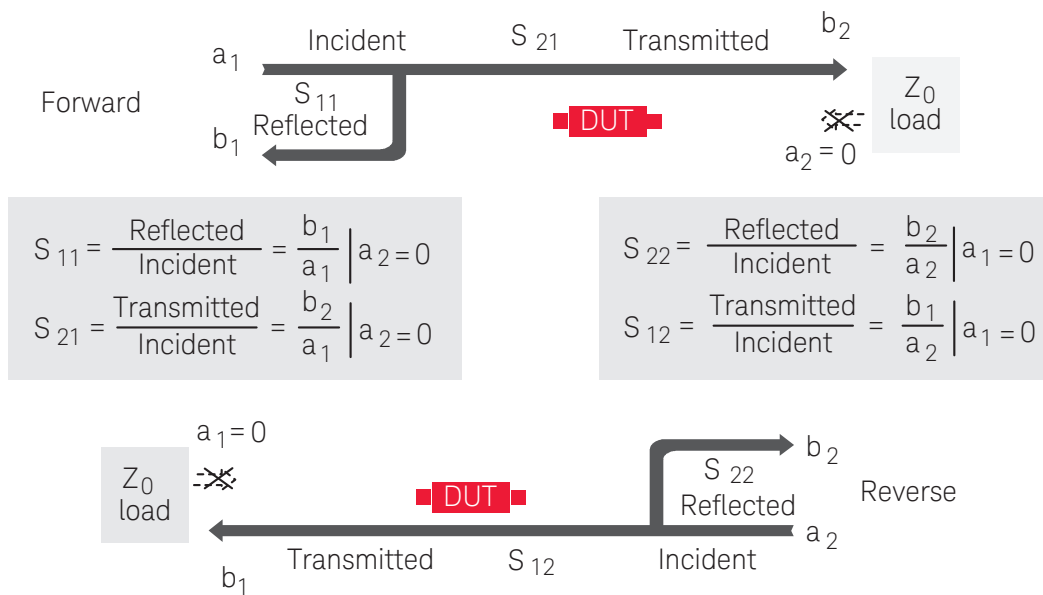


Figure 3.3: Measurement of scattering parameters [3].

Group Delay

Group delay is a measure of phase distortion, which can be calculated by differentiating the device's phase response versus frequency. Phase delay is not sufficient to describe the phase characteristics of such devices. An example

of group delay (transit time of a signal through a device versus frequency) calculation is shown in Figure 3.4.

Shift from constant group delay value indicates phase distortion and average group delay gives the transit time as shown in Figure 3.4.

$$\text{Group delay } (t_g) = -\frac{d\phi}{d\omega} = -\frac{1}{360^\circ} * \frac{d\phi}{df}.$$

where

ϕ in radians, ω in radians/sec, ϕ in degrees and f in Hz ($\omega = 2\pi f$).

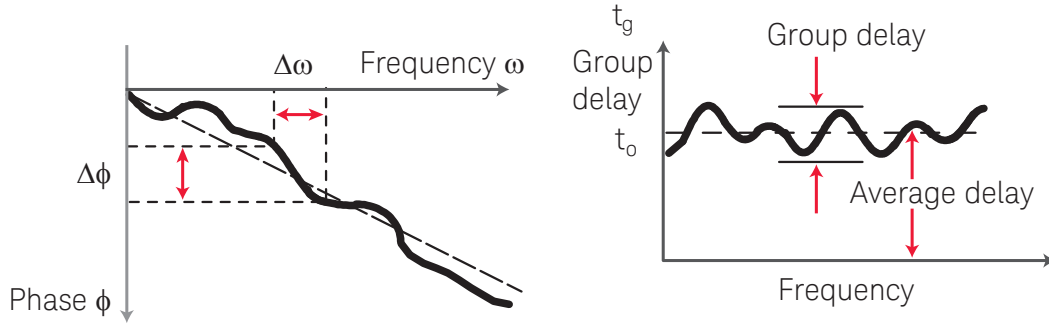


Figure 3.4: Group delay calculation [3].

The CST Microwave Studio[®] calculates group delay by performing a finite difference of the measured phase values of S_{21} to obtain $-d\phi/d\omega$ to calculate the group delay. The average value of the measured group delays at all frequency points is the transit time of the device otherwise known as average delay as shown in Figure 3.4.

Vector Network Analyzer (VNA)

A VNA can be used to measure magnitude and phase of all reflection and transmission parameters of a device under test, whose simplified block diagram is given in Figure 3.4. It can be employed for the measurement of antenna parameters including return loss characteristics, radiation pattern and gain. Two VNAs are used for measurement in this thesis, Keysight Fieldfox N9927A handheld network analyzer (30 kHz to 20 GHz) and Agilent Technologies E8362B network analyzer (10 MHz to 20 GHz).

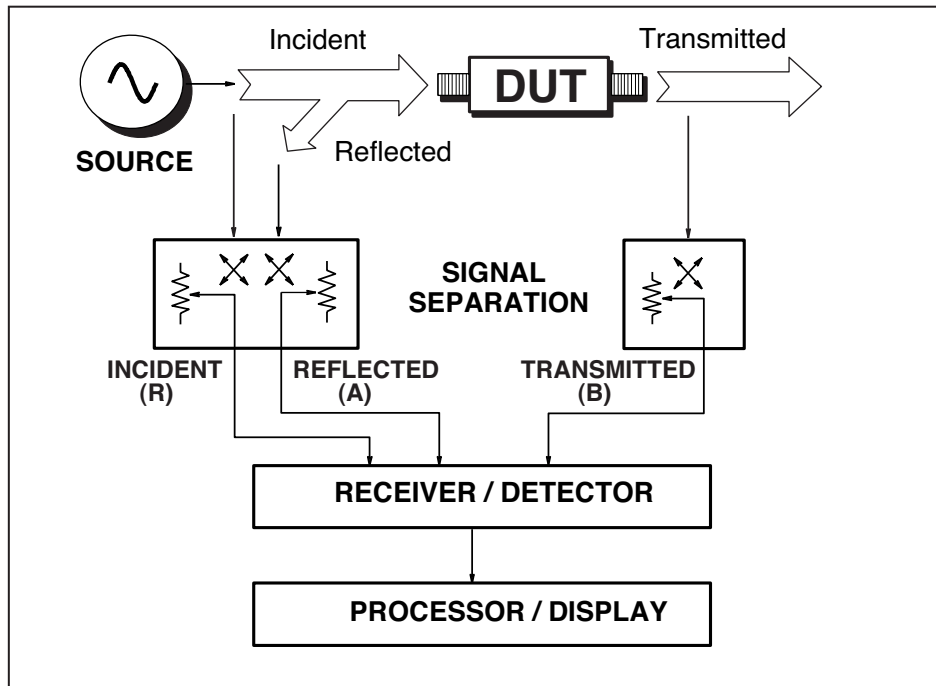


Figure 3.5: VNA block diagram [4].

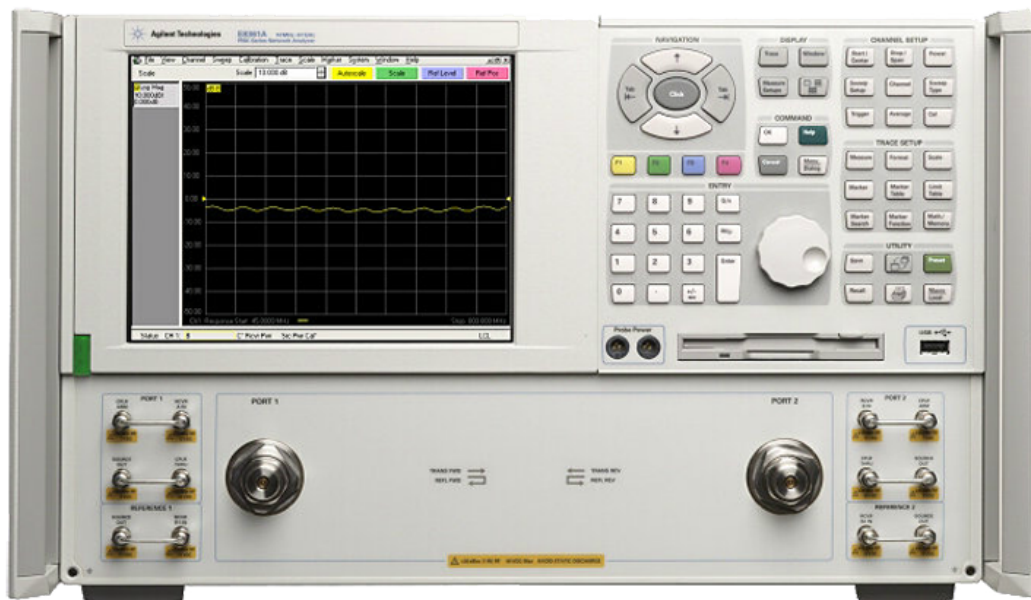


Figure 3.6: Agilent Technologies E8362B VNA (10 MHz to 20 GHz)



Figure 3.7: Keysight Fieldfox N9927A handheld VNA (30 kHz to 20 GHz)

Anechoic Chamber and Turn Table Assembly

In an anechoic chamber all the side walls, roof and the floor are covered with RF absorbers. These are having a reflection coefficient of around -40 dB in the MHz frequency region, whose performance will be much better at higher frequencies. A actual photograph of the anechoic chamber and turn table assembly is shown in Figure 3.8. The absorbering materials are of tapered to achieve good impedance matching. In order to prevent electromagnetic interferences from outside world, the chamber is built into a screened room with continuous covering of highly conductive material.



Figure 3.8: Anechoic chamber and turn table assembly.

Radiation pattern measurements are done with the antenna under test is paced on a turn table rotated by a stepper motor, whose rotation is controlled using software. A standard wideband horn is used to receive signals from the antenna under test.

Antenna Parameters: Return Loss and Bandwidth

After connecting the sufficiently long cable for VNA measurement, the calibration for the required frequency range has to be done. The S parameter corresponding to reflection characteristics (S_{11}) is measured. Bandwidth is defined as the range for which, return loss better than 10 dB. At resonances the S_{11} will be minimum.

Antenna Parameters: Radiation Pattern

An anechoic chamber is used for the farfield radiation pattern measurement. The antenna which is to be tested is mounted on a turn table controlled by computer software. At receiving end, a standard wide range horn is used. After calibration, the turn table is rotated and the measurement is taken using the VNA, which is stored and processed in a computer.

Antenna Parameters: Gain

Gain measurement is done using a gain transfer method [5, 6], in which the gain of the antenna under test is measured relative to another antenna whose gain is already available from the manufacturer. The antennas have to be tripod mounted with a minimum distance ensuring farfield separation. The reference antenna, whose gain is accurately known is aligned in the direction of maximum intensity with the other. In the calibrated VNA frequency range is selected and the normalization is done. Normalization will ensure $S_{21} = 0$ dB for the required frequency range. The next step is to replace the reference antenna with antenna to be tested. The value S_{21} represents the gain of the antenna relative to reference antenna. The total gain of the antenna under

test is obtained by adding recorded value of S_{21} of the antenna with the gain of the reference antenna at every frequency point.

3.5 Chapter Summary

This chapter explains the procedure for the planar waveguide transition design. It explains the tools and methodologies used for the simulation, measurement and fabrication of the transitions and antenna used in the thesis. CST Microwave Studio is used for all the simulations in the thesis. The measurement of scattering parameters and group delay of the transitions and measurement of gain and farfield radiation patterns of the antenna are explained in this chapter.

References

- [1] D. M. Pozar, *Microwave Engineering; 4th Edition*. Wiley, 2011.
- [2] B. C. Wadell, *Transmission Line Design Handbook*. Artech House, 1991.
- [3] Keysight Technologies, *Understanding the Fundamental Principles of Vector Network Analysis*, 2018. Application Note.
- [4] Keysight Technologies, *Exploring the Architectures of Network Analyzers*, 2018. Application Note.
- [5] C. A. Balanis, *Antenna Theory: Analysis and Design*. John Wiley and sons Inc., 2016.
- [6] J. D. Kraus and R. J. Marhefka, *Antennas*. McGrawHill Education, 2001.

Chapter 4

CPW to DSPSL Transitions

Contents

4.1 CPW to DSPSL Vertical Transitions with Via . . .	58
4.1.1 Transition Geometry and its Design	58
4.1.2 Simulation Studies	66
4.1.3 Equivalent Circuit	72
4.1.4 Measured Results	75
4.2 CPW to DSPSL Transition without Via	84
4.2.1 Transition Geometry and its Design	84
4.2.2 Simulation Studies	86
4.2.3 Equivalent Circuit	90
4.2.4 Measured Results	92
4.3 Chapter Summary	95
References	95

In this chapter, Two types (A and B) of broadband coplanar waveguide (CPW) to double-sided parallel-strip line (DSPSL) vertical transitions with a single via are presented in the first section. The transitions are composed of CPW open end with connected grounds forming the two strips of the DSPSL with single via connection. In the second section, a via-less CPW to DSPSL transition using electromagnetic (EM) coupling between the radial stub and delta stub is given. Simplified equivalent circuits for all transitions are also introduced.

4.1 CPW to DSPSL Vertical Transitions with Via

Vertical transitions are crucial components in double-layer microwave circuits to avoid the use of crossovers. DSPSL, also known as broadside coupled stripline (BCS) is a balanced transmission line, with wide range of characteristic impedances, differential signalling and simpler transition structures [1–5]. However, vertical transitions between DSPSL and CPW have been reported very little in literature. Back to back vertical transitions of DSPSL in direct and inverted forms are capable of achieving signal/phase inversion, resulting in microwave applications such as mixers, ring couplers, etc. Traditionally, vertical transitions will either use low-pass natured via connection or band-pass natured slot/cavity coupling.

Due to the wide popularity of CPW probe pads, various wideband transitions between CPW and DSPSL are proposed in recent years [6–16]. Furthermore, majority of them are built on high dielectric-constant substrates for attaining low characteristic impedances thereby easy matching to 50 Ω lines. But they are suitable for circuit design instead, using such transitions to feed antennas, will degrade the antenna performance [4]. The optimization of planar transitions using different techniques are already reported [5, 10].

In this work, a vertical broadband 50 Ω DSPSL to 50 Ω CPW transition is proposed for the first time. A simplified equivalent circuit revealing the basic low pass nature is introduced. The back-to-back transitions in 1.524 mm thickness Rogers RO4003C substrate, yield return and isolation losses better than 14.5 dB and 2.5 dB respectively, from DC to 11.5 GHz and for 1.6 mm thickness FR4 substrate, the return and insertion losses better than 15.0 dB and 4.0 dB respectively, from DC to 11.0 GHz. It has an optimized structure with a single via, which can be easily fabricated.

4.1.1 Transition Geometry and its Design

The DSPSL is two identical metal strips separated by a dielectric slab. It possesses a wide range of characteristic impedance, which validates the feasibility

in constructing new high performance microwave circuits and integrating with other microwave circuits/components without any impedance transformer. As per image theory, the middle plane of the dielectric slab is a virtual ground plane to form identical microstrip lines with half the substrate thickness ($h/2$) as shown in Figure 4.1. The relationship of the characteristic impedances between them is

$$(Z_0)_{dspsl} = 2 * (Z_0)_{microstrip}$$

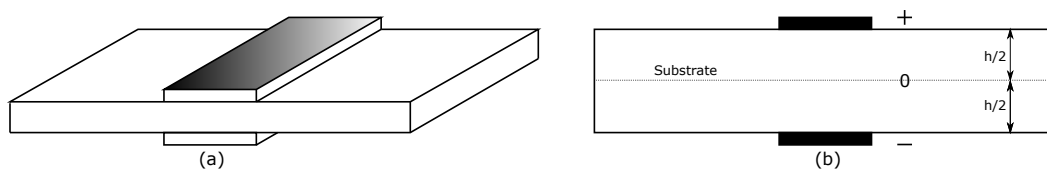


Figure 4.1: Double-sided parallel-strip line, (a) three dimensional view, (b) cross sectional view

For the unbalanced transmission lines such as microstrip line and CPW, much high impedance is not available due to the fabrication limitation. On the other hand, for the CPS and slot line, much low impedance is not available due to the small capacitance between their two strips. Like the microstrip line, the strip width is the key factor in controlling the characteristic impedance of the DSPSL also. However, offsetted top and bottom lines of the DSPSL, results in higher impedances. According to [3–5, 15–17], it finds applications in filters, rat-race hybrid couplers, power dividers and antenna feeds etc. for the frequencies ranging upto 30 GHz.

The geometrical layouts of the transitions between 50Ω CPW to 50Ω DSPSL are shown in Figure 4.2 and 4.4. To design a good transition between transmission lines gradual change in electromagnetic(EM) fields and impedance matching are required. Since realization of different characteristic impedance values of DSPSL is comparatively easier, in these designs only smooth transition of EM field from CPW mode to DSPSL mode is considered to avoid any abrupt discontinuities. However, to obtain field matching, parallel electric field of CPW is to be rotated 90° to become the vertical electric field of DSPSL. The equal magnitude currents flowing in the DSPSL conductors show 180° out of phase nature. On the other hand, due to the presence

of two ground lines in CPW, the center strip carries double the value of their individual current magnitude.

The currents of top strip line of DSPSL and ground lines of CPW have identical directions in the proposed vertical transition structure. The top strip of DSPSL is formed from the connected grounds of CPW which takes a 'Y'-shape in Type A and semi ring shape in Type B transitions respectively. The center conductor of CPW has to be connected to the bottom strip of DSPSL, and two methods can be used for this, one is using EM coupling between them, and the other is a single via connecting them directly. We choose the latter for our design because of the enhanced bandwidth (zero frequency onwards), simpler structure and compact size, since EM coupling requires comparatively large structures and low bandwidth.

Multilayer solver (Frequency domain) of CST Microwave Studio (3D planar electromagnetic solver based on MoM) is used for the parametric studies and optimization. The transitions are printed on two similar substrates, Roger's RO4003C ($\epsilon_r=3.55$ and $h=1.524$ mm) and FR4 ($\epsilon_r=4.3$ and $h=1.6$ mm). The dimensions of 50 Ω CPW is determined by CST Microwave Studio utility with the center strip width as $W_1=4.0$ mm, and the gap width as $G_1=0.35$ mm for both cases. Using image theory, the strip width of the 50 Ω DSPSL can be calculated as $W_2=4.4$ mm.

4.1.1.1 Type A

CPW grounds are connected together to form a y junction with the top metal of DSPSL as one arm, just like a power combiner circuit as shown in Figure 4.2(b). The thickness of the junction is 4 mm. The transition length is designed as approximately $\lambda/4$ at the center frequency ($L_3=7.4$ mm). The CPW center strip and the DSPSL bottom metal are circularly terminated to form the via pads with radius equal to half their width ($R_2=2$ mm). In Figure 4.2(c) after via connection ($R_1=0.75$ mm) the width of the bottom metal strip is gradually increased for a length ($L_3=7.4$ mm), to match the width of DSPSL ($W_3=4.4$ mm). Schematic layout, top view and bottom view of the proposed Type A transition is given in Figure 4.2.

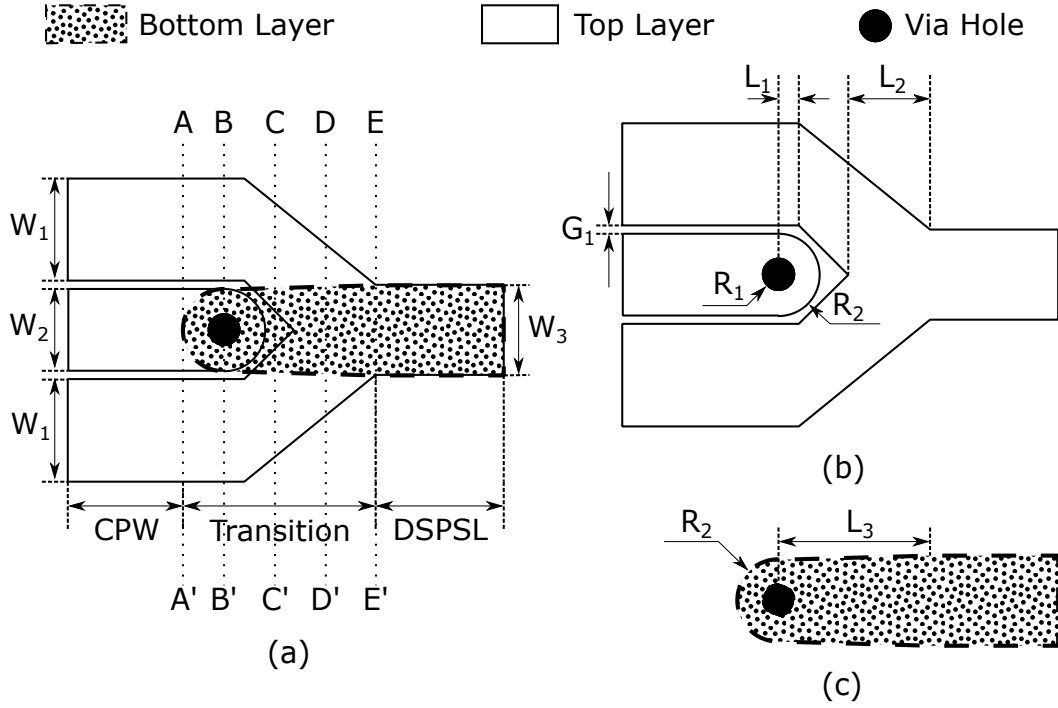


Figure 4.2: Configuration of the proposed Type A transition: (a) schematic layout, (b) top view, (c) bottom view. ($W_1=5$ mm, $W_2=4$ mm, $W_3=4.4$ mm, $G_1=0.35$ mm, $L_1=1$ mm, $L_2=2.4$ mm, $L_3=7.4$ mm, $R_1=0.75$ mm, $R_2=2$ mm)

The electric fields of both DSPSL and CPW have different characteristics. One is an unbalanced transmission line (CPW) and the other one is a balanced transmission line (DSPSL). The proposed transition rotates their electric field by 90° . The CPW has electric fields between the center strip and grounds in both sides. On the other hand DSPSL has vertical fields between the conductors.

Cross sectional electric field at AA' shows the CPW mode, which is having horizontal field distribution, and the vertical field distribution at EE' shows the DSPSL mode in Figure 4.3. At BB' the field is distributed vertically and horizontally between the radial stubs and the delta stubs. CC' is having the same field pattern with slight change in the size of the center strip and stubs. At DD' the horizontal to vertical transformation is almost complete, but still the bottom conductor is Y-shaped. The cross section at EE' completes the electric field transformation to DSPSL mode.

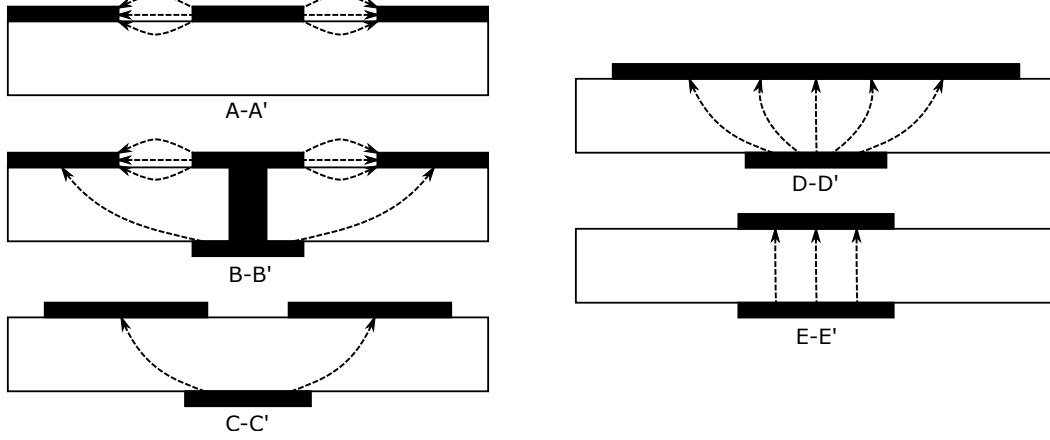


Figure 4.3: Cross-sectional views of proposed transition (Type A) and electric field distributions: (a) AA'- CPW mode, (b) EE' - DSPSL mode, (c) BB',CC',DD' - Transition modes.

4.1.1.2 Type B

As shown in Figure 4.4(b), ground conductors are circularly tapered with inner radius ($R_3=2.35$ mm) and outer radius ($R_4=7.35$ mm) to form the top metal of DSPSL. The rest of the design is exactly same as the Type A. Total transition length is ($L_4=7.35$ mm). Schematic layout, top view and bottom view of the proposed Type B transition is given in Figure 4.4.

CPW is an unbalanced transmission line and the DSPSL is a balanced transmission line. The proposed transition rotates their electric field by 90° . The CPW has electric fields between the center strip and grounds in both sides. On the other hand DSPSL has vertical fields between the conductors. Cross sectional electric field at AA' shows the CPW mode, which is having horizontal field distribution, and the vertical field distribution at EE' shows the DSPSL mode in Figure 4.5. At BB' the field is distributed vertically and horizontally between the radial stubs and the delta stubs. CC' is having the same field pattern with slight change in the size of the center strip and stubs. At DD' the horizontal to vertical transformation is almost complete, but still the bottom conductor is Y-shaped. The cross section at EE' completes the electric field transformation to DSPSL mode.

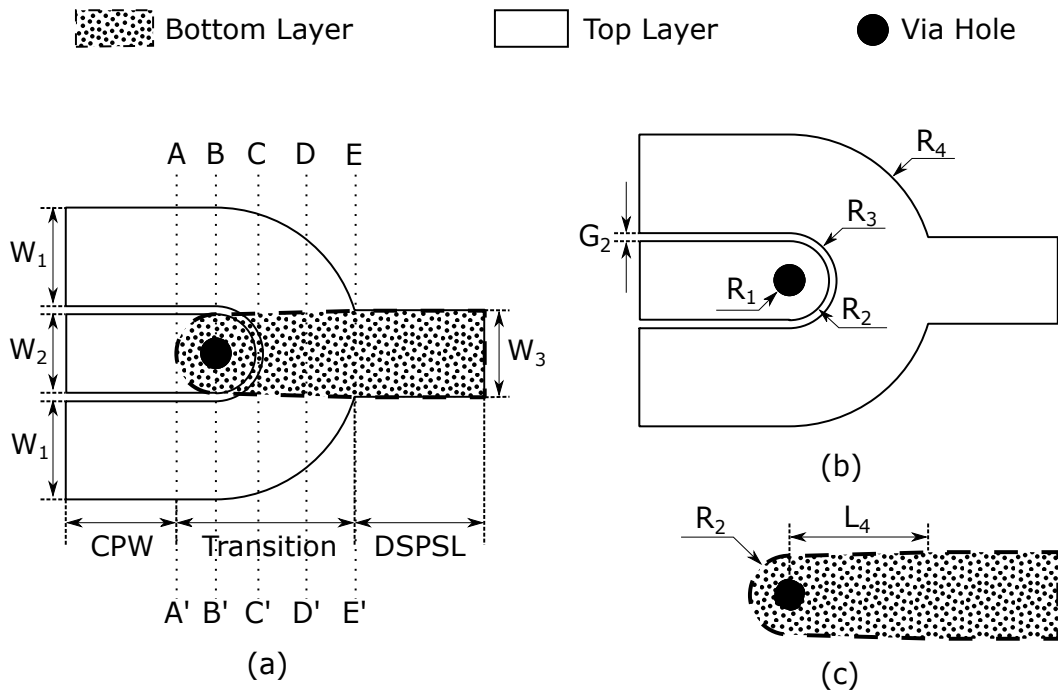


Figure 4.4: Configuration of the proposed Type B transition: (a) schematic layout, (b) top view, (c) bottom view. ($W_1=5$ mm, $W_2=4$ mm, $W_3=4.4$ mm, $G_2=0.35$ mm, $L_4=7.35$ mm, $R_1=0.75$ mm, $R_2=2$ mm, $R_3=2.35$ mm, $R_4=7.35$ mm)

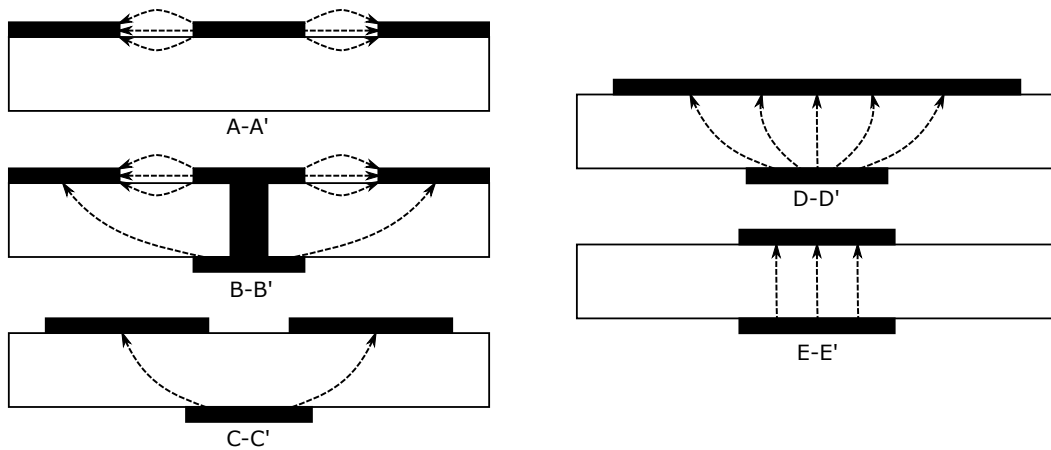


Figure 4.5: Cross-sectional views of proposed transition (Type B) and electric field distributions: (a) AA' - CPW mode, (b) EE' - DSPSL mode, (c) BB', CC', DD' - Transition modes.

4.1.1.3 CPW Open End with Connected Grounds

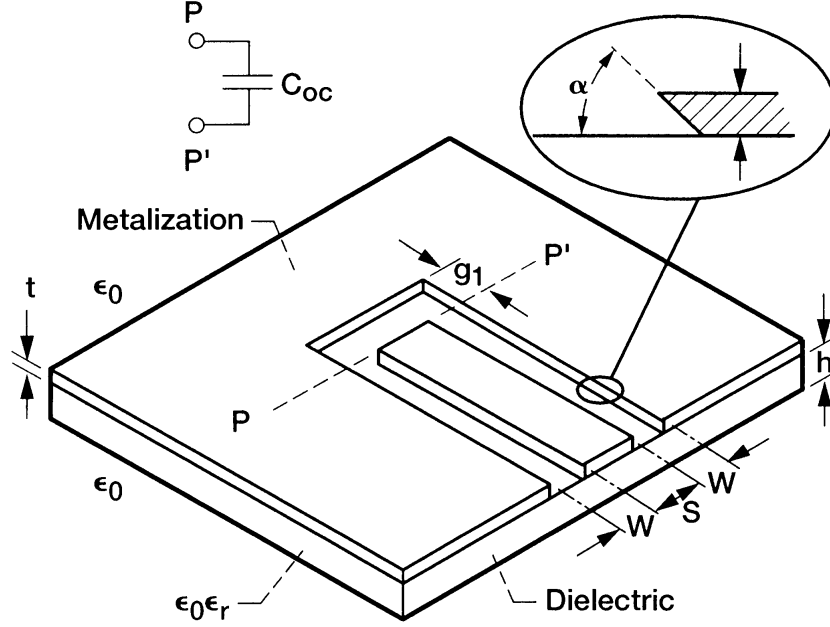


Figure 4.6: Coplanar waveguide open circuit with connected grounds. [18]

The CPW open circuit with connected grounds is shown in Figure 4.6. The electric field between the terminated center conductor and connected grounds results in reactance with capacitive nature. This reactance is the parallel combination of capacitance due to fringing fields in both the termination gap (g_1) and CPW slot (W). CPW slot capacitance is constant and other one is inversely proportional to the gap width.

The per unit length capacitance (ideal, lossless case) as per [18], is approximately

$$C = \frac{\beta}{\omega Z_0} \quad (4.1)$$

where the phase constant (β) and other variables are given by

$$\beta = \frac{2\pi f}{c} \sqrt{\epsilon_{\text{eff}}}$$

$$\omega = 2\pi f$$

ϵ_{eff} = CPW effective dielectric constant

f = frequency in Hz

c = velocity of light in free space in meters/second

Z_0 = CPW characteristic impedance

4.1.1.4 Via

In vertical transitions whenever signal has to change layers via can be used. Vias are made using either wires or by drilling and plating by an eyelet (plated through hole). There are three different cases commonly encountered for the plated-through hole or via. First, the via is used in series with the signal line when changing layers. Second, the via can be used to connect surface mount components to a ground plane on another layer and finally, vias are used to tie together ground planes on different layers. When the via is in series with the signal path, it is better to have the same characteristic impedance as the transmission lines, it is interconnecting. When it is used for grounding, it has to be as low an impedance as possible.

The simplest model for vias is simply a round wire or cylindrical wire inductor. As frequency increases, the model may need to include resistance and inductance caused by current restriction at the transition from the planar line to the via, radiation losses, and stray capacitances to nearby ground planes and across the via. As might be suspected, the via is found to radiate more than an equivalent length microstrip trace. The via model is made up of a series inductor shunted by a capacitance. Some of the capacitance is due to the open ends on the outer layers. Inner layer ground planes create a capacitance to ground along the inductor. It may be possible to minimize any discontinuity (over some bandwidth) by equating these to the distributed inductance and capacitance of a transmission line with the desired characteristic impedance.

4.1.2 Simulation Studies

Simulation studies of Type A (Y-shaped connected grounds) and Type B (round connected grounds) CPW to DSPSL transition is done on a back to back configurations. This configuration has planar signal feeds at both ends (CPWs) as shown in Figures 4.7 and 4.12. The CPW center strip width and the gap is adjusted so that the 50Ω characteristic impedance is assured. The metalization widths and gaps are chosen such that the etching can be done easily. The 50Ω terminations ensure proper matching with 50Ω testing ports of the simulator and the vector network analyzer. The transitions are printed on two similar substrates, Roger's RO4003C ($\epsilon_r=3.55$ and $h=1.524$ mm) and FR4 ($\epsilon_r=4.3$ and $h=1.6$ mm).

The three dimensional electromagnetic solver used in CST Microwave Studio for analyzing and modeling planar devices is the Multilayer solver. This Method of Moments (MoM) based solver have automatic system for de-embedding of ports, generation of layer stacks from the three dimensional model and edge mesh refinement. Design of planar filters, antennas and feeding networks are typical applications of this solver.

4.1.2.1 Type A

The simulation studies on various sensitive parameters of Type A transition on the substrate Roger's RO4003C ($\epsilon_r=3.55$ and $h=1.524$ mm), is done to optimize the geometric configuration. For this transition, the Y-connected ground junction thickness (L_3), the CPW length offset distances (L_1), the via radius (R_1) and the CPW ground width (W_1) are the parametrically analyzed.

Table 4.1: Geometrical parameters of the proposed transition (Type A) (in mm).

Parameter	W_1	W_2	W_3	G_1	R_1	R_2	R_3	R_4	
Value	5	4	4.4	0.35	0.75	2	2.35	7.35	
Parameter	L_1	L_2	L_3	L_4	L_5	L_6	L_7	L_8	L_9
Value	1	2.4	4	8.6	6.24	7.6	6.24	7.4	7.4

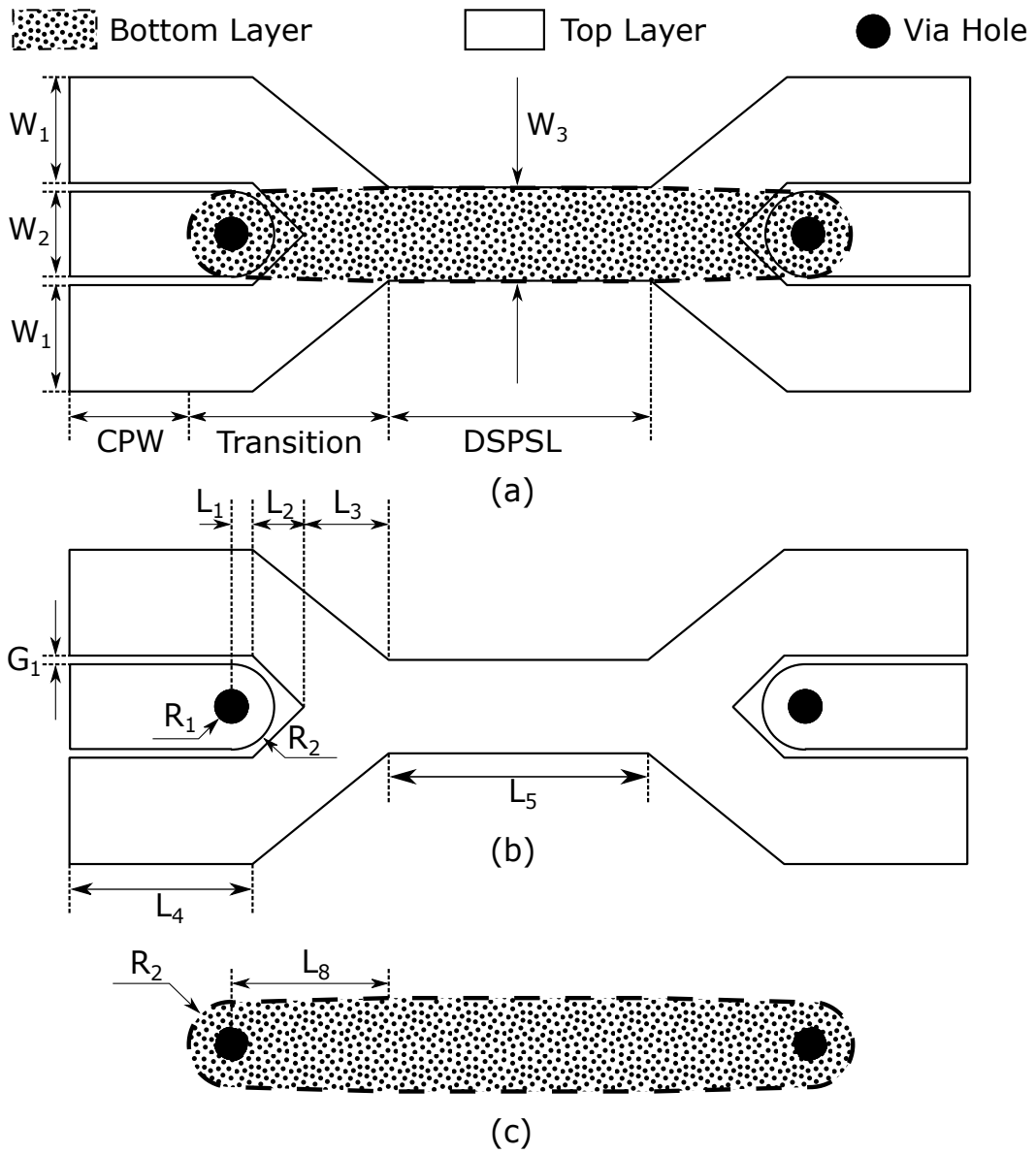


Figure 4.7: Configuration of the back-to-back transitions (Type A): (a) schematic layout, (b) top view and (c) bottom view.

Geometrical parameters of the proposed transition (Type A) is given in Table 4.1. Simulation studies of the Y-connected ground junction thickness (L_3), the CPW length offset distances (L_1), the via radius (R_1) and the CPW ground width (W_1) are shown in Figures 4.8, 4.9, 4.10 and 4.11.

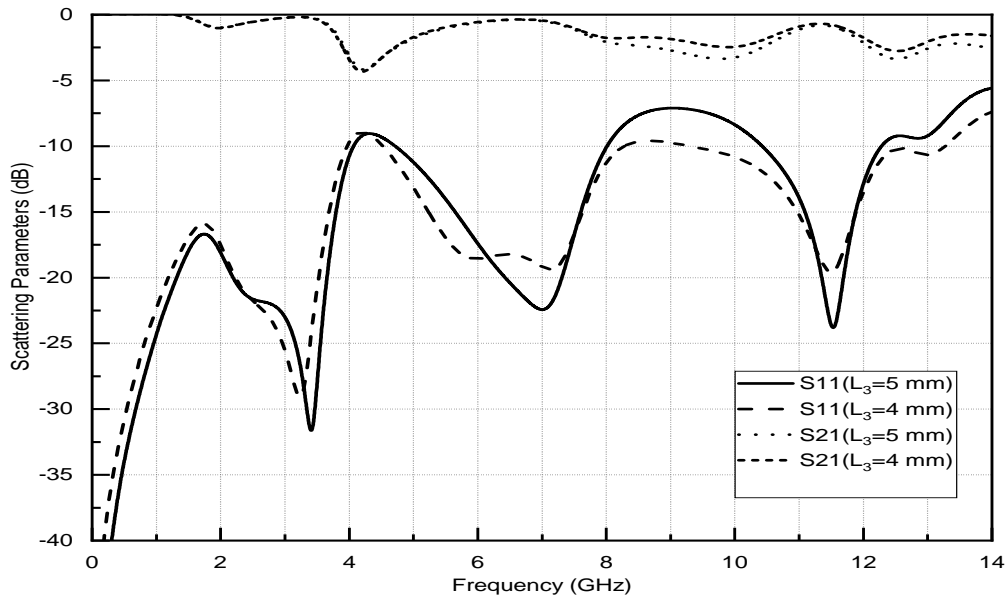


Figure 4.8: Simulated scattering parameters of the back-to-back transitions (Type A) against frequency with different Y-junction thicknesses (L_3).

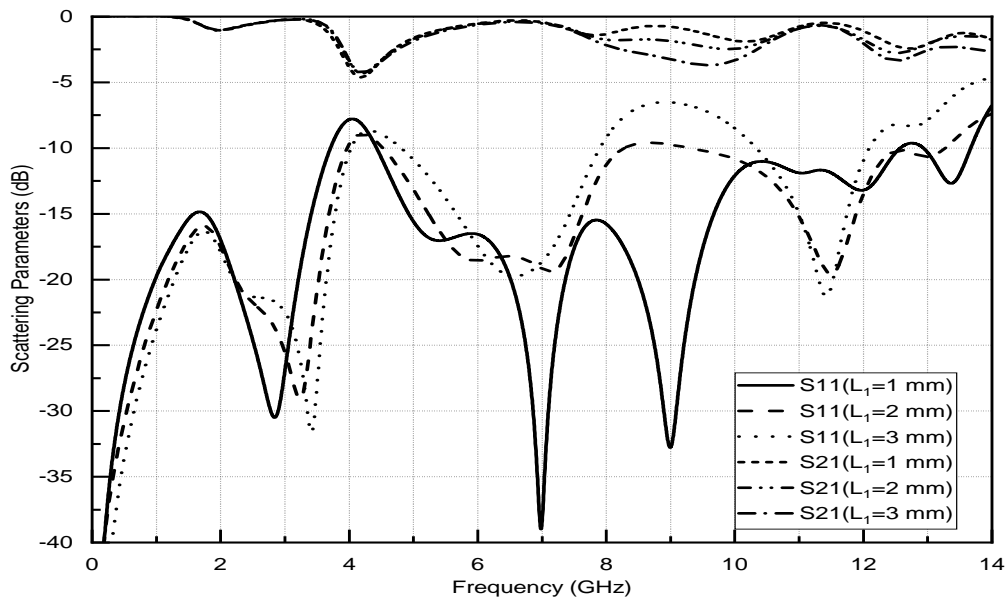


Figure 4.9: Simulated scattering parameters of the back-to-back transitions (Type A) against frequency with different CPW length offset distances (L_1).

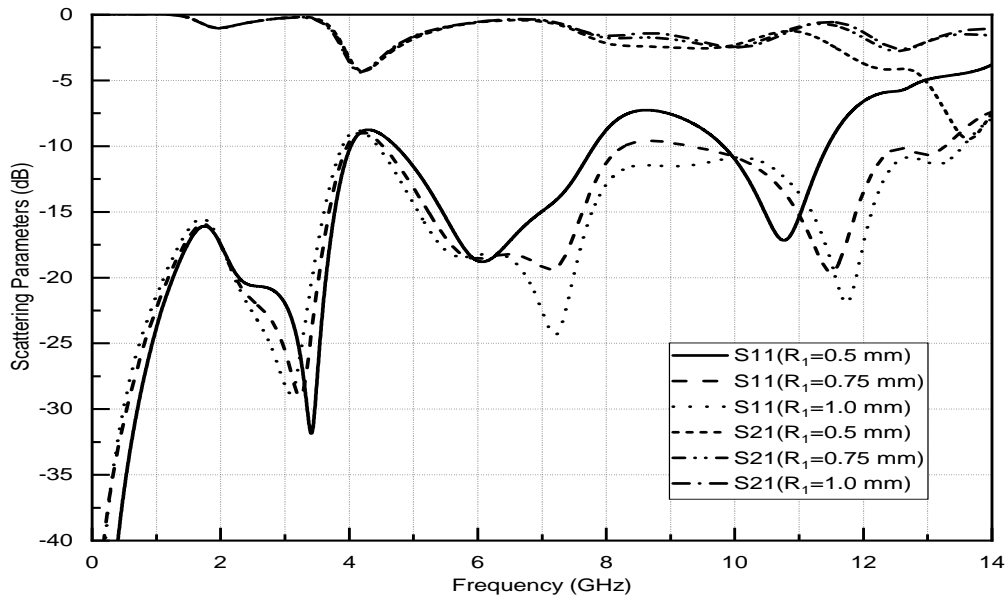


Figure 4.10: Simulated scattering parameters of the back-to-back transitions (Type A) against frequency with different layer interconnecting via radii (R_1).

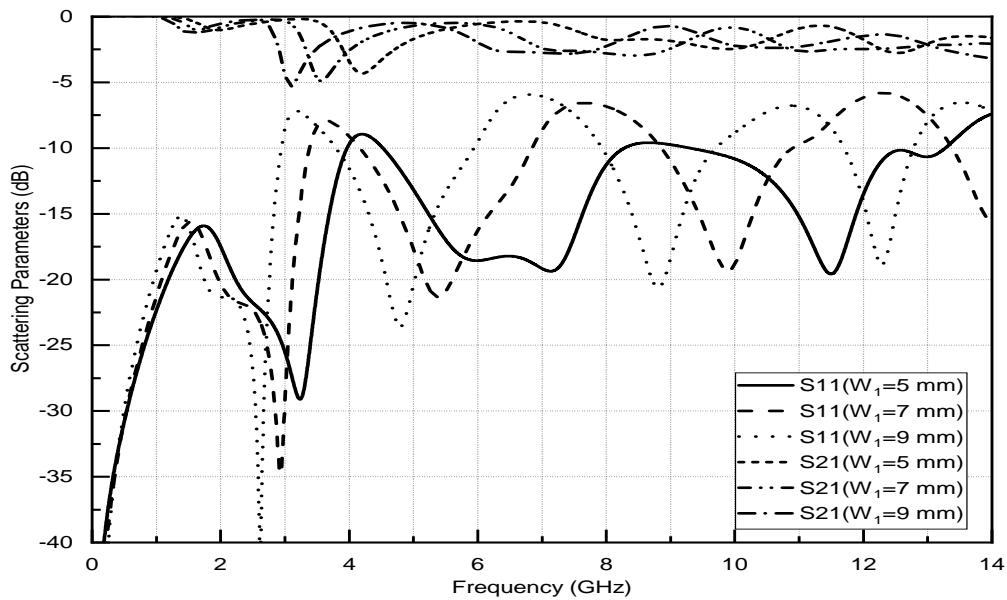


Figure 4.11: Simulated scattering parameters of the back-to-back transitions (Type A) against frequency with different CPW ground widths (W_1).

4.1.2.2 Type B

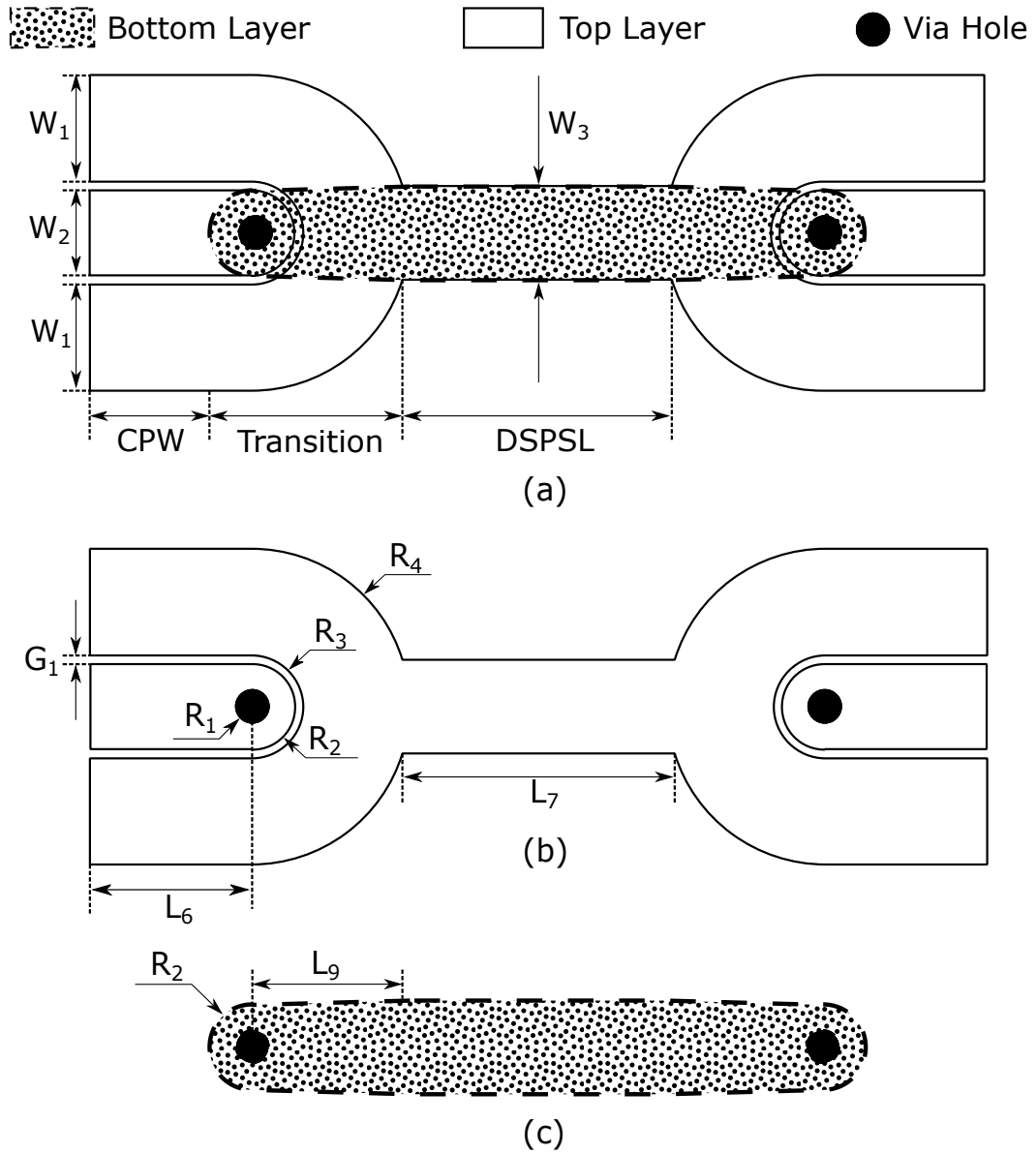


Figure 4.12: Configuration of the back-to-back transitions (Type B): (a) schematic layout, (b) top view and (c) bottom view.

Geometrical parameters of the proposed transition (Type B) is given in Table 4.2.

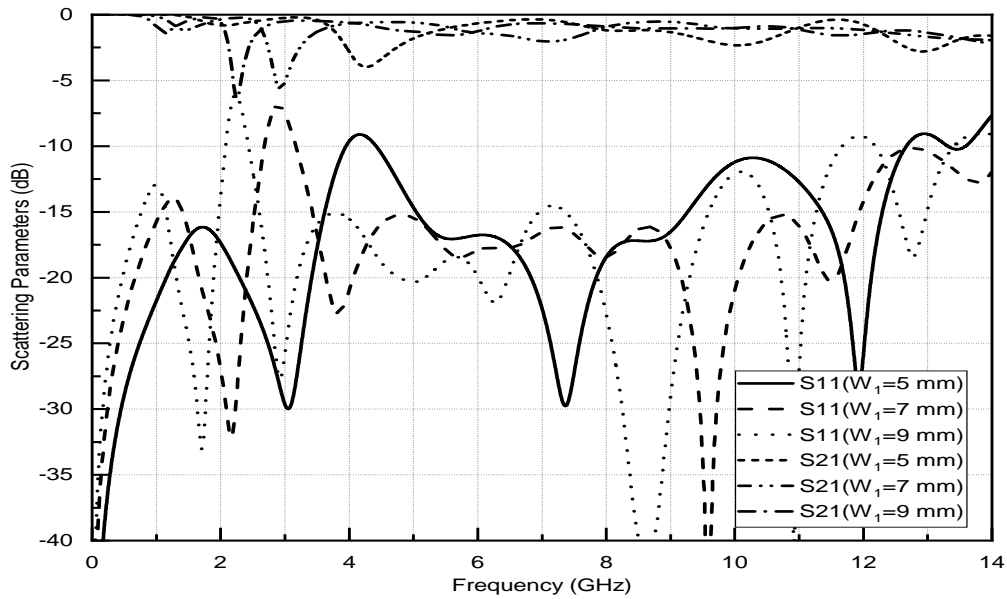


Figure 4.13: Simulated scattering parameters of the back-to-back transitions (Type B) against frequency with different CPW ground widths (W_1).

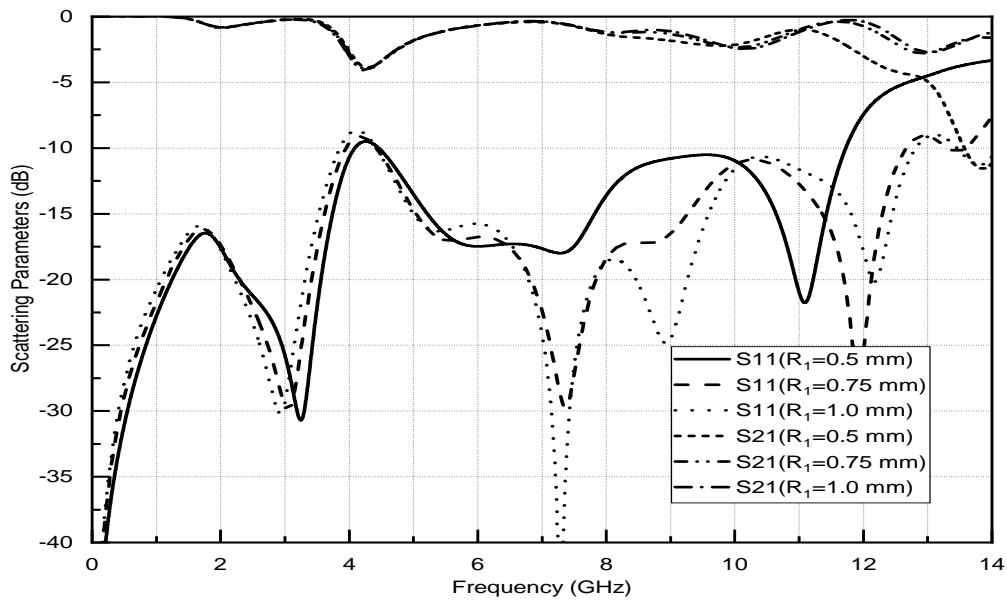


Figure 4.14: Simulated scattering parameters of the back-to-back transitions (Type B) against frequency with different layer interconnecting via radii (R_1).

Table 4.2: Geometrical parameters of the proposed transition (Type B) (in mm).

Parameter	W_1	W_2	W_3	G_1	R_1	R_2	R_3	R_4	
Value	5	4	4.4	0.35	0.75	2	2.35	7.35	
Parameter	L_1	L_2	L_3	L_4	L_5	L_6	L_7	L_8	L_9
Value	1	2.4	4	8.6	6.24	7.6	6.24	7.4	7.4

For the Type B transition on the substrate Roger’s RO4003C ($\epsilon_r=3.55$ and $h=1.524$ mm), the via radius (R_1) and the CPW ground width (W_1) are the sensitive parameters used for the simulation studies and optimization as shown in Figures 4.13 and 4.14.

4.1.3 Equivalent Circuit

4.1.3.1 CPW Open End with Connected Grounds

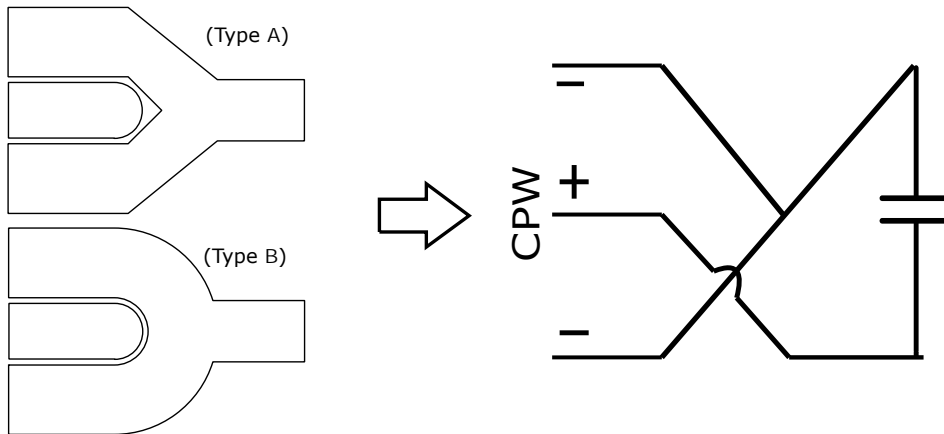


Figure 4.15: Simplified equivalent circuit of CPW with connected grounds.

The CPW open circuit with connected grounds is shown in Figure 4.15, [18]. The electric field between the terminated center conductor and connected grounds results in reactance with capacitive nature. This reactance is the

parallel combination of capacitance due to fringing fields in both the termination gap and CPW slot.

4.1.3.2 Via

A via is used in series with the signal line whenever we wish a signal to change layers in a two sided or multilayer circuit. Simplified equivalent circuit of via will approximately characterize its electrical response. It will be practical enough for developmental and understanding purposes, but accurate responses will have limited bandwidth. The via structure basically involves an upper pad, via cylinder and lower pad [19]. The lower frequency response of the via, tend to look capacitive (low impedance). At higher frequencies, the upper and lower pads of the via remain capacitive, but the cylindrical part will become more inductive in nature (high impedance). An approximate equivalent circuit which excludes coupling effects, for determining the response of the transition is given in the Figure 4.16.

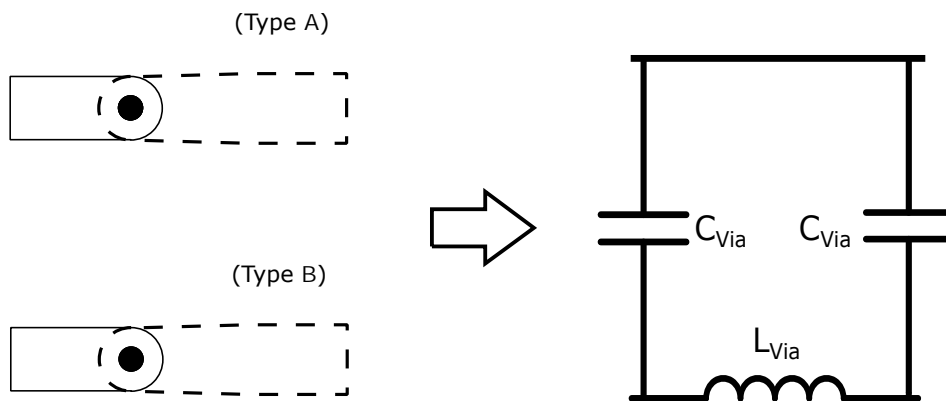


Figure 4.16: Simplified equivalent circuit of via (Lumped).

4.1.3.3 Simplified Equivalent Circuit

The equivalent circuit behaves like a Π network LC low pass filter which has capacitive components to ground and inductive series components as shown in Figures 4.17 and 4.18. Transitions involving multiple vias will have the cascading effect of several low pass filter sections which will provide greater roll off.

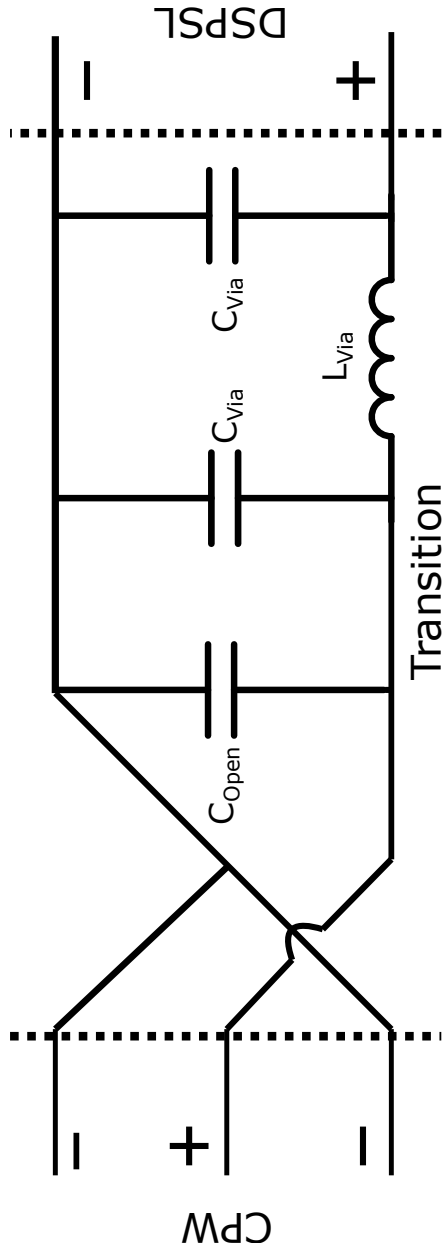


Figure 4.17: Simplified equivalent circuit of a single transition (Type A and Type B).

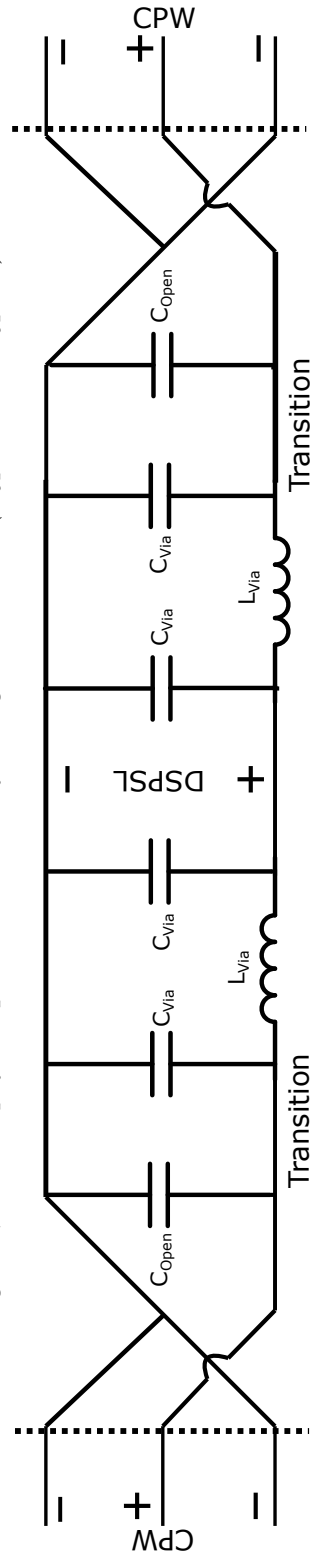


Figure 4.18: Simplified equivalent circuit of the back to back configuration of the transition (Type A and Type B).

4.1.4 Measured Results

4.1.4.1 Type A

The scattering parameters of the back-to-back transitions were simulated and measured using multilayer solver (Frequency domain) of CST Microwave Studio and Keysight Fieldfox N9927A handheld network analyzer respectively, are illustrated in Figures 4.19 and 4.21, which show good match. The actual photographs of top and bottom views of all transitions are also shown in Figures 4.20 and 4.22. Table 4.3 shows the measured insertion and return losses of the transitions for different substrates.

From the measured group delays shown in Figure 4.25, average delay deviation for 30 kHz to 14 GHz is only about 0.021 ns (Type A - Rogers RO4003C) and 0.016 ns (Type A - FR4) which are relatively very small. Phase of the scattering parameter S_{21} is shown in Figures 4.23 and 4.24, indicating the good transmission phase linearity of the transitions.

The insertion loss associated with a single transition, $IL_{Transition}$, can be calculated as;

$$IL_{Transition} = (IL_{Total} - L_{CPW} - L_{DSPSL} - L_{SMA})/2$$

where, IL_{Total} is the total measured insertion loss, L_{CPW} and L_{DSPSL} are the insertion losses of the CPW and DSPSL lines respectively, and L_{SMA} is the insertion loss of SMA connectors. According to [6, 7, 9, 11–13], the transmission loss of DSPSL and CPW sections are about 0.03 dB/mm and 0.04 dB/mm, respectively and insertion loss of a single SMA connector is around 0.09 dB. Therefore maximum in band insertion loss for a single transition is approximately 0.76 dB and 1.51 dB for the substrates Rogers RO4003C and FR4 respectively.

Table 4.3: Measured losses of the back-to-back transitions (Type A).

Substrate	Bandwidth (GHz)	Insertion loss (dB)	Return loss (dB)
Rogers RO4003C	0.0 - 12.1	≤ 2.5	≥ 9.0
FR4	0.0 - 11.0	≤ 4.0	≥ 15.0

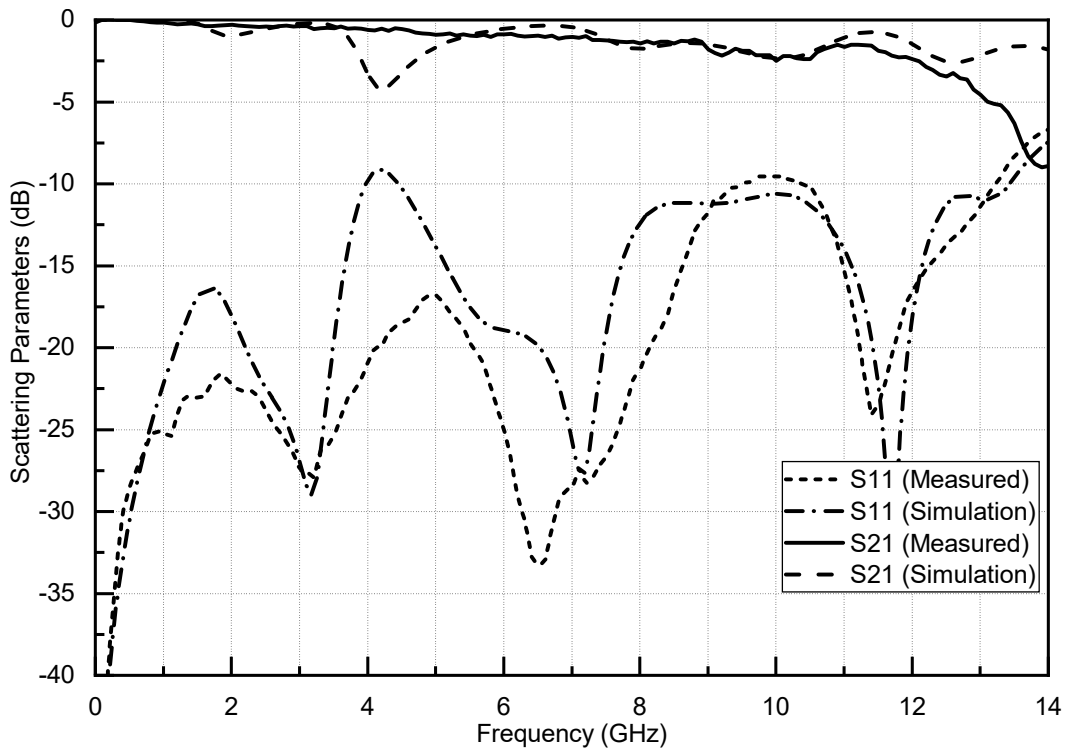


Figure 4.19: Simulated and measured scattering parameters of the back-to-back transitions- Type A (Rogers RO4003C)



(a) Top view



(b) Bottom view

Figure 4.20: Actual photograph of the back-to-back transitions - Type A (Rogers RO4003C)

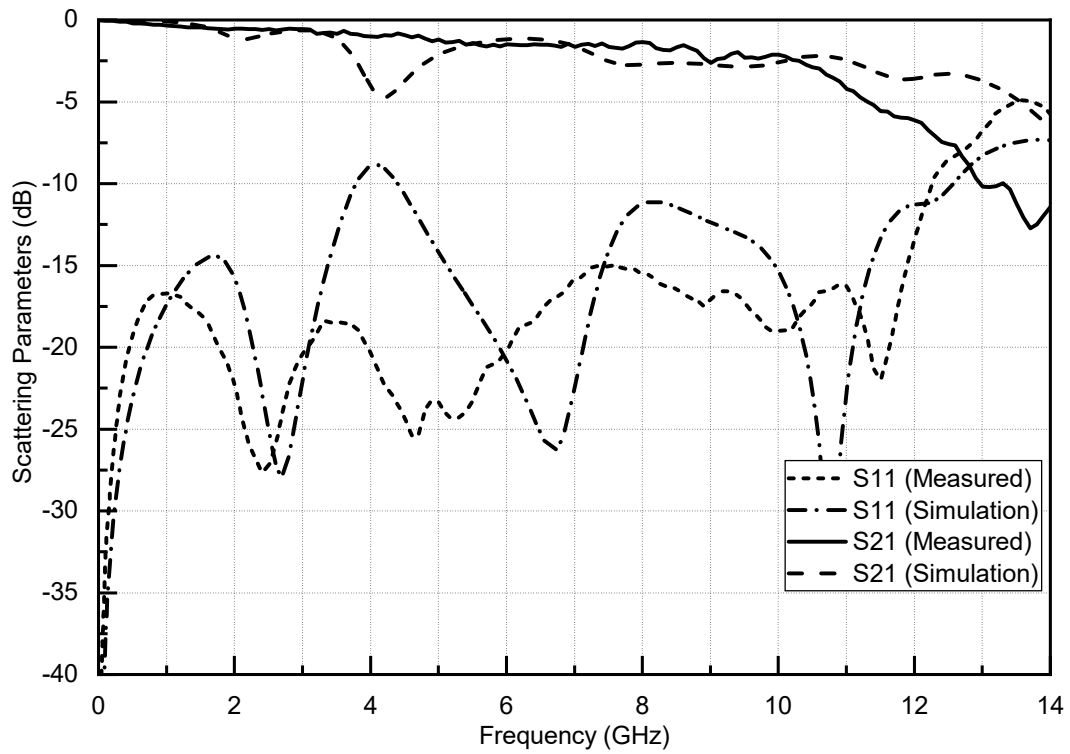
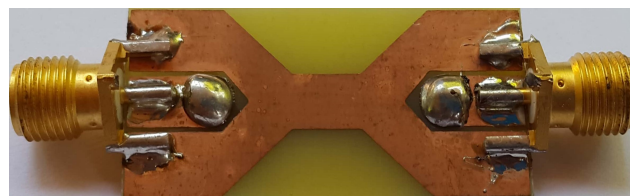


Figure 4.21: Simulated and measured scattering parameters of the back-to-back transitions - Type A (FR₄)



(a) Top view



(b) Bottom view

Figure 4.22: Actual photograph of the back-to-back transitions - Type A (FR₄)

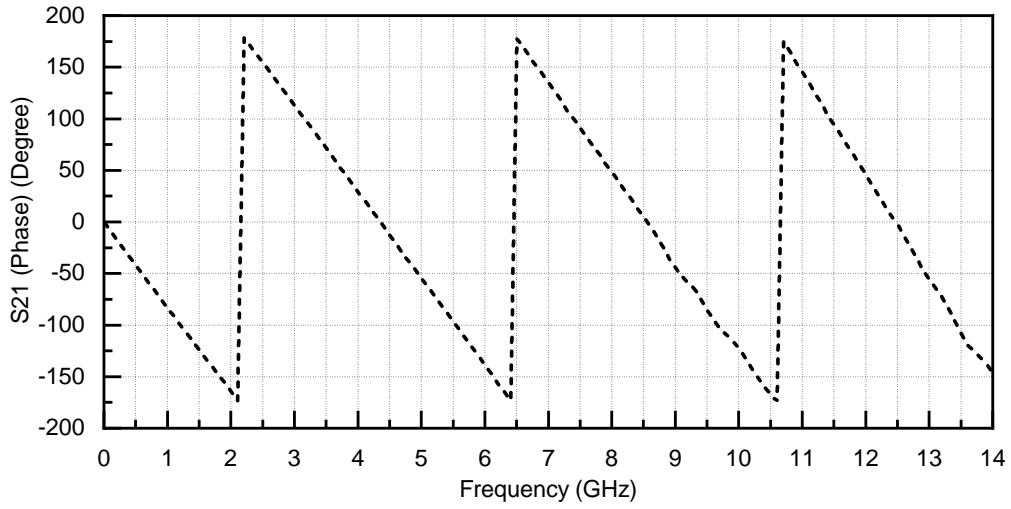


Figure 4.23: Measured scattering parameter S_{21} phase (in degrees) of the back-to-back transitions - Type A (Rogers RO4003C).

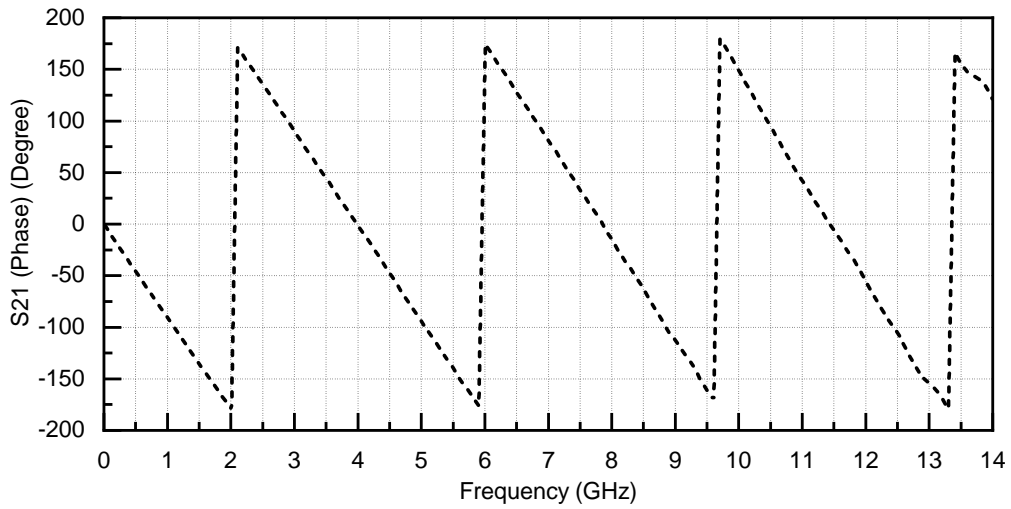


Figure 4.24: Measured scattering parameter S_{21} phase (in degrees) of the back-to-back transitions - Type A (FR4).

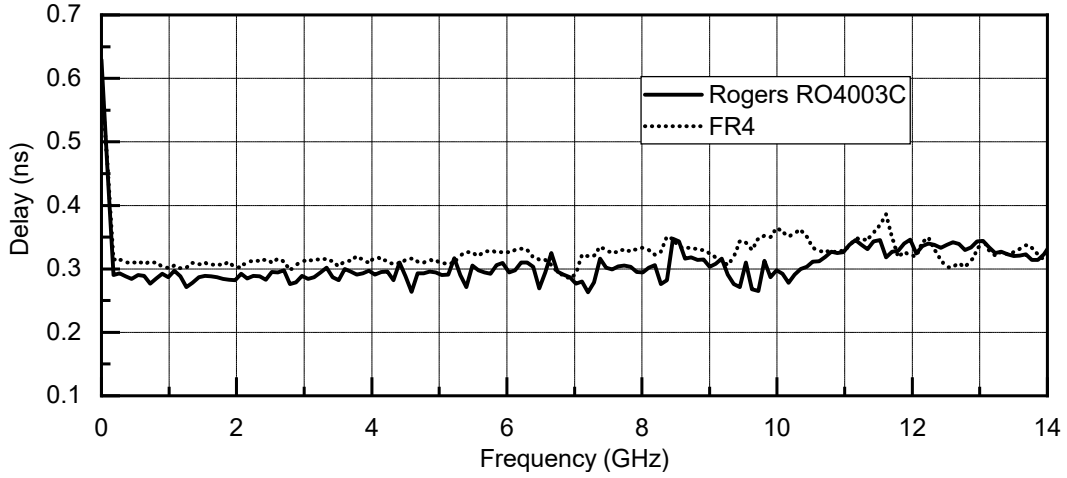


Figure 4.25: Measured group delays of the back-to-back transitions - Type A

4.1.4.2 Type B

The scattering parameters of the back-to-back transitions were simulated and measured using multilayer solver (Frequency domain) of CST Microwave Studio and Keysight Fieldfox N9927A handheld network analyzer respectively, are illustrated in Figures 4.26 and 4.29, which show good match. The actual photographs of top and bottom views of all transitions are also shown in Figures 4.28 and 4.30. Table 4.4 shows the measured insertion and return losses of the transitions for different substrates.

From the measured group delays as shown in Figure 4.32, average delay deviation for 30 kHz to 14 GHz is only about 0.014 ns (Type B - Rogers RO4003C) and 0.020 ns (Type B - FR4) which are relatively very small. Phase of the scattering parameter S_{21} is shown in Figures 4.27 and 4.31, indicating the good transmission phase linearity of the transitions.

The insertion loss associated with a single transition, $IL_{Transition}$, can be calculated as;

$$IL_{Transition} = (IL_{Total} - L_{CPW} - L_{DSPSL} - L_{SMA})/2$$

where, IL_{Total} is the total measured insertion loss, L_{CPW} and L_{DSPSL} are the insertion losses of the CPW and DSPSL lines respectively, and L_{SMA} is the insertion loss of SMA connectors. According to [6, 7, 9, 11–13], the transmission loss of DSPSL and CPW sections are about 0.03 dB/mm and 0.04

dB/mm, respectively and insertion loss of a single SMA connector is around 0.09 dB . Therefore maximum in band insertion loss for a single transition is approximately 0.76 dB and 1.51 dB for the substrates Rogers RO4003C and FR4 respectively.

Table 4.4: Measured losses of the back-to-back transitions (Type B).

Substrate	Bandwidth (GHz)	Insertion loss (dB)	Return loss (dB)
Rogers RO4003C	0.0 - 11.5	≤ 2.5	≥ 14.5
FR4	0.0 - 10.7	≤ 4.0	≥ 13.4

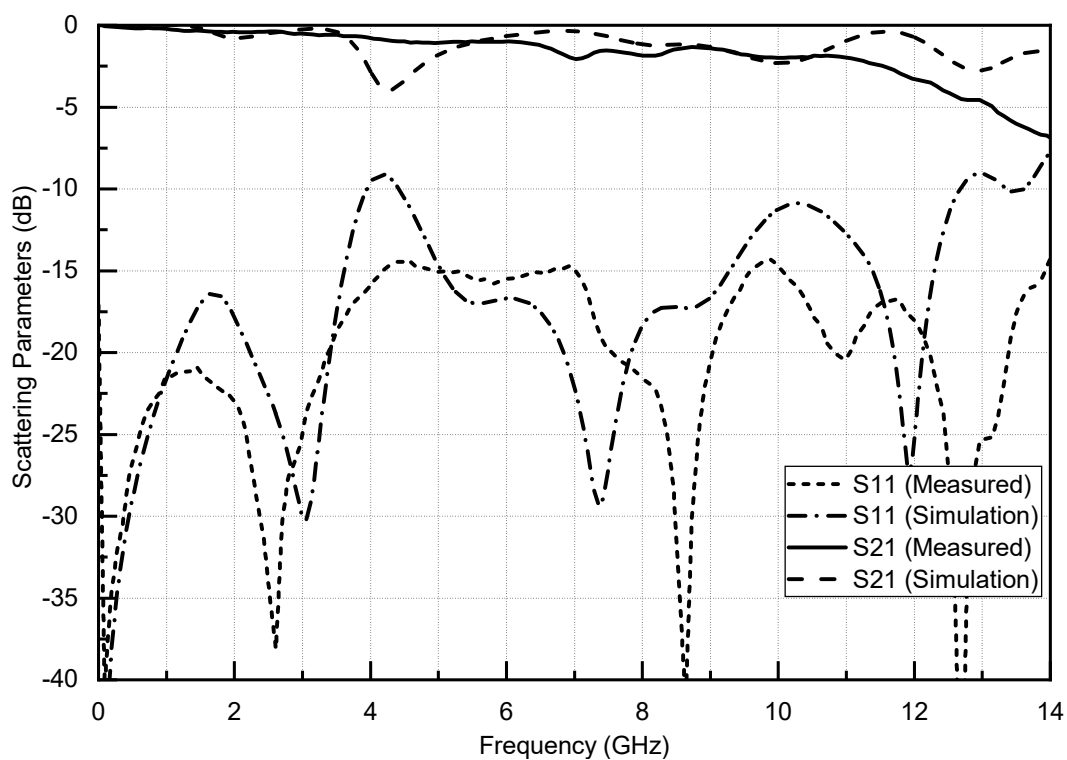


Figure 4.26: Simulated and measured scattering parameters of the back-to-back transitions - Type B (Rogers RO4003C)

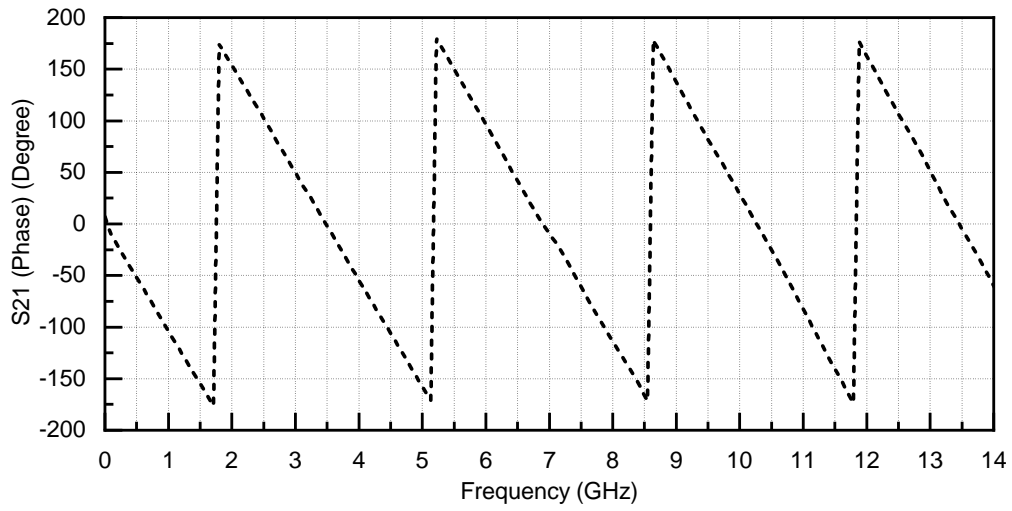
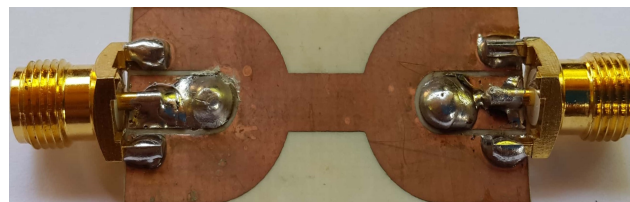


Figure 4.27: Measured scattering parameter S_{21} phase (in degrees) of the back-to-back transitions - Type B (Rogers RO4003C).



(a) Top view



(b) Bottom view

Figure 4.28: Actual photograph of the back-to-back transitions - Type B (Rogers RO4003C)

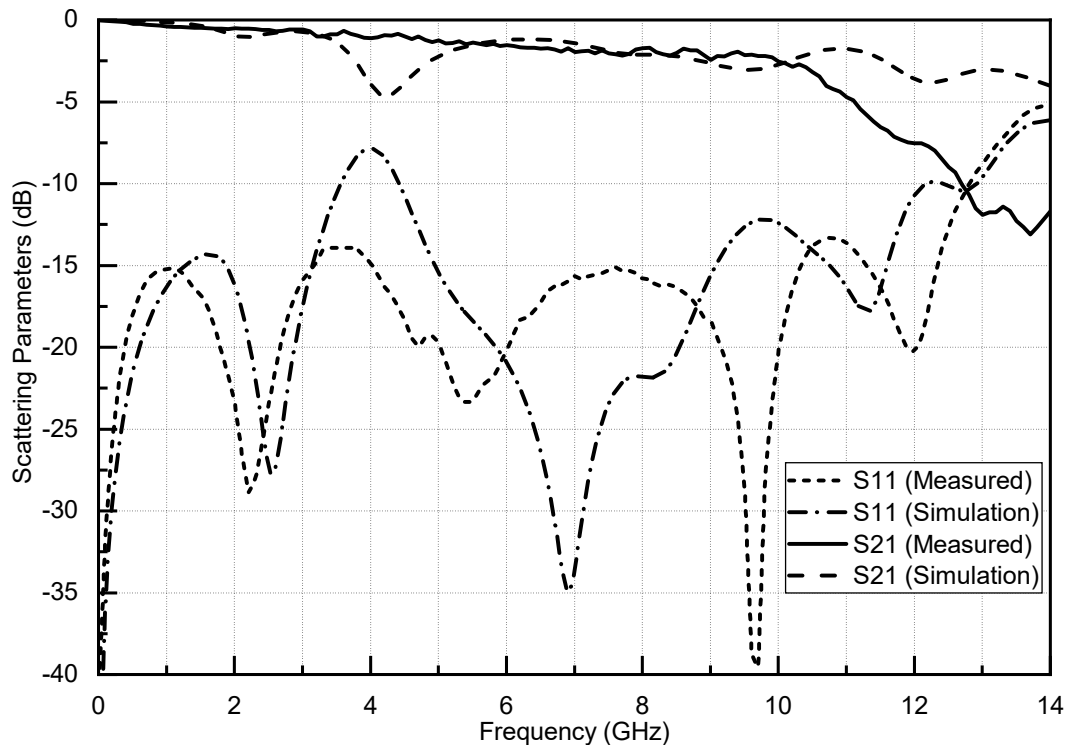
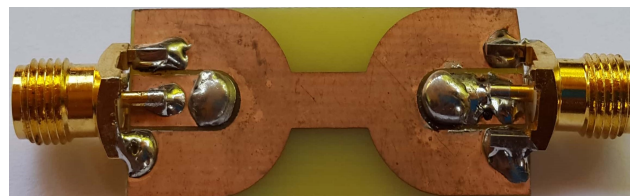


Figure 4.29: Simulated and measured scattering parameters of the back-to-back transitions - Type B (FR4)



(a) Top view



(b) Bottom view

Figure 4.30: Actual photograph of the back-to-back transitions - Type B (FR4).

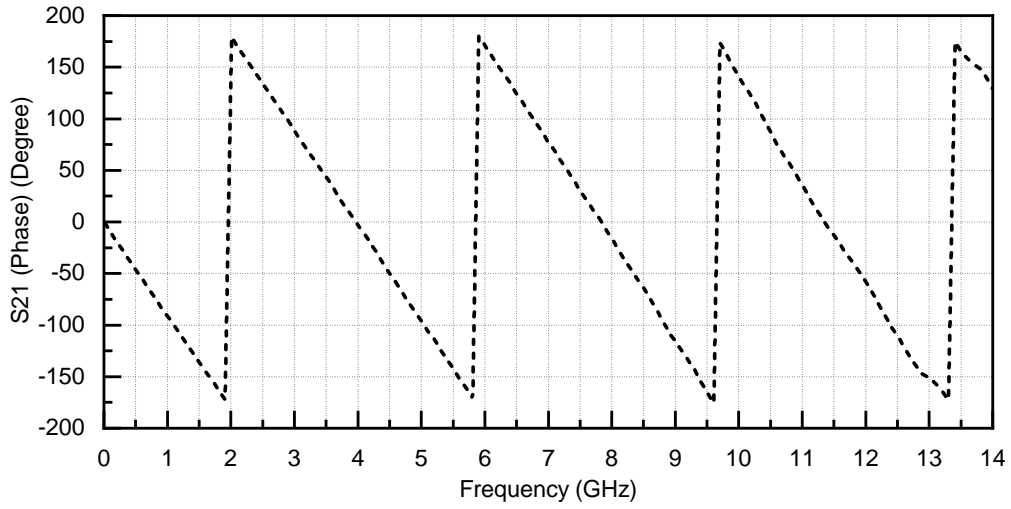


Figure 4.31: Measured scattering parameter S_{21} phase (in degrees) of the back-to-back transitions - Type B (FR4).

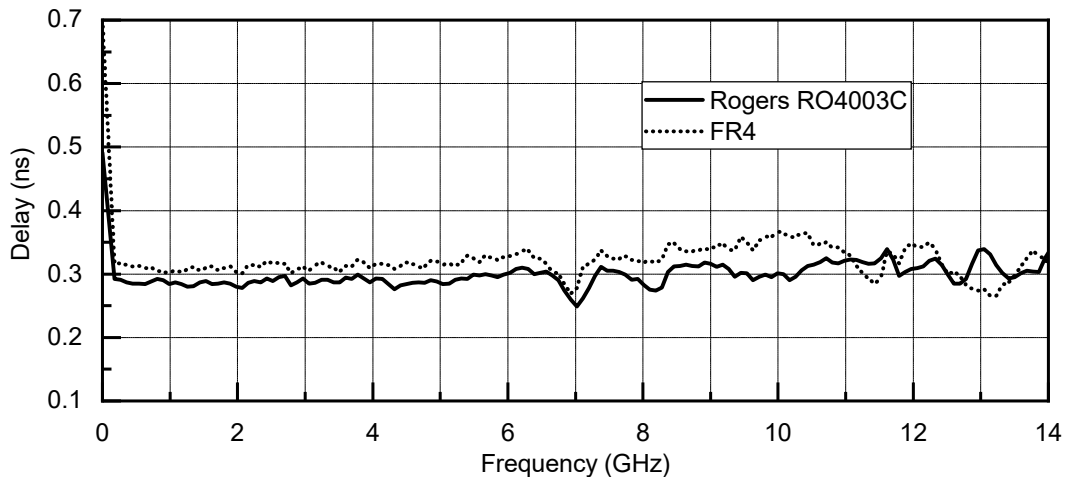


Figure 4.32: Measured group delays of the back-to-back transitions (a). Type A; (b). Type B.

4.2 CPW to DSPSL Transition without Via

4.2.1 Transition Geometry and its Design

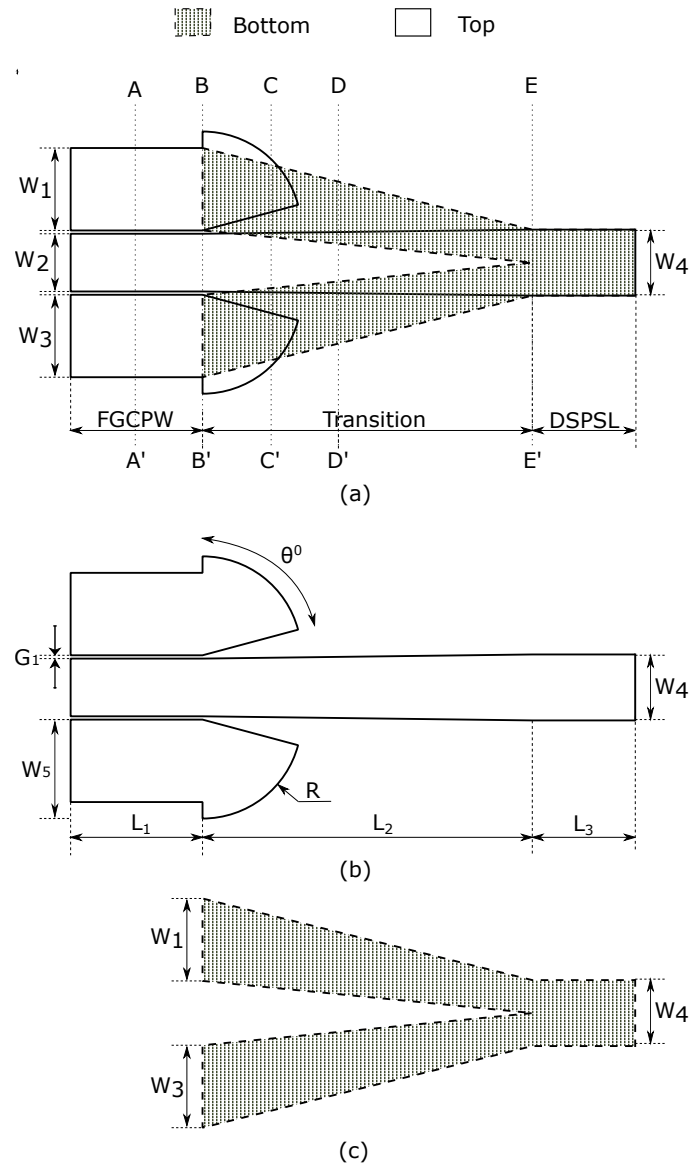


Figure 4.33: Configuration of the via-less transition: (a) schematic layout, (b) top view, (c) bottom view. ($W_1=5$ mm, $W_2=3.5$ mm, $W_3=5$ mm, $W_4=4$ mm, $W_5=6$ mm, $G_1=0.2$ mm, $\theta^0=70^\circ$, $L_1=8$ mm, $L_2=20$ mm, $L_3=6$ mm)

In this transition, the terminated CPW grounds are modified into radial stubs for vertical coupling between layers. The DSPSL in the bottom layer is split into two delta stubs for easy coupling from the CPW grounds. This via-less design reduces structural complexity, performance imbalances and fabrication difficulties. The tapered structure used for connecting the CPW center line to the top DSPSL line, gives rise to better bandwidth and low insertion losses.

The proposed transition is between 50Ω CPW and 50Ω DSPSL in a Roger's RT/Duroid 5870 with thickness 0.5 mm and a dielectric constant of 2.31 as shown in Figure 4.33. The DSPSL is fabricated on both sides with opposing but equal magnitude currents in lines. The CPW is fabricated on the top of the substrate. Both ground lines together and the center strip of CPW carry equal current with π radians phase difference. The signal lines, which carry equal magnitude current and which are in phase are connected together in top side of the substrate. The currents which are half in magnitude, available in the CPW grounds are coupled to the next layer using the radial stub - delta stub combination. Both of the Y-shaped delta stubs contributes to the total currents in the DSPSL bottom line.

DSPSL top signal strip is linearly tapered to match the width of CPW center strip. The linear tapering mentioned above combined with the electromagnetic (EM) coupling of the radial stub and the delta stub ensures the field and impedance matching. The overlapping area of the stubs are optimized to ensure maximum EM coupling. The radial stub length is approximately $\lambda/4$ at the center frequency of the bandwidth. The radial stub angle is optimized to 70° . Both the stubs converts the horizontally aligned electric field of the CPW to the vertically aligned field of DSPSL. The length of the transition is 20mm.

Multilayer solver (Frequency domain) of CST Microwave Studio (3D planar electromagnetic solver based on MoM) is used for the parametric studies and optimization. The transitions are printed on Roger's RT/Duroid 5870 with thickness 0.5 mm and a dielectric constant of 2.31. The dimensions of 50Ω CPW is determined by CST Microwave Studio utility with the center strip width as $W_1=3.5$ mm, and the gap width as $G_1=0.2$ mm for both cases. Using image theory, the strip width of the 50Ω DSPSL can be calculated as $W_2=3.5$ mm.

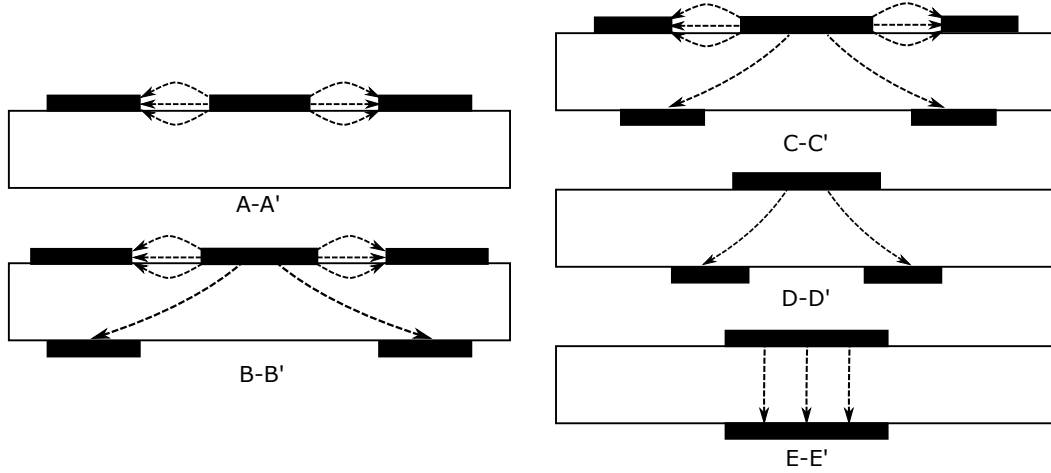


Figure 4.34: Cross-sectional views of proposed transition (Type B) and electric field distributions: (a) AA'- CPW mode, (b) EE' - DSPSL mode, (c) BB',CC',DD' - Transition modes.

The electric fields of both DSPSL and CPW have different characteristics. One is an unbalanced transmission line (CPW) and the other one is a balanced transmission line (DSPSL). The proposed transition rotates their electric field by 90° . The CPW has electric fields between the center strip and grounds in both sides. On the other hand DSPSL has vertical fields between the conductors.

Cross sectional electric field at AA' shows the CPW mode, which is having horizontal field distribution, and the vertical field distribution at EE' shows the DSPSL mode as in Figure 4.34. At BB' the field is distributed vertically and horizontally between the radial stubs and the delta stubs. CC' is having the same field pattern with slight change in the size of the center strip and stubs. At DD' the horizontal to vertical transformation is almost complete, but still the bottom conductor is Y-shaped. The cross section at EE' completes the electric field transformation to DSPSL mode.

4.2.2 Simulation Studies

Simulation studies of the via-less CPW to DSPSL transition, printed on Roger's RT Duroid 5870 ($\epsilon_r=2.31$ and $h=0.5$ mm), is done on a back to back

configuration with CPW signal feeds at both ends as in Figure 4.35.

Multilayer solver (Frequency domain) of CST Microwave Studio (3D planar electromagnetic solver based on MoM) is used for the parametric studies and optimization. The dimensions of 50 Ω CPW is determined by CST Microwave Studio utility with the center strip width as $W_1=3.5$ mm, and the gap width as $G_1=0.2$ mm. Using image theory, the strip width of the 50 Ω DSPSL can be calculated as $W_2=4.0$ mm as in Table 4.5. For this transition, the transition length (L_2), radial stub length (W_5), radial stub angle (θ°) and CPW ground width (W_1) are the sensitive parameters used for the simulation studies and optimization as shown in Figures 4.36, 4.37, 4.38 and 4.39.

Table 4.5: Geometrical parameters of the proposed transition (in mm).

Parameter	W_1	W_2	W_3	W_4	W_5	R	θ°	L_1	L_2	L_3	G_1
Value	5	3.5	5	4	6	6	70°	8	20	6	0.2

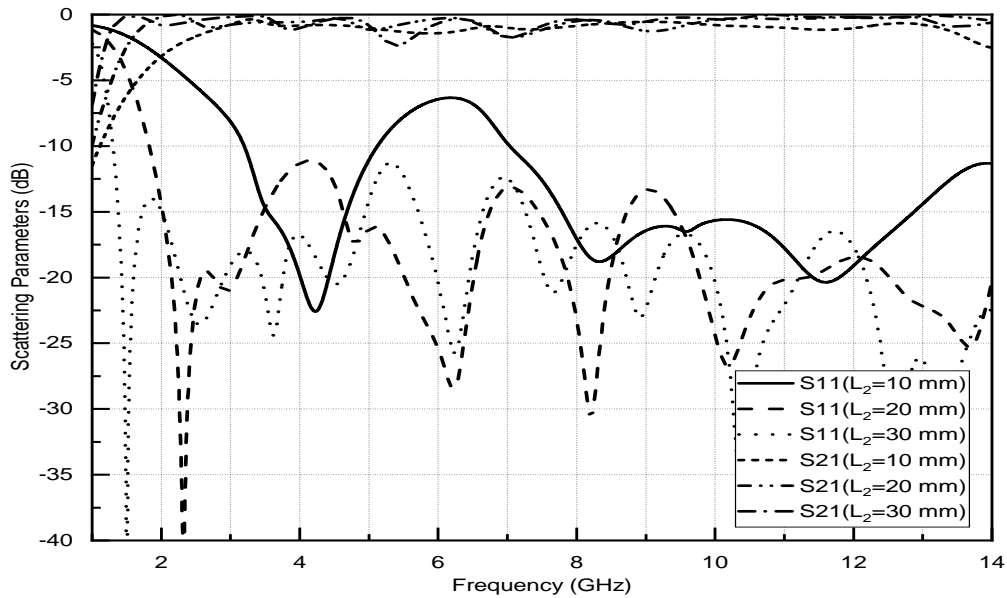


Figure 4.36: Simulated scattering parameters of the back-to-back via-less transitions against frequency with different transition lengths (L_2).

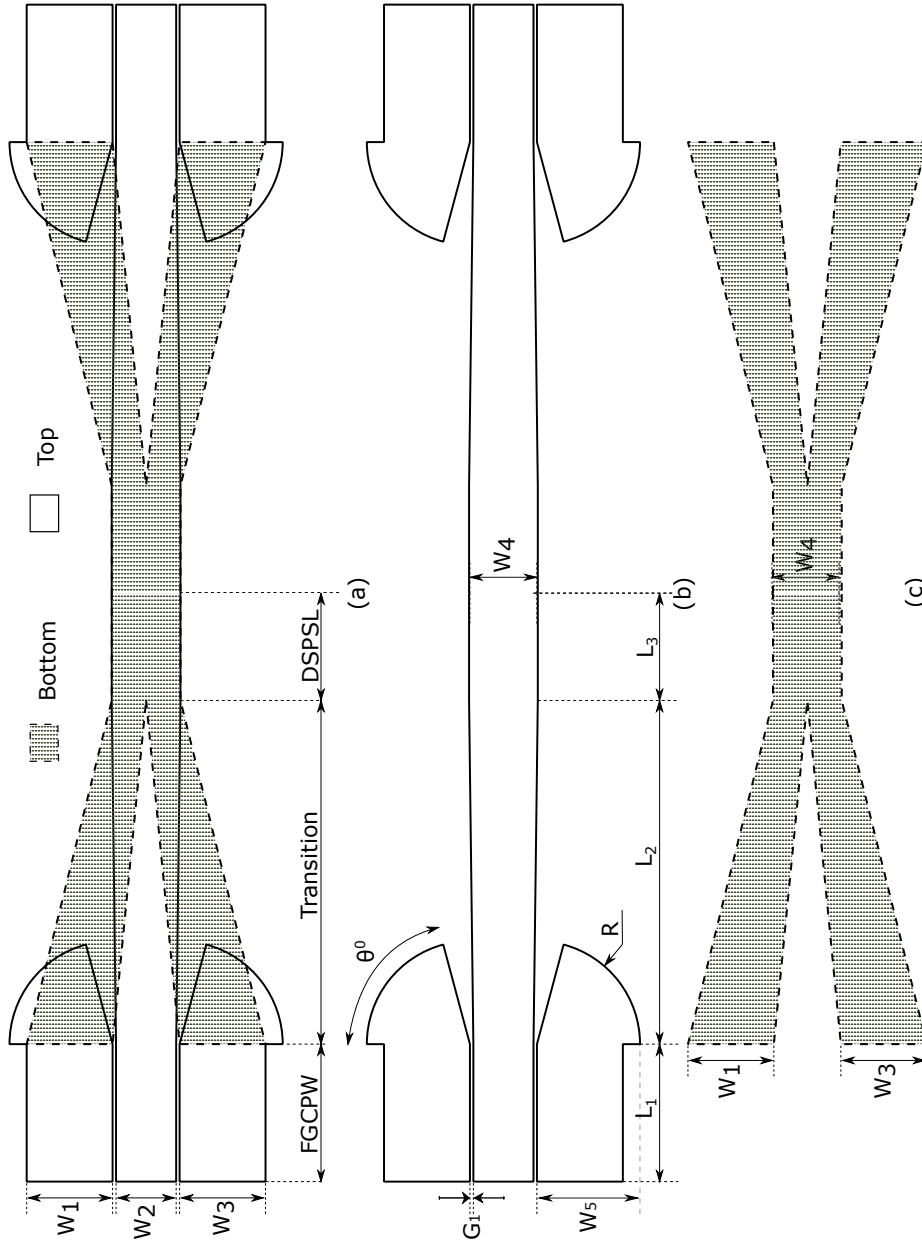


Figure 4.35: Configuration of the back to back via-less transitions: (a) schematic layout, (b) top view, (c) bottom view. ($W_1=5$ mm, $W_2=3.5$ mm, $W_3=5$ mm, $W_4=4$ mm, $W_5=6$ mm, $G_1=0.2$ mm, $\theta^0=70^\circ$, $L_1=8$ mm, $L_2=20$ mm, $L_3=6$ mm)

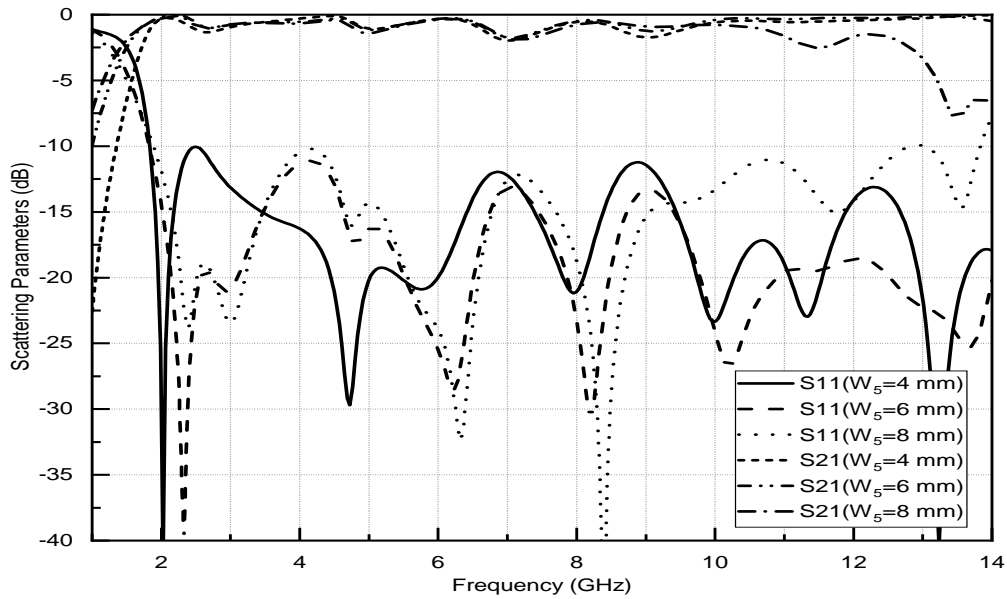


Figure 4.37: Simulated scattering parameters of the back-to-back via-less transitions against frequency with different radial stub lengths (W_5).

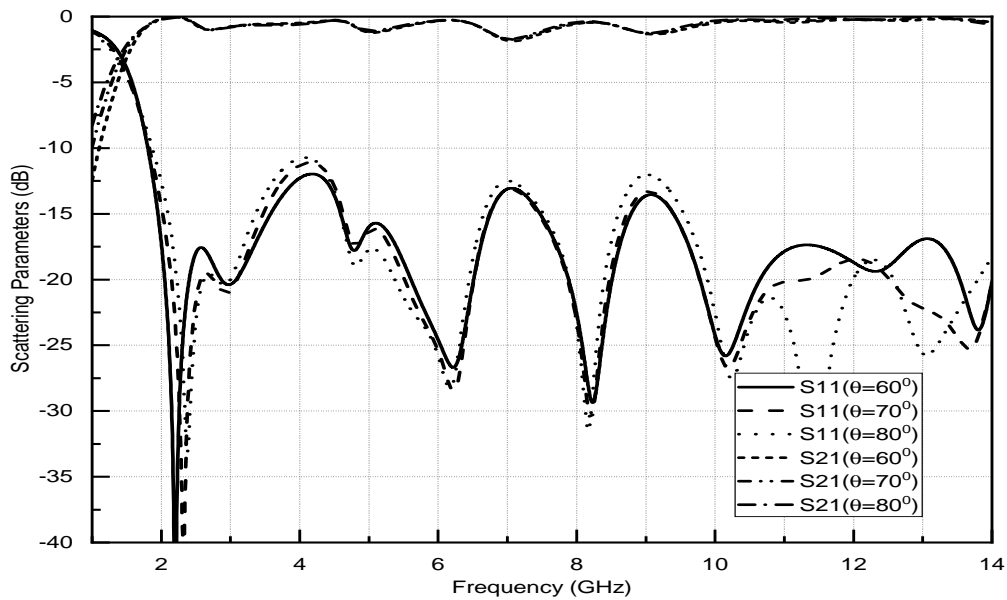


Figure 4.38: Simulated scattering parameters of the back-to-back via-less transitions against frequency with different radial stub angles (θ°).

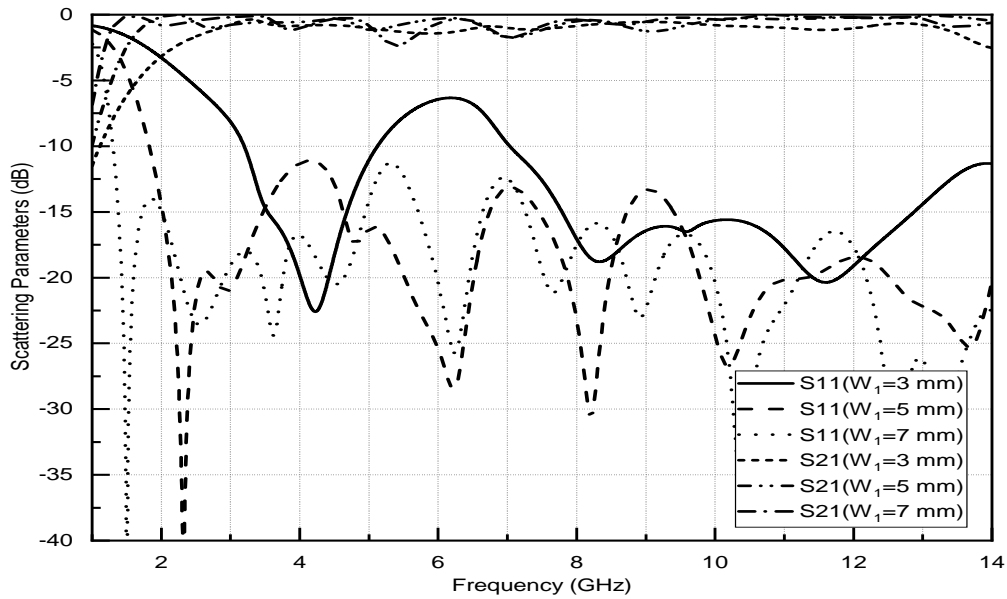


Figure 4.39: Simulated scattering parameters of the back-to-back via-less transitions against frequency with different CPW ground widths (W_1).

4.2.3 Equivalent Circuit

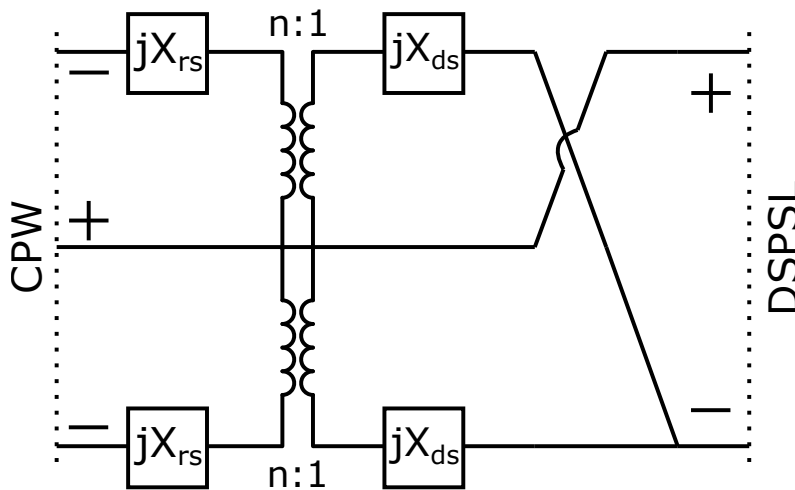


Figure 4.40: Simplified equivalent circuit of a single via-less transition.

The centre conductor of the CPW is integrated with the top plane of the DSPSL. The bottom end of the DSPSL is connected to two open delta stubs. The end of the delta stubs are aligned with the radial stub arms of the CPW on opposite sides of the substrate. The lengths of both stubs are designed to allow wider bandwidth. The natural gap between the two transmission line structures, blocks DC which is a requirement in some microwave circuit designs.

The present transition design is capable of inducing strong coupling between the electromagnetic fields of the stubs at top and bottom layers. As a result, the high frequency signal can be effectively transferred between DSPSL and CPW through resonant coupling. The equivalent circuit model is equivalent to the parallel combination of two delta to radial stub via-less coupling, as shown in Figures 4.40 and 4.41. In the equivalent circuit, X_{rs} and X_{ds} represent the reactances of the open radial and delta stubs respectively. The transformer turns ratio n describes the magnitude of the coupling between the stubs. The bandwidth of operation is limited due to the frequency dependence of the reactance of the stubs (X_{rs} and X_{ds}) used in the transition design. To ensure a broadband transition, mutual cancellation of reactances X_{rs} and X_{ds} is needed, even though one of them will be scaled by the magnitude of coupling (transformer turns ratio n) upon transferring to primary of the transformer. This can be achieved by properly designing and optimizing the size and shape of the stubs.

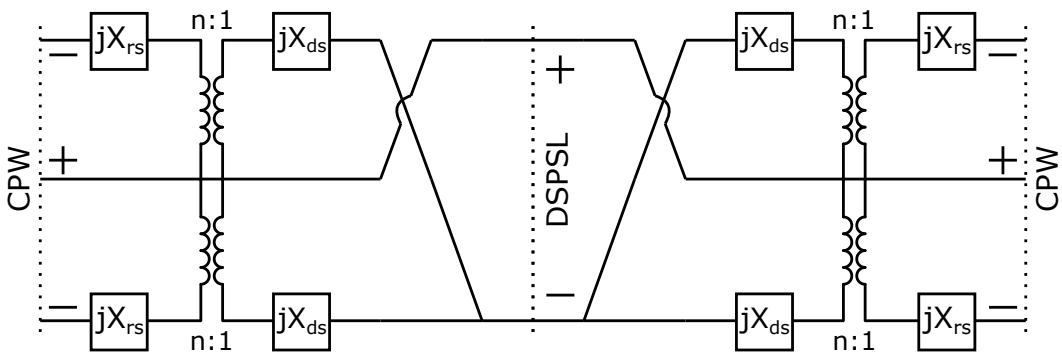


Figure 4.41: Simplified equivalent circuit of the back to back configuration of the via-less transitions.

4.2.4 Measured Results

The scattering parameters of the back-to-back via-less transition was simulated and measured using multilayer solver (Frequency domain) of CST Microwave Studio and Keysight Fieldfox N9927A handheld network analyzer respectively, are illustrated in Figure 4.42, which show good match. The actual photographs of top and bottom views of the transition is shown in Figure 4.43. Table 4.6 shows the measured insertion and return losses of the transitions for the substrate Rogers RT Duroid 5870.

From the measured group delay shown in Figure 4.45, average delay deviation for 1.0 GHz to 11 GHz is only about 0.028 ns which is relatively very small. Phase of the scattering parameter S_{21} is shown in Figure 4.44, indicating the good transmission phase linearity of the transition.

The insertion loss associated with a single transition, $IL_{Transition}$, can be calculated as;

$$IL_{Transition} = (IL_{Total} - L_{CPW} - L_{DSPSL} - L_{SMA})/2$$

where, IL_{Total} is the total measured insertion loss, L_{CPW} and L_{DSPSL} are the insertion losses of the CPW and DSPSL lines respectively, and L_{SMA} is the insertion loss of SMA connectors. According to [6, 7, 9, 11–13], the transmission loss of DSPSL and CPW sections are about 0.03 dB/mm and 0.04 dB/mm, respectively and insertion loss of a single SMA connector is around 0.09 dB. Therefore maximum in band insertion loss for a single transition is approximately 0.41 dB for the substrate Rogers RT Duroid 5870.

Table 4.6: Measured losses of the back-to-back via-less transitions.

Substrate	Bandwidth (GHz)	Insertion loss (dB)	Return loss (dB)
Rogers RT Duroid 5870	1.76 - 10.10	≤ 2.0	≥ 10.0

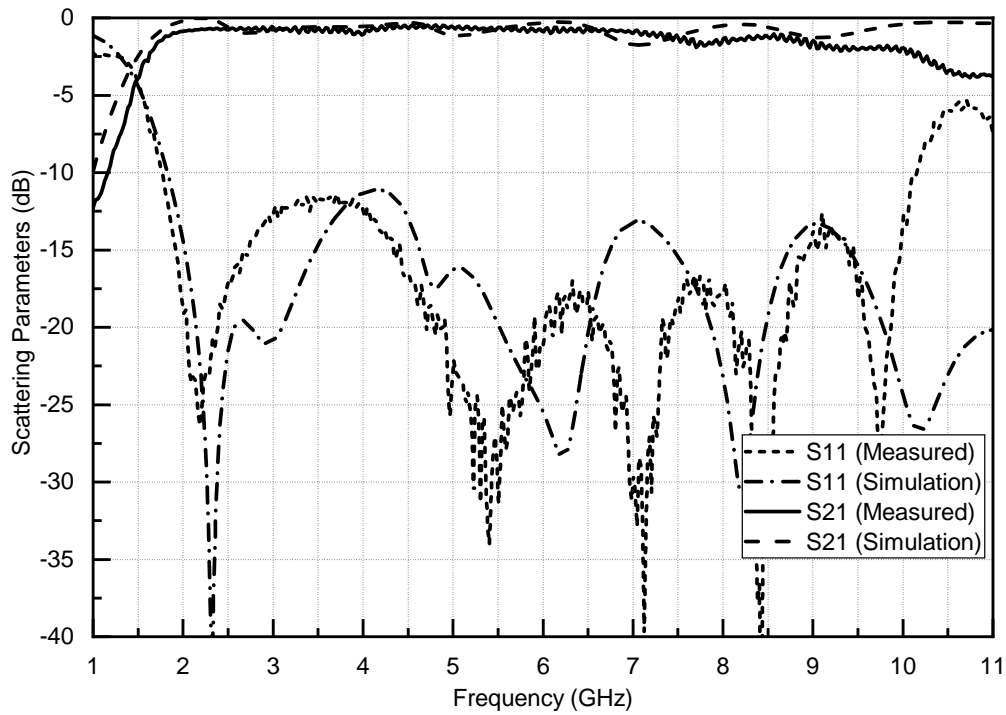
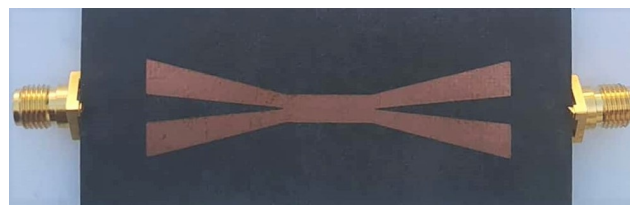


Figure 4.42: Simulated and measured scattering parameters of the back-to-back via-less transitions.



(a) Top View



(b) Bottom View

Figure 4.43: Actual photograph of the back-to-back via-less transitions.

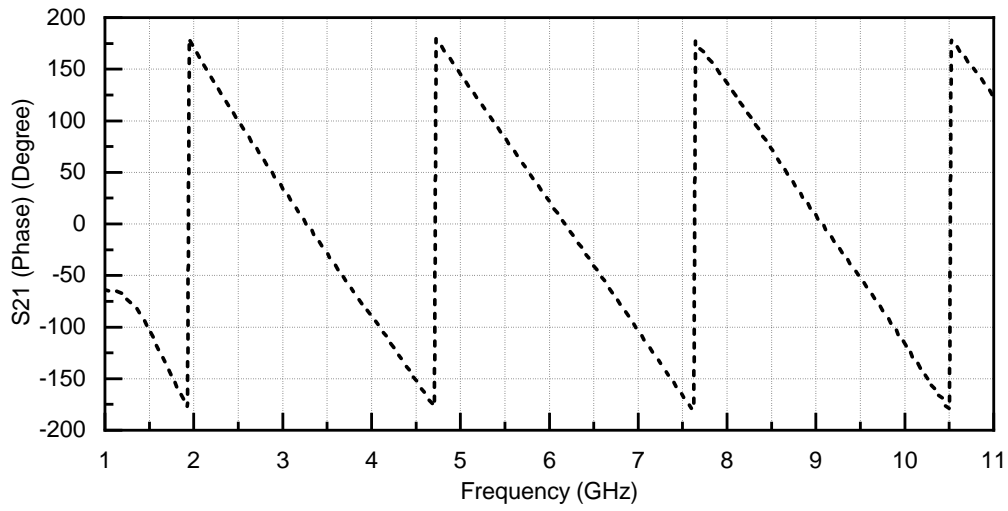


Figure 4.44: Measured scattering parameter S_{21} phase (in degrees) of the back-to-back via-less transitions.

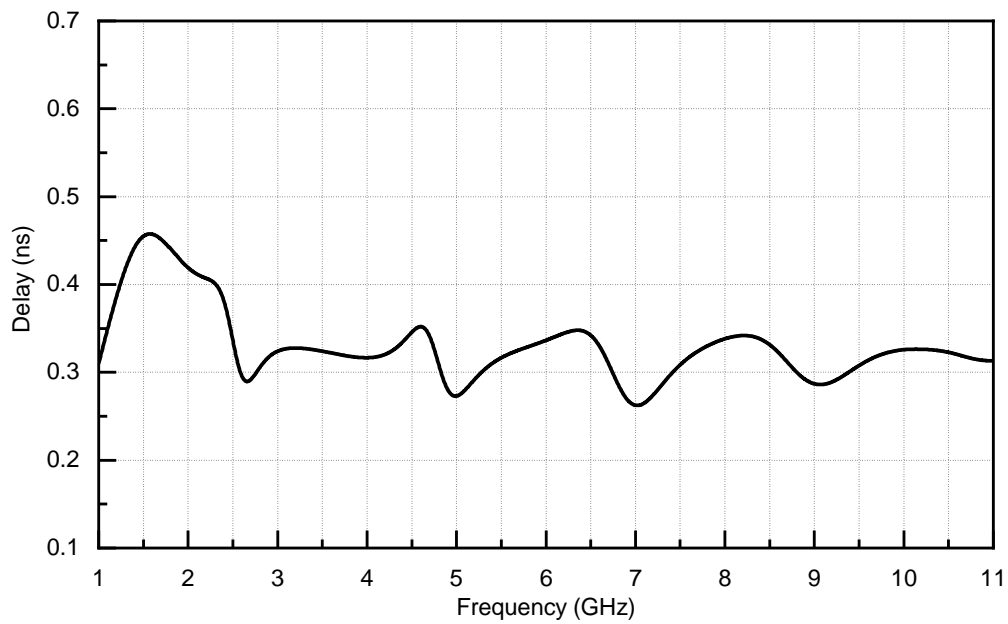


Figure 4.45: Measured group delays of the back-to-back via-less transitions.

4.3 Chapter Summary

The vertical broadband transitions between DSPSL and CPW has been designed, optimized and measured for the first time. The proposed transitions (Types A and B) are based on a single via connection and connected CPW grounds. An approximate equivalent circuit, which is a Π network, LC low pass filter is discussed. Transitions are fabricated on Rogers RO4003C and FR4 substrates, using the standard photolithography process. A via-less transition is designed, prototyped in Rogers RT Duroid 5870, and measured, in the second part of the chapter and its equivalent circuit is discussed. These transitions are useful in many applications like antenna feeds and passive and active microwave components. Besides the vertical transitions of DSPSL in flipped back-to-back form are capable of achieving phase inversion, useful especially in applications like ring couplers, mixers, doublers, etc.

References

- [1] D. M. Pozar, *Microwave Engineering; 4th Edition*. Wiley, 2011.
- [2] B. C. Wadell, *Transmission Line Design Handbook*. Artech House, 1991.
- [3] H. A. Wheeler, "Transmission-line properties of parallel strips separated by a dielectric sheet," *IEEE Transactions on Microwave Theory and Techniques*, vol. 13, pp. 172–185, March 1965.
- [4] J. M. Rochelle, "Approximations for the symmetrical parallel-strip transmission line (letters)," *IEEE Transactions on Microwave Theory and Techniques*, vol. 23, pp. 712–714, Aug 1975.
- [5] Sang-Gyu Kim and Kai Chang, "Ultrawide-band transitions and new microwave components using double-sided parallel-strip lines," *IEEE Transactions on Microwave Theory and Techniques*, vol. 52, pp. 2148–2152, Sep. 2004.

- [6] J.-X. Chen, J.-L. Li, and Q. Xue, “Novel via-less double-sided parallel strip line to coplanar waveguide transition,” *Microwave and Optical Technology Letters*, vol. 48, no. 9, pp. 1717–1718, 2006.
- [7] X. Y. Zhang, J. Chen, and Q. Xue, “Broadband transition between double-sided parallel-strip line and coplanar waveguide,” *IEEE Microwave and Wireless Components Letters*, vol. 17, pp. 103–105, Feb 2007.
- [8] S. Bulja, D. Mirshekar-Syahkal, and M. Yazdanpanahi, “Novel wide-band transition between finite ground coplanar waveguide (fgcpw) and balanced stripline,” in *2009 European Microwave Integrated Circuits Conference (EuMIC)*, pp. 301–303, Sep. 2009.
- [9] C. H. Ahn and K. Chang, “Wideband coplanar stripline to double-sided parallel-strip line transition,” *Electronics Letters*, vol. 45, pp. 748–749, July 2009.
- [10] P. L. Carro and J. de Mingo, “Analysis and synthesis of double-sided parallel-strip transitions,” *IEEE Transactions on Microwave Theory and Techniques*, vol. 58, pp. 372–380, Feb 2010.
- [11] T. W. Eubanks and K. Chang, “Low-loss ultra-wideband double-sided parallel-strip line transition and power divider,” *Electronics Letters*, vol. 46, pp. 93–94, January 2010.
- [12] W. . Lu, C. Cheng, and H. . Zhu, “Wideband coplanar waveguide to edges-even broadside-coupled stripline transition,” *Electronics Letters*, vol. 47, pp. 1286–1287, November 2011.
- [13] W. Lu, Y. Bo, and H. Zhu, “A broadband transition design for a conductor-backed coplanar waveguide and a broadside coupled stripline,” *IEEE Microwave and Wireless Components Letters*, vol. 22, pp. 10–12, Jan 2012.
- [14] W. Lu, H. Tong, Y. Bo, and H. Zhu, “Design and study of enhanced wideband transition between coplanar waveguide and broadside coupled

- stripline,” *IET Microwaves, Antennas Propagation*, vol. 7, pp. 715–721, June 2013.
- [15] Y.-G. Kim and K. W. Kim, “Design of an ultra-wideband transition from double-sided parallel stripline to coplanar waveguide,” *International Journal of Antennas and Propagation*, pp. 1–8, 2013.
- [16] J. Chen, C. K. Chin, and Q. Xue, “Double-sided parallel-strip line with an inserted conductor plane and its applications,” *IEEE Transactions on Microwave Theory and Techniques*, vol. 55, pp. 1899–1904, Sep. 2007.
- [17] J. X. Chen, *Double-sided parallel-strip line circuit analysis and applications to microwave component designs*. PhD thesis, City University of Hong Kong, 2008.
- [18] R. N. Simons, *Coplanar Waveguide Circuits, Components and Systems*. Wiley-IEEE Press, 2004.
- [19] B. J. LaMeres, “Characterization of a printed circuit board via,” Master’s thesis, University of Colorado, Colorado Springs, May 2000.

Chapter 5

Applications of CPW to DSPSL Transitions

Contents

5.1 CPW to CPW Phase Inverted Vertical Transitions	99
5.1.1 Transition Geometry and its Design	99
5.1.2 Equivalent Circuit	104
5.1.3 Measured Results	104
5.2 CPW Fed UWB Antipodal Vivaldi Antenna . . .	114
5.2.1 Antenna Geometry and its Design	115
5.2.2 Simulation Studies	118
5.2.3 Measured Results	121
5.3 Chapter Summary	126
References	126

In this chapter, a new method for designing a pair of structurally similar CPW to CPW transitions with phase inversion is proposed for the first time. A simplified equivalent circuit clearly showing the second order low pass nature and phase inversion is introduced. A CPW fed Ultra-WideBand (UWB) Antipodal Vivaldi Antenna (AVA) is also developed as an application of the transition.

5.1 CPW to CPW Phase Inverted Vertical Transitions

In multilayer microwave circuits phase inverting vertical transitions are extremely useful in generating differential signals for mixers, doublers and differential amplifiers etc. However, inverted phase vertical transitions between CPWs have not reported yet. Majority of the vertical transitions between CPWs are in phase and electromagnetically coupled between stacked CPWs [1, 2]. CPWs with finite-width ground planes are known as CPW or FWCPW (finite - width coplanar waveguide) [3]. Via connection (low-pass) between layers or Cavity coupling (band-pass) are usually used for achieving vertical transitions. A lot of new transitions between the balanced line DSPSL (otherwise broadside coupled stripline (BCS)) and the unbalanced line coplanar waveguide (CPW) are proposed in recent years [4–10]. Majority of them are made on high permittivity substrates, so that low characteristic impedance realizations are practically difficult. The optimized transitions in planar form using different methods are already reported [11–14].

5.1.1 Transition Geometry and its Design

The transition design flow can be summarized as, first choosing a configuration (which ensures smooth electromagnetic (EM) field transition), method (EM coupling/via) and dielectric(substrate) according to the requirements. In the second stage line lengths and impedances are calculated using approximate transition center frequency ensuring impedance matching and physical realizability. In final step a model for simulation taking all parasitic effects into account is created and optimized to meet the specifications.

The schematic layout of the transitions are shown in Figures 5.1 and 5.2. It utilizes the CPW - DSPSL transition reported earlier in which horizontal EM fields are rotated orthogonally (90°) from CPW mode to DSPSL mode, which is vertical in nature [9].

Due to the balanced nature of the transmission line DSPSL strips carry equal magnitude but phase inversed currents. On the other hand CPW's

finite width grounds carry half the currents of its center conductor due to the unbalanced nature. Almost all the transitions are made using either EM proximity coupling or single/multiple via configurations. Here a low pass natured, two via configuration, which can be easily manufactured is selected.

Parametric studies of the structures are done using the planar EM solver (multilayer solver) in the CST Microwave Studio. Prototyping are done using two almost identical substrates; Rogers RO4003C with permittivity 3.55 and height 1.524 mm and FR4 with permittivity value 4.3 and height 1.6 mm. The conductor width of 4.4 mm of DSPSL and a gap width of 0.35 mm with center conductor width of 4 mm and finite ground width of 5 mm, ensures 50 Ω characteristic impedances for both. Geometrical parameters of the proposed transitions (in mm) are given in Tables 5.1 and 5.2.

Both types are identical in nature apart from the structure of connected grounds in CPWs, which form a single strip for the via connection between layers. The Type A employs a 'y' junction and Type B utilizes circular tapering for the connected grounds. The length of a single transition between FGPCW and DSPSL is made quarter wavelength ($\lambda/4=7.4$ mm) at the approximate transition center frequency (7 GHz).

Cross-sectional views of both transitions (Type A and B) and electric field distributions are given in Figure 5.3. The electric fields of both DSPSL and CPW have different characteristics. One is an unbalanced transmission line (CPW) and the other one is a balanced transmission line (DSPSL). The proposed transition rotates their electric field by 90°. The CPW has electric fields between the center strip and grounds in both sides. On the other hand DSPSL has vertical fields between the conductors.

Cross sectional electric fields at AA' and II' show the CPW mode, which are having horizontal field distribution, and the vertical field distribution at EE' shows the DSPSL mode as in Figure 5.3. At BB' and HH' the field is distributed vertically and horizontally between the vias, via pads and CPW grounds. At CC' and GG' the horizontal to vertical transformation is almost complete, but still the ground conductor yet to be merged. At DD' and FF' the field pattern is almost like an inverted microstrip. The cross section at EE' completes the electric field transformation to DSPSL mode.

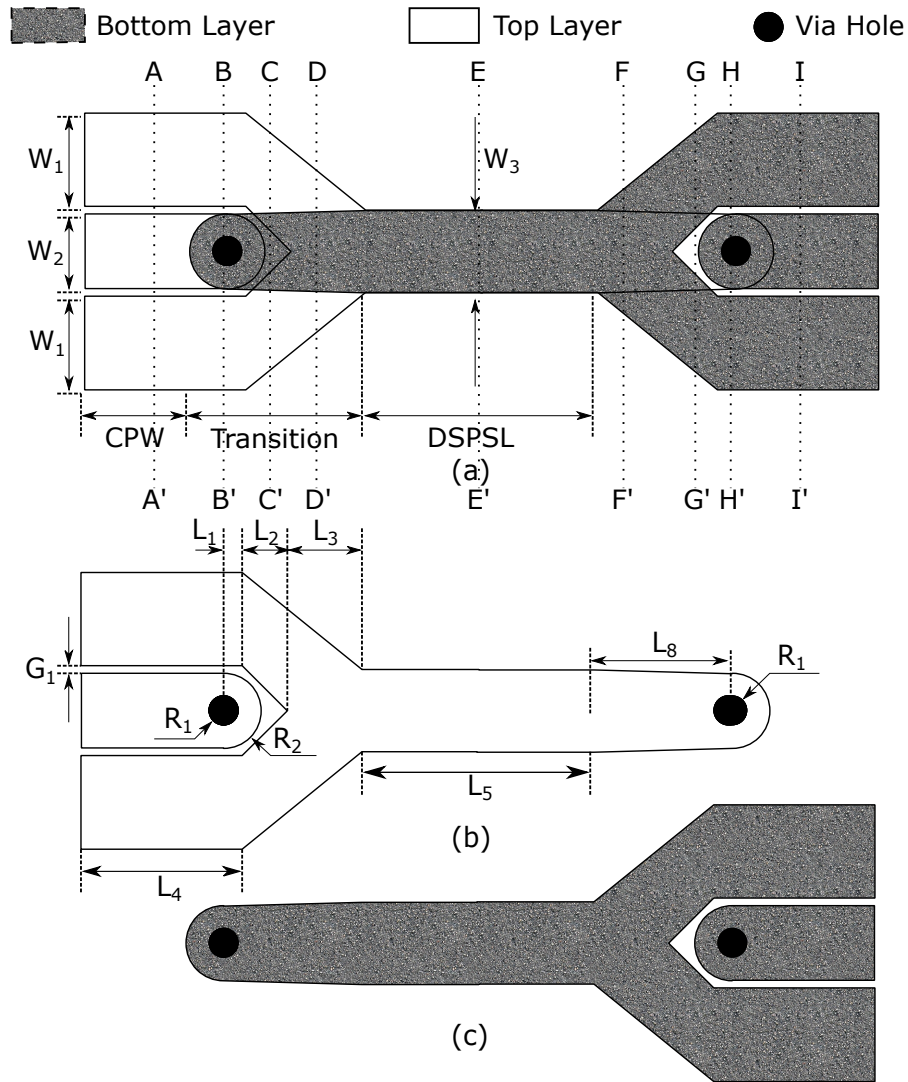


Figure 5.1: Configuration of the CPW to CPW transitions (Type A): (a) schematic layout, (b) top view and (c) bottom view.

Table 5.1: Geometrical parameters of the proposed transition (Type A) (in mm).

Parameter	W_1	W_2	W_3	G_1	R_1	R_2	L_1	L_2	L_3	L_4	L_5	L_8
Value	5	4	4.4	0.35	0.75	2	1	2.4	4	8.6	6.24	7.4

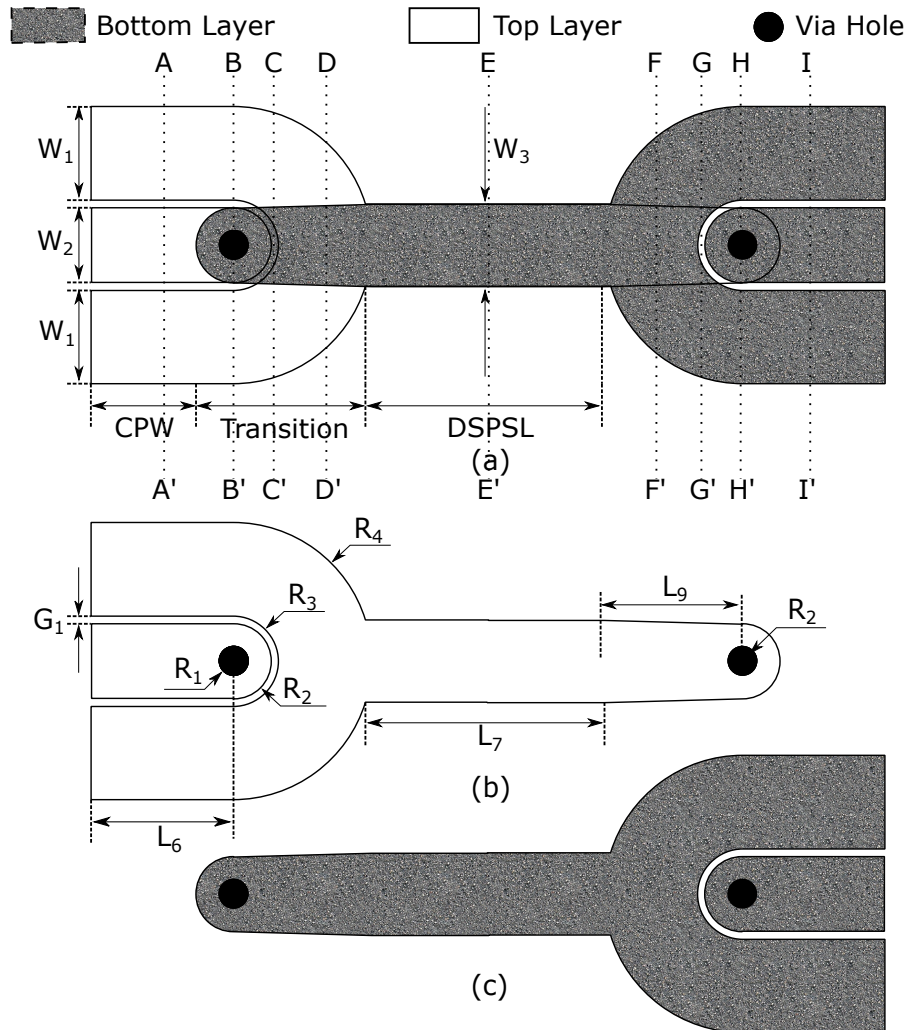


Figure 5.2: Configuration of the CPW to CPW transitions (Type B): (a) schematic layout, (b) top view and (c) bottom view.

Table 5.2: Geometrical parameters of the proposed transition (Type B) (in mm).

Parameter	W_1	W_2	W_3	G_1	R_1	R_2	R_3	R_4	L_6	L_7	L_9
Value	5	4	4.4	0.35	0.75	2	2.35	7.35	7.6	6.24	7.4

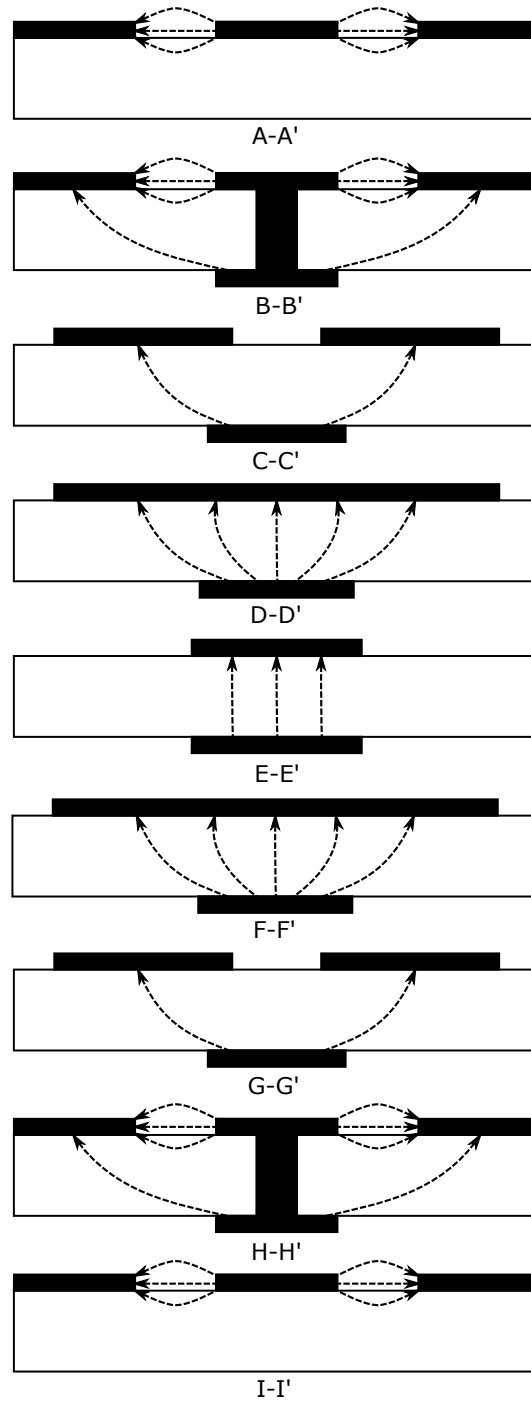


Figure 5.3: Cross-sectional views of both transitions (Type A and B) and electric field distributions: (a) AA', II'- CPW modes, (b) EE' - DSPSL mode, (c) BB', CC', DD', FF', GG', HH' - Transition modes.

5.1.2 Equivalent Circuit

A second order low pass, lumped LC Π network shown in Figure 5.4, approximates the nature of the transitions. Open ended CPW with connected grounds results in capacitive nature (C_{Open}) at both ends. The simplified lumped equivalent of a single via between layers is a Π network with capacitive nature at low frequencies and inductive at high frequencies. The vias are present whenever the signal switches layers and they are in series with the signal lines. Phase inverting nature of the transition is well established in the equivalent circuit where the connected grounds of CPW in one side is connected to the center conductor of the other side.

5.1.3 Measured Results

5.1.3.1 Type A

The scattering parameters of the back-to-back transitions were simulated and measured using multilayer solver (Frequency domain) of CST Microwave Studio and Keysight Fieldfox N9927A handheld network analyzer respectively, are illustrated in Figures 5.5 and 5.8, which show good agreement. The actual photographs of top and bottom views of all transitions are also shown in Figures 5.6 and 5.9. Table 5.3 shows the measured insertion and return losses of the transitions for different substrates.

From the measured group delays as shown in Figure 5.11, average delay deviation for 30 kHz to 14 GHz is only about 0.0548 ns (Type A - Rogers RO4003C) and 0.0644 ns (Type A - FR4) which are relatively very small. Phase of the scattering parameter S_{21} is shown in Figures 5.7 and 5.10, indicating the good transmission phase linearity of the transitions.

The insertion loss associated with a single transition, $IL_{Transition}$, can be calculated as;

$$IL_{Transition} = (IL_{Total} - L_{CPW} - L_{SMA})$$

where, IL_{Total} is the total measured insertion loss, L_{CPW} is the insertion losses of the CPW line, and L_{SMA} is the insertion loss of SMA connectors.

According to [5, 15], the insertion losses of CPW lines are about 0.04 dB/mm and that of a SMA connector is around 0.09 dB . The maximum

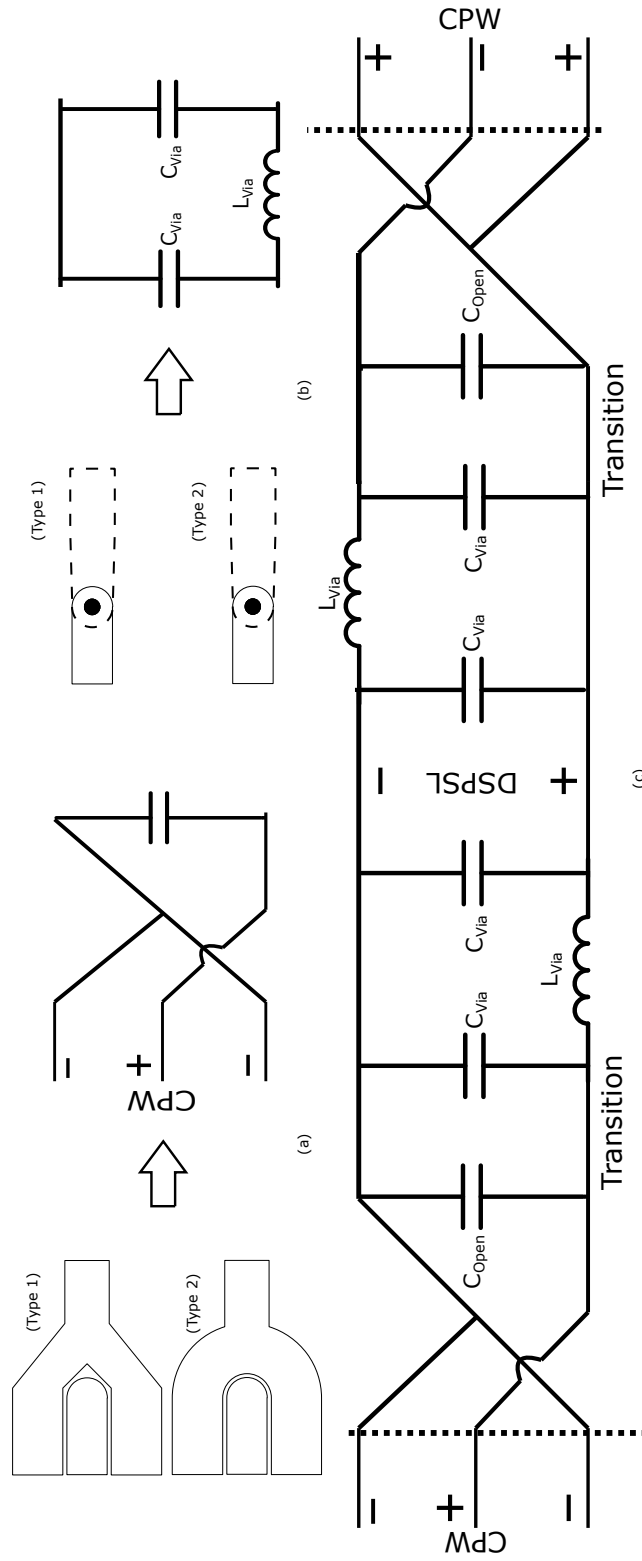


Figure 5.4: Simplified equivalent circuit of CPW with connected grounds, (b) equivalent circuit of via (Lumped), (c) complete equivalent circuit of the transitions (Type A & Type B)

Table 5.3: Measured losses of the transitions (Type A).

Type	Substrate	Bandwidth (GHz)	Insertion loss (dB)	Return loss (dB)
A	Rogers RO4003C	0.0 - 12.5	≤ 3	≥ 7.5
		0.0 - 8.5, 10 - 12	≤ 3	≥ 10
	FR4	0.0 - 11.0	≤ 3	≥ 7.5
		0.0 - 7.4, 8.9 - 11	≤ 3	≥ 10

insertion loss for the transition is approximately 1.7 dB and 2.2 dB for the substrates Rogers RO4003C and FR4 respectively in the bandwidth.

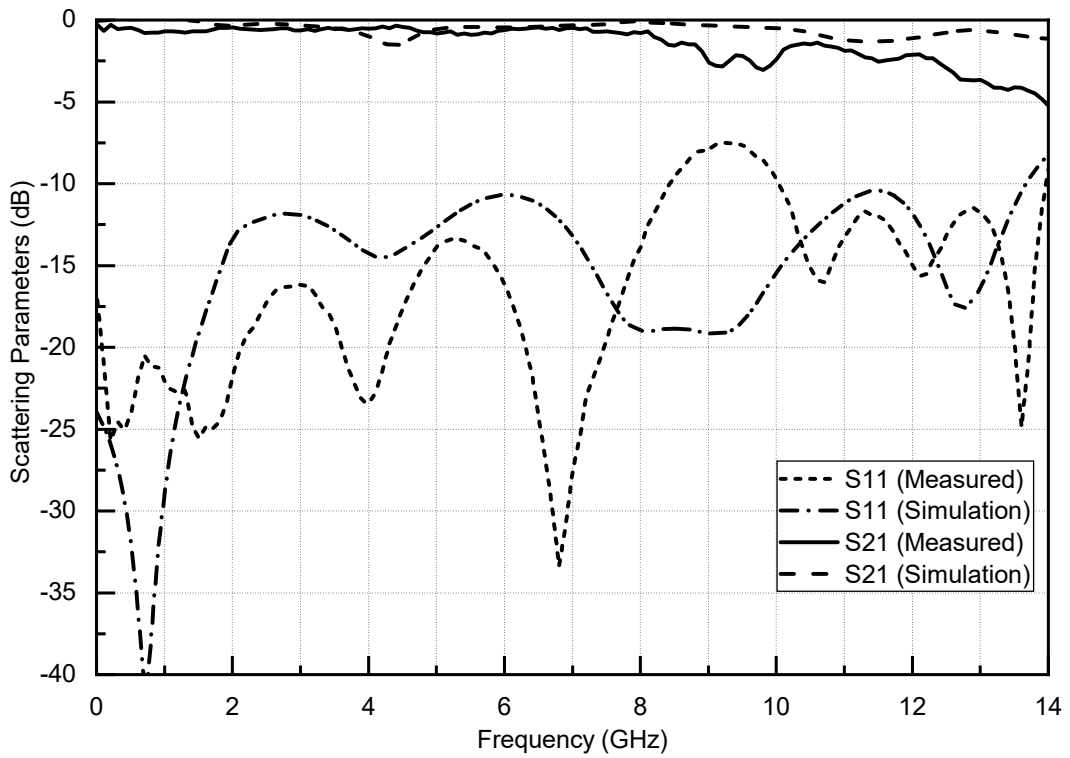
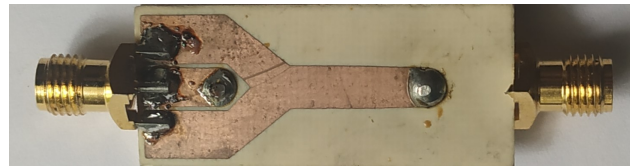
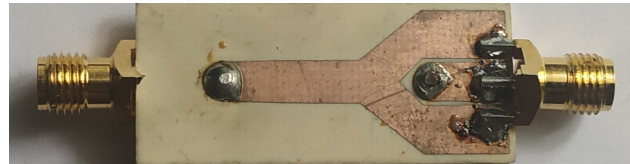


Figure 5.5: Simulated and measured scattering parameters of the CPW to CPW transition - Type A (Rogers RO4003C)



(a) Top view



(b) Bottom view

Figure 5.6: Actual photograph of the CPW to CPW transition transitions - Type A (Rogers RO4003C).

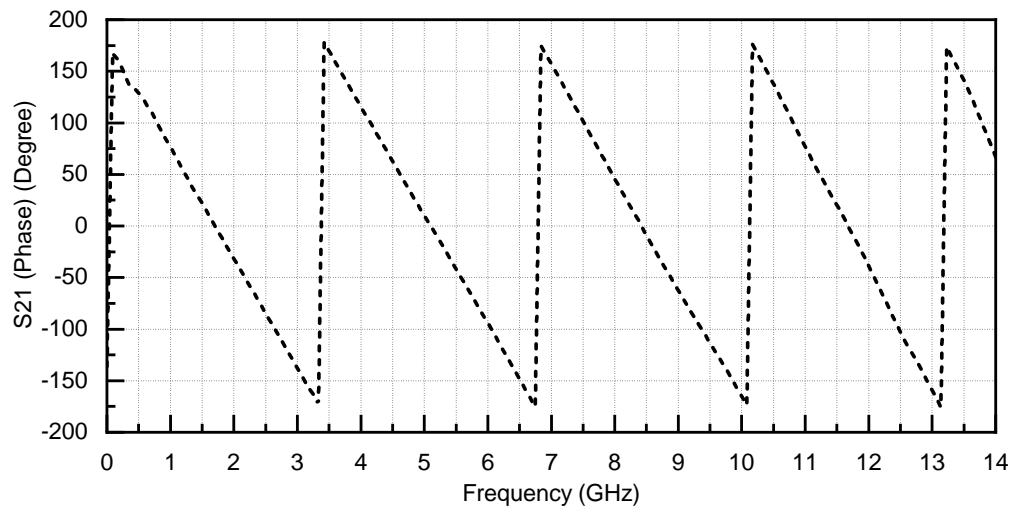


Figure 5.7: Measured scattering parameter S_{21} phase (in degrees) of the CPW to CPW transition - Type A (Rogers RO4003C).

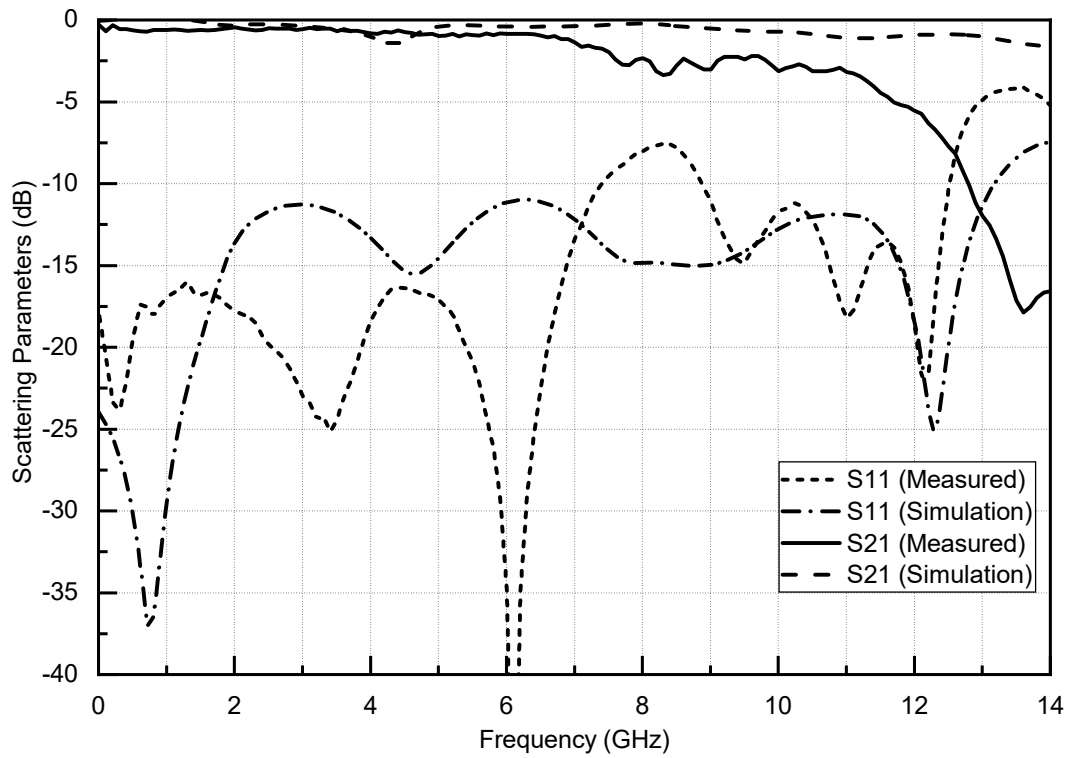


Figure 5.8: Simulated and measured scattering parameters of the CPW to CPW transition - Type A (FR4).



(a) Top view



(b) Bottom view

Figure 5.9: Actual photograph of the CPW to CPW transition transitions - Type A (FR4).

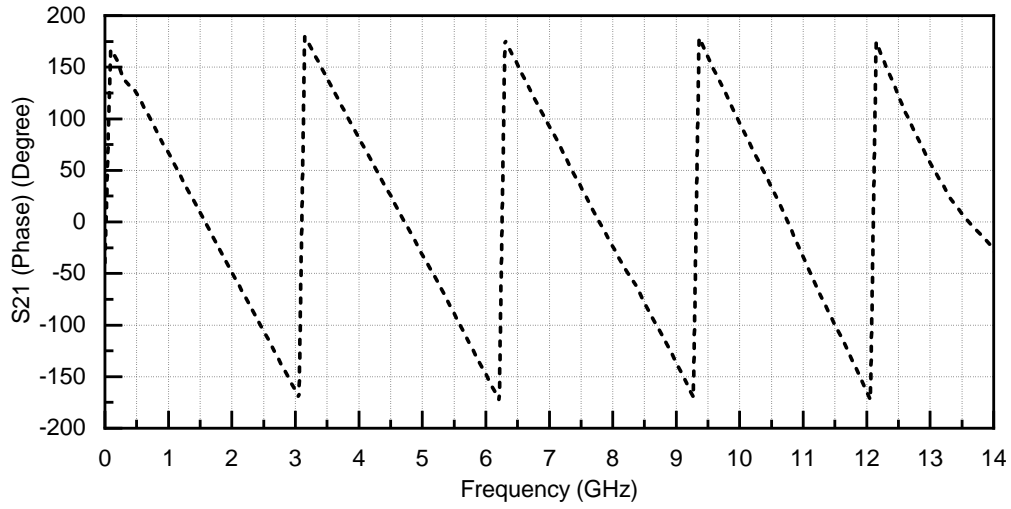


Figure 5.10: Measured scattering parameter S_{21} phase (in degrees) of the CPW to CPW transitions - Type A (FR4).

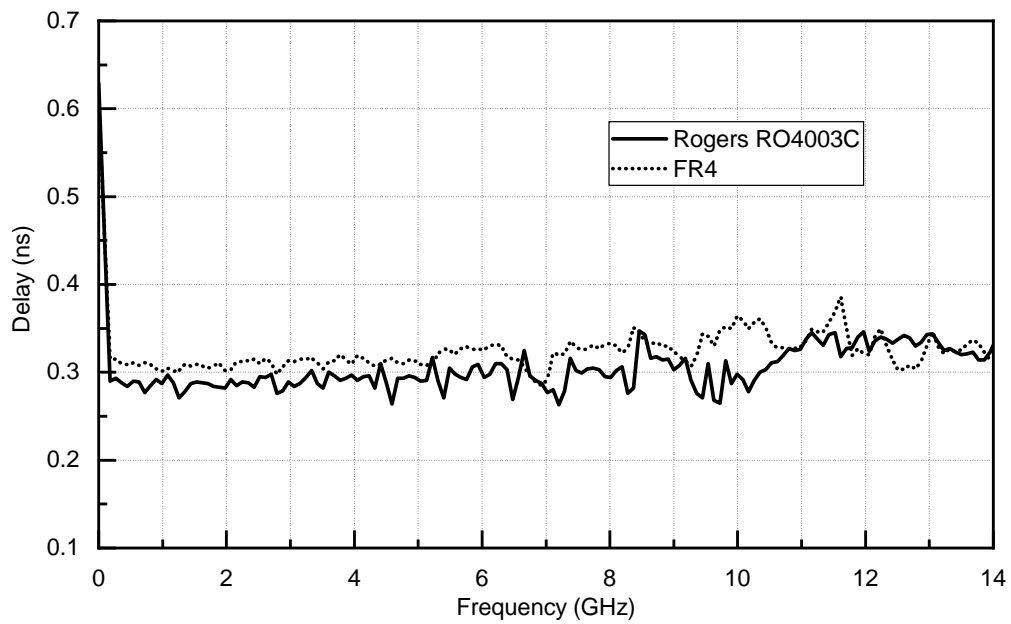


Figure 5.11: Measured group delays of the CPW to CPW transitions - Type A

5.1.3.2 Type B

The scattering parameters of the back-to-back transitions were simulated and measured using multilayer solver (Frequency domain) of CST Microwave Studio and Keysight Fieldfox N9927A handheld network analyzer respectively. They are illustrated in Figures 5.12 and 5.14, which show good agreement. The actual photographs of top and bottom views of all transitions are also shown in Figures 5.13 and 5.15. Table 5.4 shows the measured insertion and return losses of the transitions for different substrates.

From the measured group delays as shown in Figure 5.18, average delay deviation for 30 kHz to 14 GHz is only about 0.0528 ns (Type B - Rogers RO4003C) and 0.0670 ns (Type B - FR4) which are relatively very small. Phase of the scattering parameter S_{21} is shown in Figures 5.16 and 5.17, indicating the good transmission phase linearity of the transitions.

The insertion loss associated with a single transition, $IL_{Transition}$, can be calculated as;

$$IL_{Transition} = (IL_{Total} - L_{CPW} - L_{SMA})$$

where, IL_{Total} is the total measured insertion loss, L_{CPW} is the insertion losses of the CPW line, and L_{SMA} is the insertion loss of SMA connectors.

According to [5, 15], the insertion losses of CPW lines are about 0.04 dB/mm and that of a SMA connector is around 0.09 dB . The maximum insertion loss for the transition is approximately 1.5 dB and 2.2 dB for the substrates Rogers RO4003C and FR4 respectively in the bandwidth.

Table 5.4: Measured losses of the transitions (Type B).

Type	Substrate	Bandwidth (GHz)	Insertion loss (dB)	Return loss (dB)
B	Rogers RO4003C	0.0 - 11.2	≤ 2	≥ 14
	FR4	0.0 - 11	≤ 3.5	≥ 7.5
		0.0 - 7.6, 8.9 - 11	≤ 3.5	≥ 10

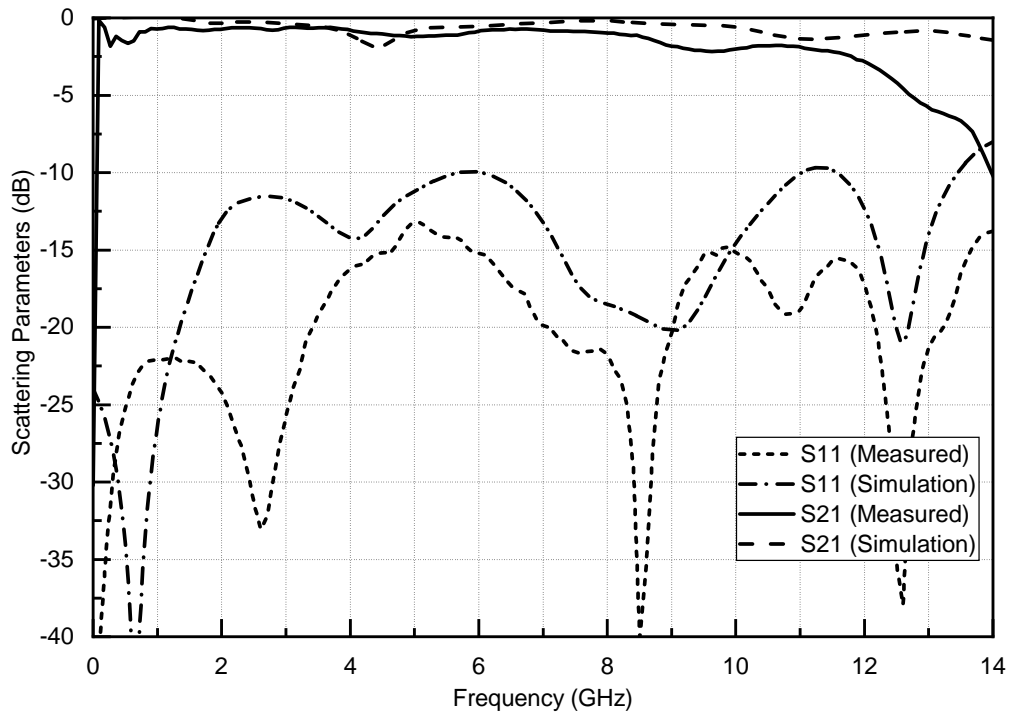


Figure 5.12: Simulated and measured scattering parameters of the CPW to CPW transition - Type B (Rogers RO4003C).



(a) Top view



(b) Bottom view

Figure 5.13: Actual photograph of the CPW to CPW transition transitions - Type B (Rogers RO4003C).

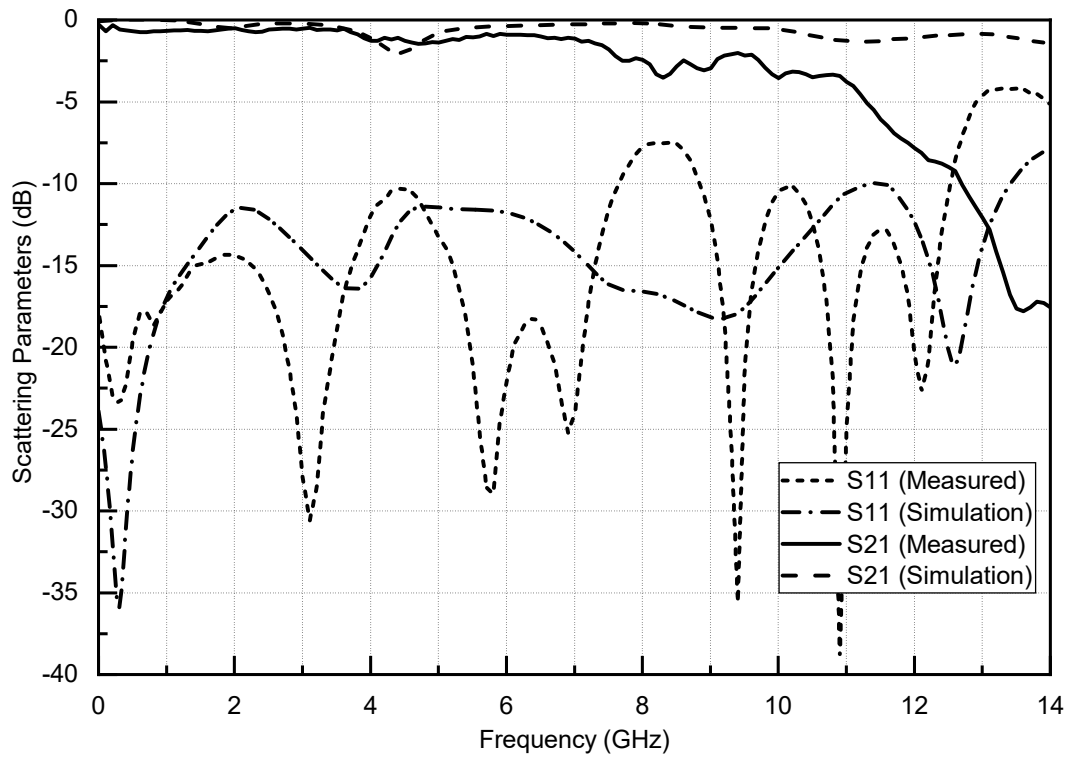
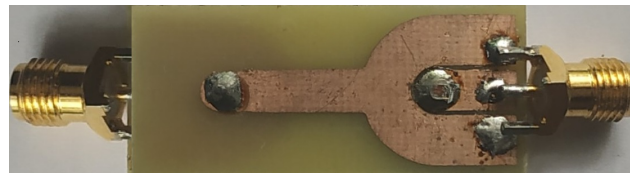


Figure 5.14: Simulated and measured scattering parameters of the CPW to CPW transition - Type B (FR4).



(a) Top view



(b) Bottom view

Figure 5.15: Actual photograph of the CPW to CPW transition transitions - Type B (FR4).

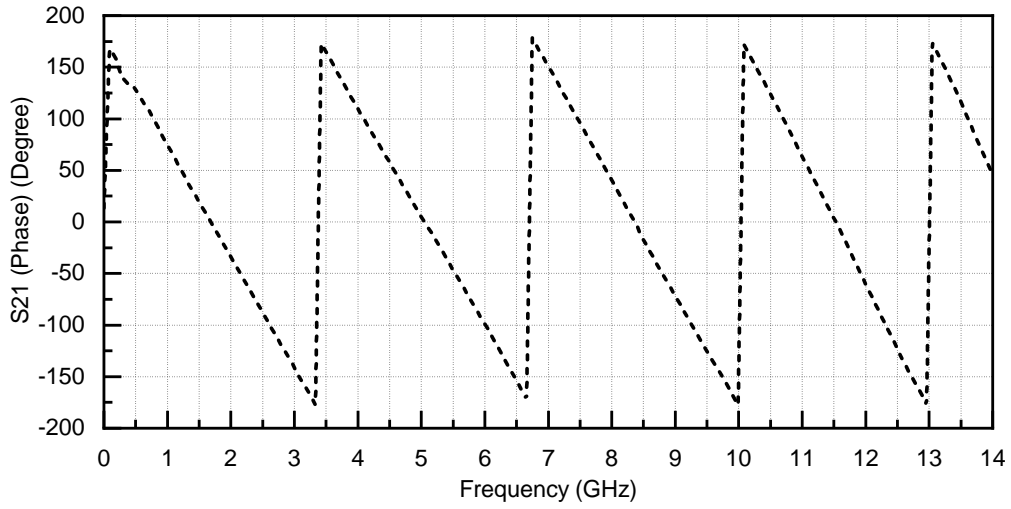


Figure 5.16: Measured scattering parameter S_{21} phase (in degrees) of the CPW to CPW transitions - Type B (Rogers RO4003C).

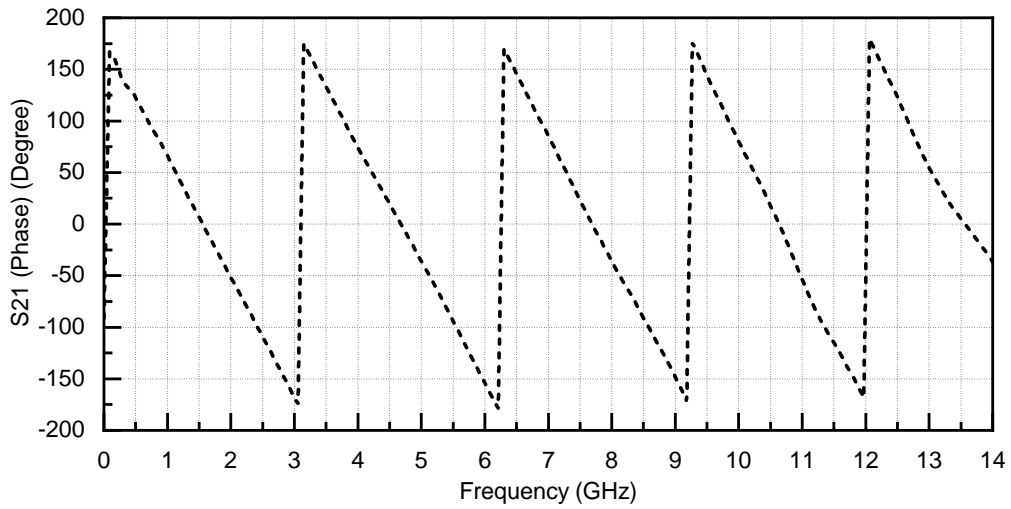


Figure 5.17: Measured scattering parameter S_{21} phase (in degrees) of the CPW to CPW transitions - Type B (FR4).

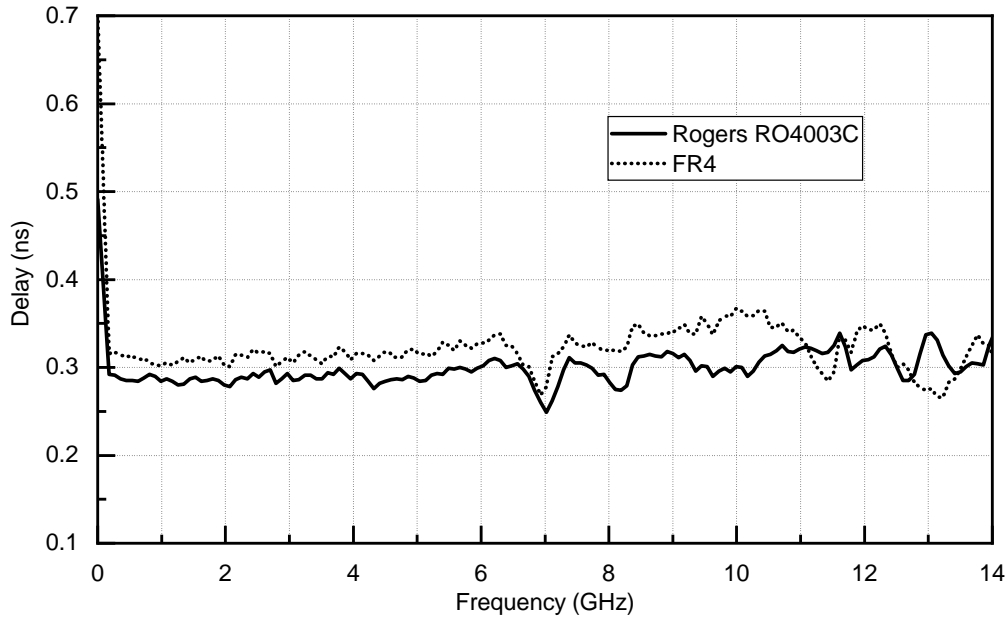


Figure 5.18: Measured group delays of the CPW to CPW transitions - Type B

5.2 CPW Fed UWB Antipodal Vivaldi Antenna

The vivaldi antenna is a tapered slot antenna which is wideband in nature, introduced by Gibson in 1979 [16]. As shown by Gazit in 1988 [17], the bandwidth enhancement can be achieved for vivaldi by making it antipodal in nature. The UWB applications like imaging and wireless communication systems extensively use antipodal vivaldi antennas (AVAs). The bandwidth constraints in different vivaldi antennas are limited by the feeding transitions. The feeding structure of AVA is the DSPSL structure, therefore transitions to the DSPSL structure is extremely important. AVAs have skewed electric field components result in the poor cross polarization and at higher frequencies this skew results in serious beam tilt also. These problems can be avoided to a limit by using thin substrates with limited range of application. The balanced AVA (BAVA) introduced by Langley in 1993 [18], with three layered

structure, reduces this problem, though it is having high cost and slightly difficult manufacturing procedure.

5.2.1 Antenna Geometry and its Design

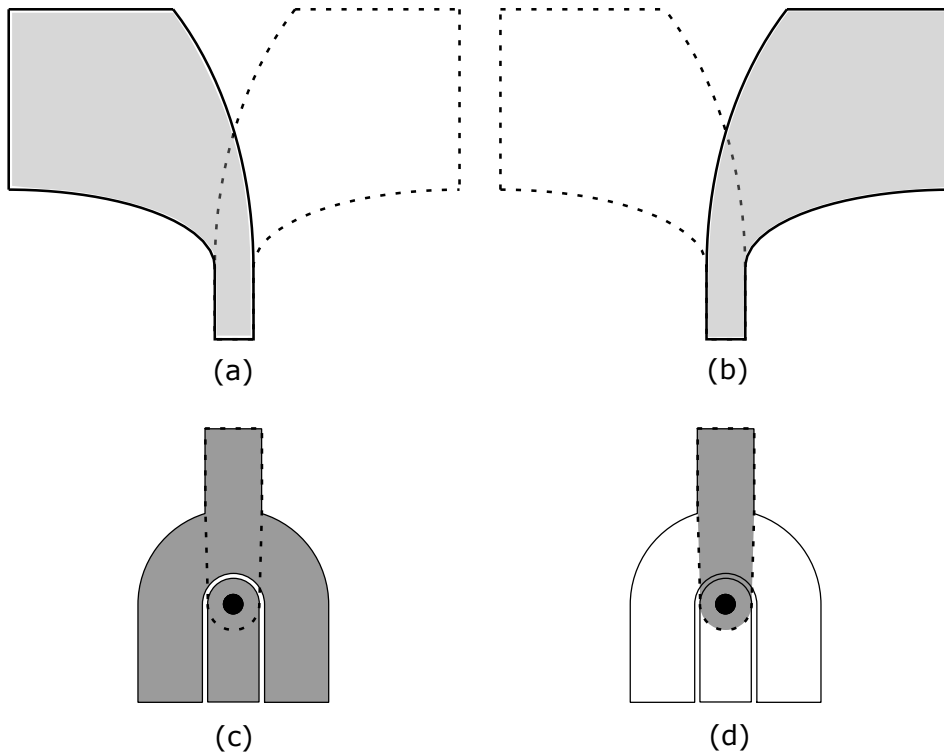


Figure 5.19: Configuration of the Antipodal Vivaldi Antenna: (a) top view, (b) bottom view. ; Configuration of the proposed Type B transition: (c) top view, (d) bottom view.

The proposed CPW fed UWB antipodal vivaldi antenna is made from the conventional differentially fed antipodal vivaldi antenna and the type B, single via vertical transition from CPW to DSPSL described in Section 4.1. The feed transition structure from CPW to DSPSL makes the antenna well suited for many microwave integrated circuits utilizing CPW pads [19]. The detailed simulation and experimental studies of the transition is given in the Chapter 4. CPW is an unbalanced transmission line and the DSPSL is a balanced

transmission line. The transition rotates their electric field by 90° . The CPW has electric fields between the center strip and grounds in both sides. On the other hand DSPSL has vertical fields between the conductors.

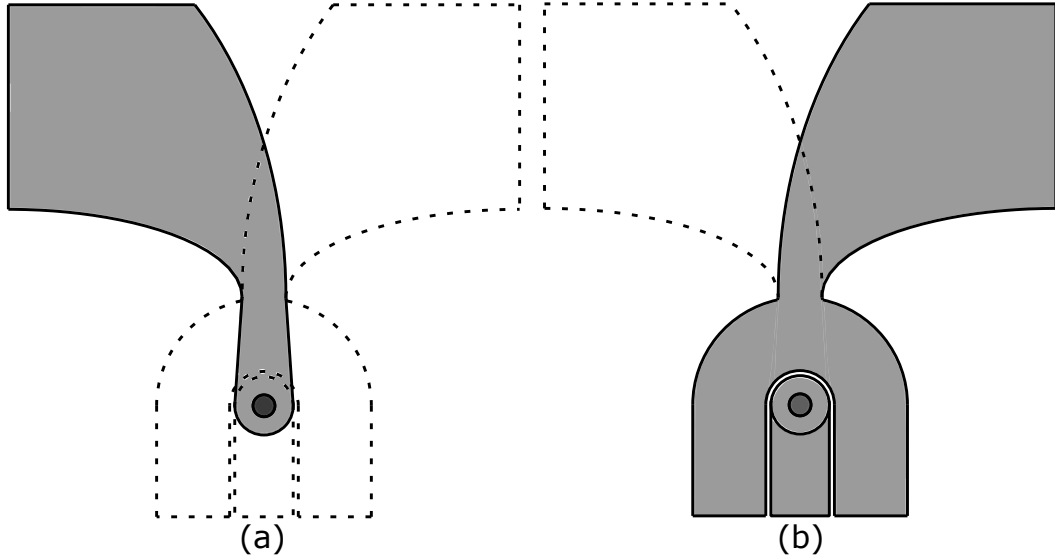


Figure 5.20: Schematic layout of the proposed Antenna: (a) top view, (b) bottom view.

CPW ground conductors are circularly tapered with inner radius ($R_4=2.35$ mm) and outer radius ($R_5=7.35$ mm) to form the top metal of DSPSL. The transition length is designed as approximately $\lambda/4$ at the center frequency ($L_2=7.4$ mm). The CPW center strip and the DSPSL bottom metal are circularly terminated to form the via pads with radius equal to half their width ($R_2=2$ mm). In Figure 5.21 after via connection ($R_1=0.75$ mm) the width of the bottom metal strip is gradually decreased for a length ($L_8=7.4$ mm), to match the width of DSPSL ($W_5=3$ mm).

The antenna design objective is to make it small while maintaining CPW feeding structure in the UWB range (3.1 - 10.6 GHz) of operation. Intersection of $1/4$ portion of two ellipses forms the main radiating structure. The primary radii and secondary radii of the ellipses are (W_4+W_5, W_4) and (L_5, L_3) respectively. The length L_4 controls the length of radiating structure, eventhough L_5 is the primary radius of the bigger ellipse. Corresponding to

the parameter, L_4 , the W_6 decides the width of the top side of the flared structure. The total size of the antenna is $35 \text{ mm} \times 35 \text{ mm}$.

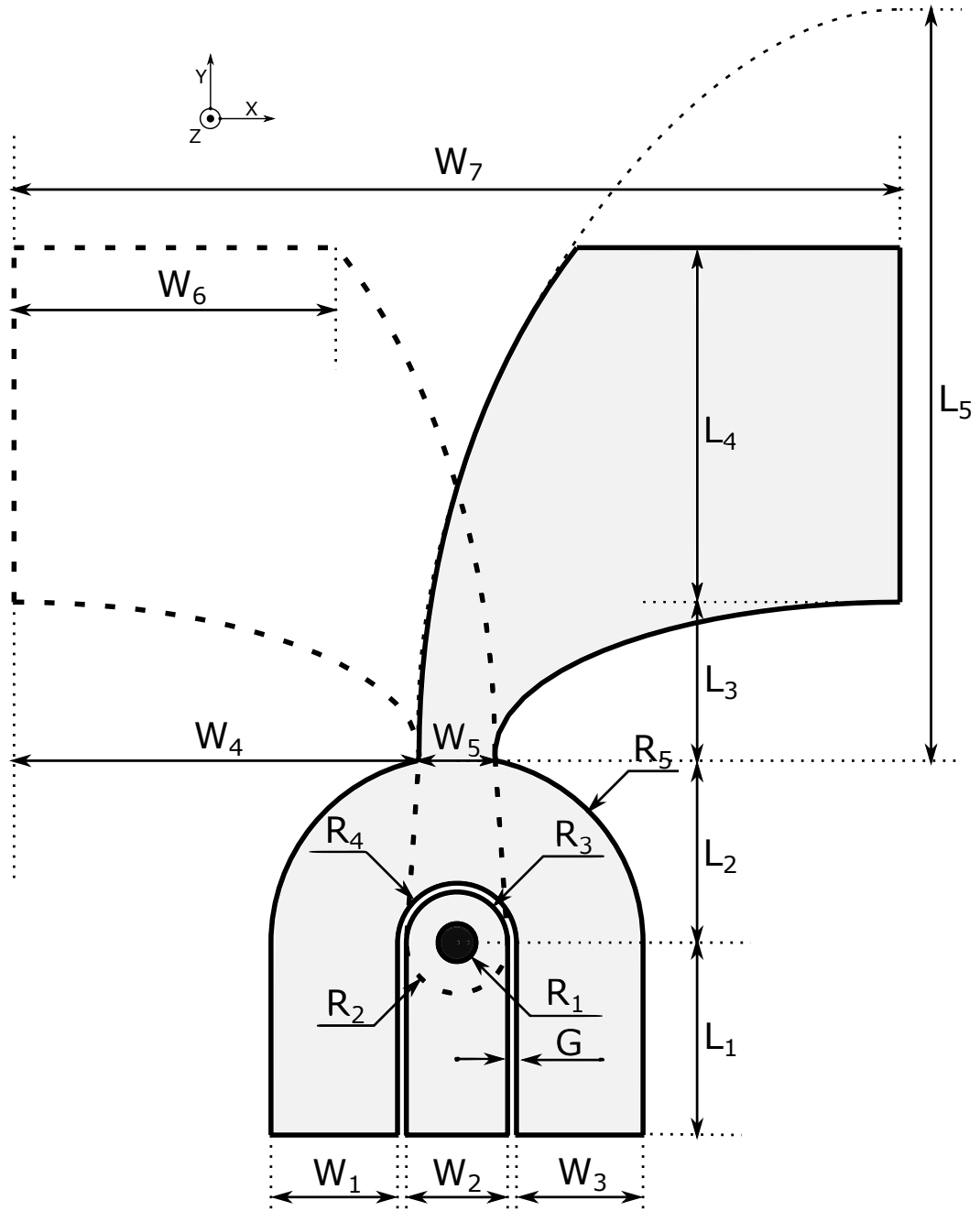


Figure 5.21: Configuration of the proposed Antenna.

Table 5.5: Geometrical parameters of the proposed Antenna (in mm).

Parameter	W_1	W_2	W_3	W_4	W_5	W_6	W_7	G	L_1
Value	5	4	5	16	3	12.8	35	0.35	7.6
Parameter	L_2	L_3	L_4	L_5	R_1	R_2	R_3	R_4	R_5
Value	7.35	6.05	14	27	0.75	2	2	2.35	7.35

The antenna is printed on the substrate FR4 ($\epsilon_r=4.3$ and $h=1.6$ mm). The dimensions of 50 Ω CPW is determined by CST Microwave Studio utility with the center strip width as $W_2=4.0$ mm, and the gap width as $G=0.35$ mm. Using image theory, the strip width of the DSPSL can be calculated as $(Z_0)_{dspst} = 2 * (Z_0)_{microstrip}$. The geometrical parameters of the antenna is given in the Table 5.5.

5.2.2 Simulation Studies

Multilayer solver (Frequency domain) of CST Microwave Studio (3D planar electromagnetic solver based on MoM) is used for the parametric studies and optimization. The CPW center strip width and the gap is adjusted so that the 50 Ω characteristic impedance is assured. The metalization widths and gaps are chosen such that the etching can be done easily. The 50 Ω termination ensure proper matching with 50 Ω testing ports of the simulator and the vector network analyzer.

The parametric analysis and optimization of the feeding transition is done in the section 4.1. The sensitive parameters of the antenna radiating structure (L_3 and L_4) are parametrically analyzed in Figures 5.22 and 5.23. The antenna lies in the X-Y plane. The three dimensional radiation patterns (absolute value of the power flow (dB) in farfield) of the antenna at frequencies 4 GHz, 6 GHz and 9 GHz are shown in Figures 5.24, 5.25 and 5.26 respectively. Red colour indicates maximum magnitude of the radiation and from red to violet the magnitude decreases.

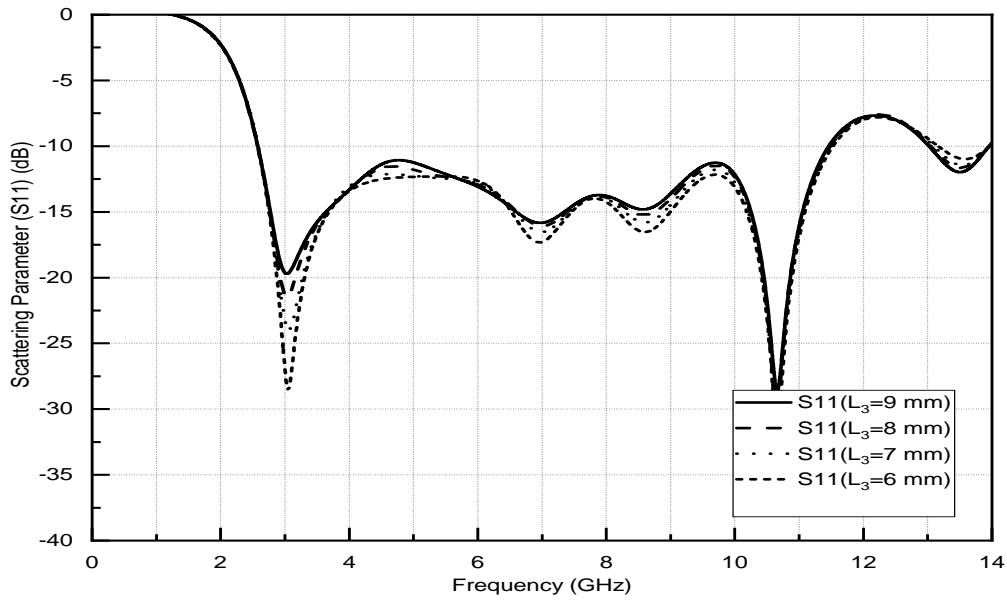


Figure 5.22: Simulated return losses of the proposed Antenna against frequency with different values of L_3 .

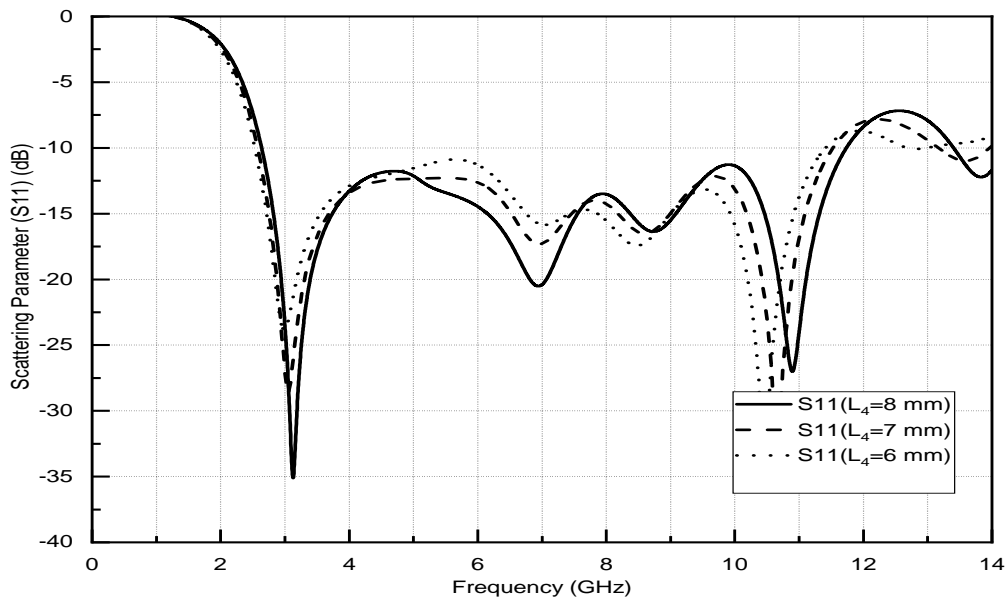


Figure 5.23: Simulated return losses of the proposed Antenna against frequency with different values of L_4 .

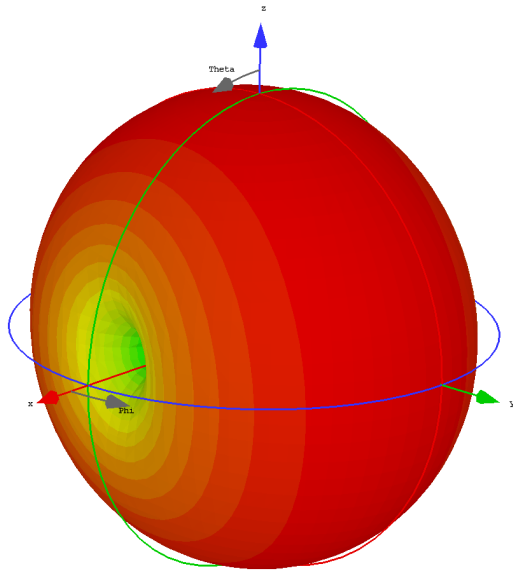


Figure 5.24: Simulated radiation pattern of the proposed Antenna at 4 GHz.

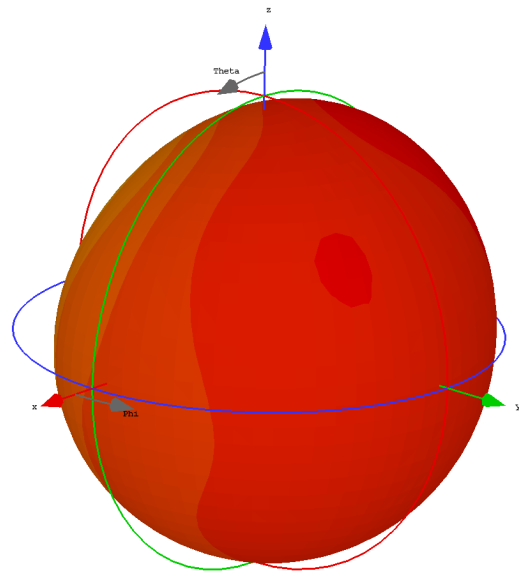


Figure 5.25: Simulated radiation pattern of the proposed Antenna at 6 GHz.

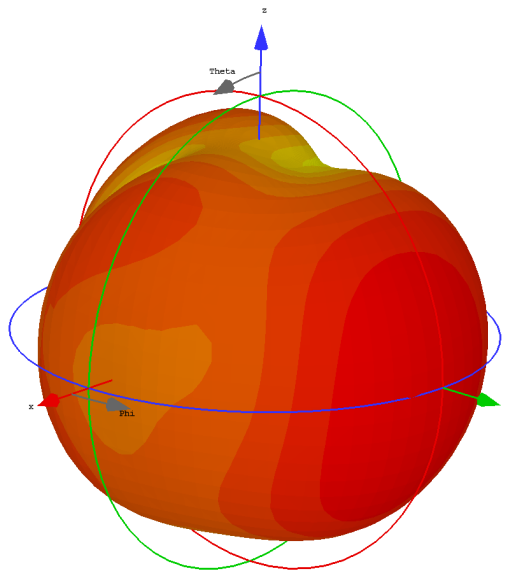


Figure 5.26: Simulated radiation pattern of the proposed Antenna at 9 GHz.

5.2.3 Measured Results

The return loss of the antenna was simulated and measured using time domain solver CST Microwave Studio and Agilent Technologies E8362B vector network analyzer (10 MHz to 20 GHz) respectively, are illustrated in Figure 5.27, which show good agreement. The antenna shows measured return losses better than 10 dB for the frequency range, 2.97 - 10.93 GHz. Major resonances are observed at frequencies 3.75 GHz, 5.75 GHz and 10.25 GHz.

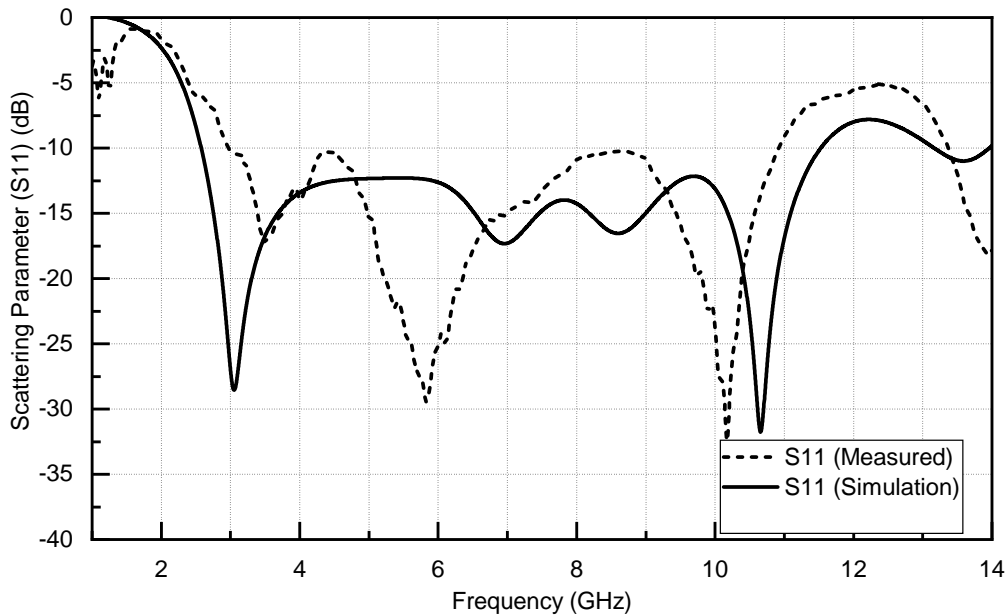
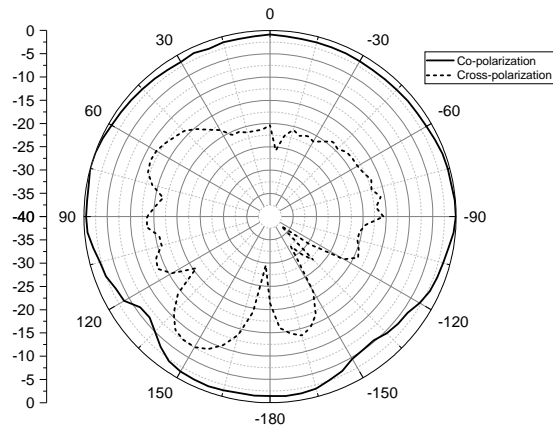
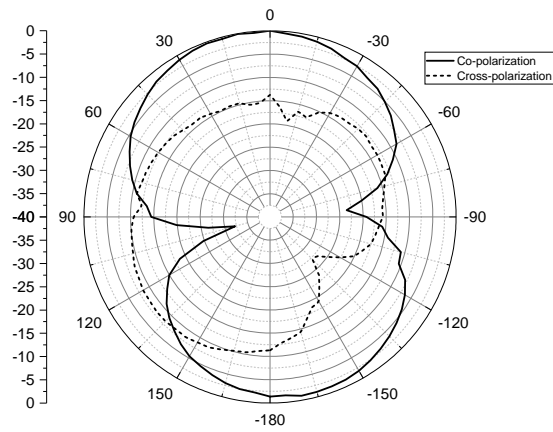


Figure 5.27: Simulated and Measured return loss (dB) of the proposed Antenna against frequency.

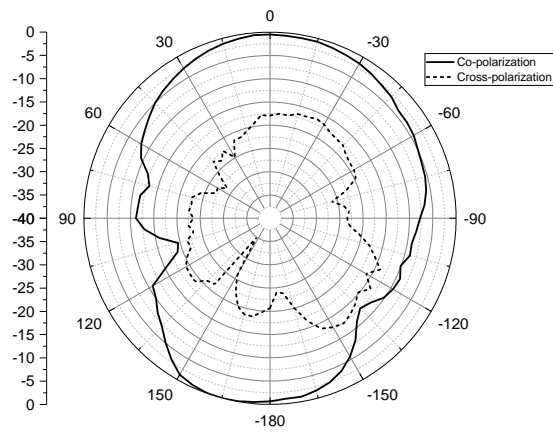
Radiation patterns (2D polar plot) of the antenna at frequencies 4 GHz, 6 GHz and 9 GHz are shown for different cross-sectional planes (X-Y, Y-Z and X-Z) in Figures 5.28, 5.29 and 5.30 for co and cross polarizations. Each pattern is normalized with respect to the peak value of the corresponding plane. The actual photographs of top and bottom views of the antenna are also shown in Figure 5.31. Measured gain of the antenna is shown in Figure 5.32, which has an average value of 3.84 dBi, for the 3.1 - 10.6 GHz band.



(a) Y-Z Plane

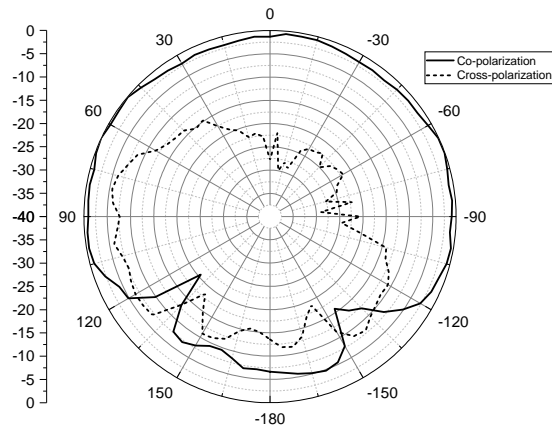


(b) X-Z Plane

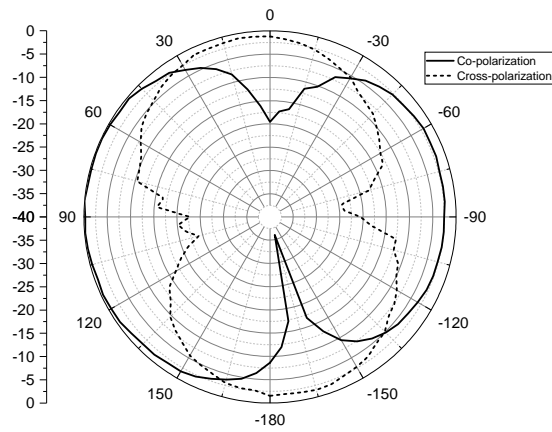


(c) X-Y Plane

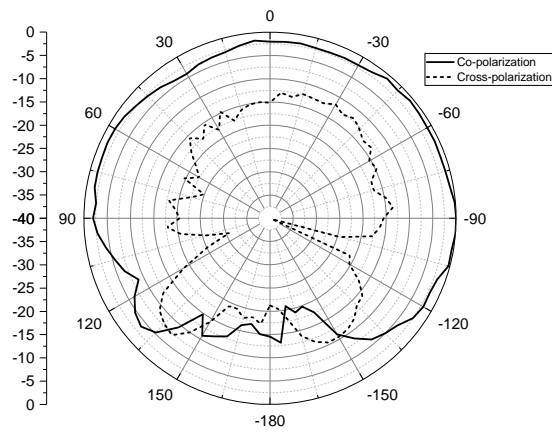
Figure 5.28: Measured radiation pattern of the proposed Antenna at 4 GHz.



(a) Y-Z Plane

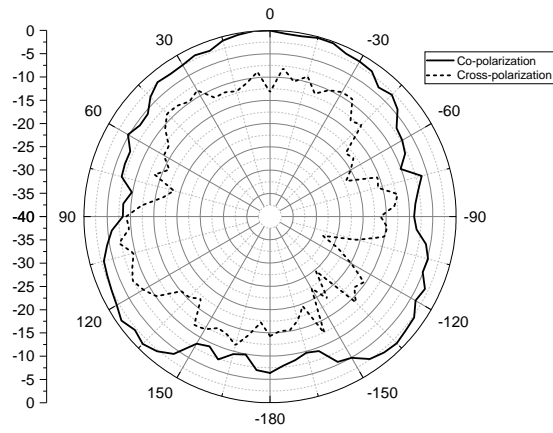


(b) X-Z Plane

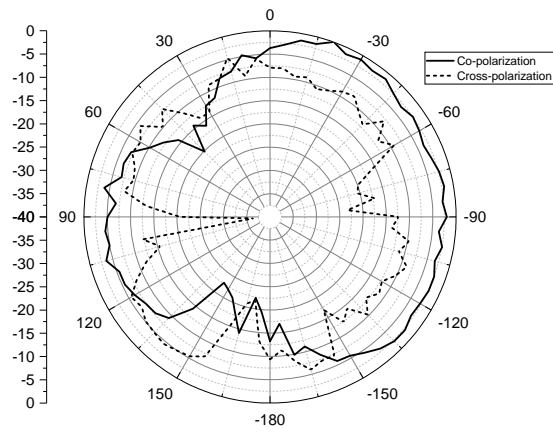


(c) X-Y Plane

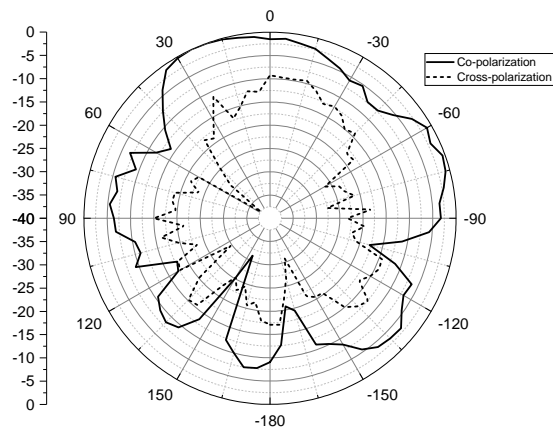
Figure 5.29: Measured radiation pattern of the proposed Antenna at 6 GHz.



(a) Y-Z Plane

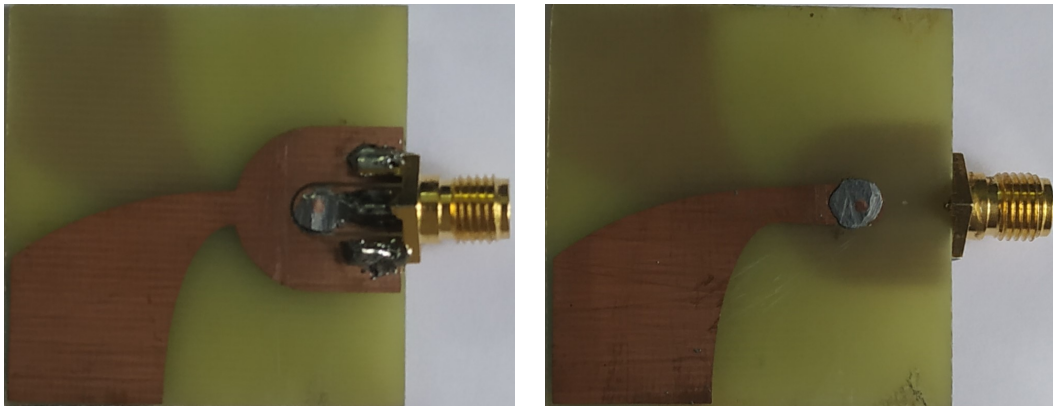


(b) X-Z Plane



(c) X-Y Plane

Figure 5.30: Measured radiation pattern of the proposed Antenna at 9 GHz.



(a) Top view

(b) Bottom view

Figure 5.31: Actual photograph of the proposed Antenna.

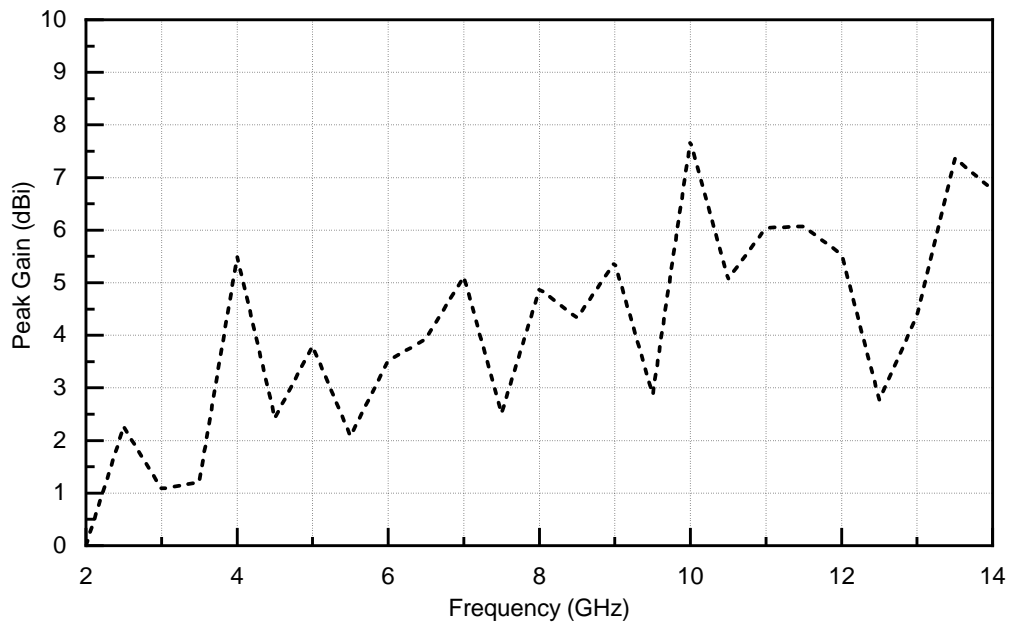


Figure 5.32: Measured peak gain of the proposed Antenna against frequency.

5.3 Chapter Summary

Ultra-wideband CPW to CPW, vertical transitions with phase inverting nature have been designed, optimized and prototyped for the first time. The proposed transitions utilize two types of CPW to DSPSL transitions. A summarized design procedure for the transitions is discussed. The simplified equivalent circuit of the transition is a Π shaped, low pass LC network. Using standard photolithography process, transitions are prototyped on both FR4 and RO4003C substrates. Moreover, out of phase, vertical transitions are useful in the microwave applications like differential amplifiers, mixers, doublers etc.

A compact CPW Fed UWB Antipodal Vivaldi Antenna has been designed, optimized and prototyped on the cost effective substrate (FR4). The CPW fed AVA structures are very rare in literature [19]. The gain and radiation pattern of the antenna are measured. The proposed antenna utilizes the CPW to DSPSL transition as feeding structure and elliptically tapered flares as radiators.

References

- [1] R. W. Jackson and D. W. Matolak, "Surface-to-surface transition via electromagnetic coupling of coplanar waveguides," *IEEE Transactions on Microwave Theory and Techniques*, vol. 35, pp. 1027–1032, Nov 1987.
- [2] R. N. Simons, R. A. Lee, K. A. Shalkhausere, J. Owens, J. Demarco, J. Leen, and D. Sturzebecher, "Finite width coplanar waveguide patch antenna with vertical fed through interconnect," in *IEEE Antennas and Propagation Society International Symposium. 1996 Digest*, vol. 2, pp. 1338–1341 vol.2, July 1996.
- [3] P. L. Carro and J. de Mingo, "Analysis and synthesis of double-sided parallel-strip transitions," *IEEE Transactions on Microwave Theory and Techniques*, vol. 58, pp. 372–380, Feb 2010.

- [4] H. A. Wheeler, "Transmission-line properties of parallel strips separated by a dielectric sheet," *IEEE Transactions on Microwave Theory and Techniques*, vol. 13, pp. 172–185, March 1965.
- [5] J. M. Rochelle, "Approximations for the symmetrical parallel-strip transmission line (letters)," *IEEE Transactions on Microwave Theory and Techniques*, vol. 23, pp. 712–714, Aug 1975.
- [6] Sang-Gyu Kim and Kai Chang, "Ultrawide-band transitions and new microwave components using double-sided parallel-strip lines," *IEEE Transactions on Microwave Theory and Techniques*, vol. 52, pp. 2148–2152, Sep. 2004.
- [7] J.-X. Chen, J.-L. Li, and Q. Xue, "Novel via-less double-sided parallel strip line to coplanar waveguide transition," *Microwave and Optical Technology Letters*, vol. 48, no. 9, pp. 1717–1718, 2006.
- [8] X. Y. Zhang, J. Chen, and Q. Xue, "Broadband transition between double-sided parallel-strip line and coplanar waveguide," *IEEE Microwave and Wireless Components Letters*, vol. 17, pp. 103–105, Feb 2007.
- [9] S. Bulja, D. Mirshekar-Syahkal, and M. Yazdanpanahi, "Novel wide-band transition between finite ground coplanar waveguide (fgcpw) and balanced stripline," in *2009 European Microwave Integrated Circuits Conference (EuMIC)*, pp. 301–303, Sep. 2009.
- [10] C. H. Ahn and K. Chang, "Wideband coplanar stripline to double-sided parallel-strip line transition," *Electronics Letters*, vol. 45, pp. 748–749, July 2009.
- [11] T. W. Eubanks and K. Chang, "Low-loss ultra-wideband double-sided parallel-strip line transition and power divider," *Electronics Letters*, vol. 46, pp. 93–94, January 2010.
- [12] W. . Lu, C. Cheng, and H. . Zhu, "Wideband coplanar waveguide to edges-even broadside-coupled stripline transition," *Electronics Letters*, vol. 47, pp. 1286–1287, November 2011.

- [13] W. Lu, Y. Bo, and H. Zhu, "A broadband transition design for a conductor-backed coplanar waveguide and a broadside coupled stripline," *IEEE Microwave and Wireless Components Letters*, vol. 22, pp. 10–12, Jan 2012.
- [14] W. Lu, H. Tong, Y. Bo, and H. Zhu, "Design and study of enhanced wideband transition between coplanar waveguide and broadside coupled stripline," *IET Microwaves, Antennas Propagation*, vol. 7, pp. 715–721, June 2013.
- [15] D. M. Pozar, *Microwave Engineering; 4th Edition*. Wiley, 2011.
- [16] P. J. Gibson, "The vivaldi aerial," in *1979 9th European Microwave Conference*, pp. 101–105, Sep. 1979.
- [17] E. Gazit, "Improved design of the vivaldi antenna," *IEE Proceedings H (Microwaves, Antennas and Propagation)*, vol. 135, pp. 89–92(3), April 1988.
- [18] J. D. S. Langley, P. S. Hall, and P. Newham, "Novel ultrawide-bandwidth vivaldi antenna with low crosspolarisation," *Electronics Letters*, vol. 29, pp. 2004–2005, Nov 1993.
- [19] Z. Wang, Y. Yin, J. Wu, and R. Lian, "A miniaturized cpw-fed antipodal vivaldi antenna with enhanced radiation performance for wideband applications," *IEEE Antennas and Wireless Propagation Letters*, vol. 15, pp. 16–19, 2016.

Chapter 6

Conclusion and Future Prospects

Contents

6.1	Conclusions	129
6.2	Major Contributions	130
6.3	Suggestions for Future Work	131

This chapter highlights the conclusions drawn from the research work on Coplanar Waveguide to Double-Sided Parallel-Strip Line Transitions and the major contributions of the thesis. This is followed by a few recommendations for future work.

6.1 Conclusions

The objective of the thesis was to design and develop new transitions between the planar waveguides CPW and DSPSL and their applications. An introduction to the background theory of the planar waveguides, transitions and their applications were shortly discussed. The methodologies used in this thesis are explained in brief. The evolution, design, simulation, fabrication and measurement of two single via vertical transitions (Type A & B) and a via-less transition are proposed in this thesis. Simplified equivalent circuit for each transitions were developed for better understanding. Applications to the transitions, like CPW to CPW inverted phase vertical transitions and CPW fed UWB AVA are developed and measured.

6.2 Major Contributions

The vertical broadband transitions between DSPSL and CPW has been designed, optimized and measured for the first time. The proposed transitions (Types A and B) are based on a single via connection and connected CPW grounds. An approximate equivalent circuit, which is a Π network, LC low pass filter is discussed. Transitions are fabricated on Rogers RO4003C and FR4 substrates, using the standard photolithography process. A via-less transition also is designed, prototyped in Rogers RT Duroid 5870, and measured. Its equivalent circuit is presented. These transitions are useful in many applications like antenna feeds and passive and active microwave components. Besides the vertical transitions of DSPSL in flipped back-to-back form are capable of achieving phase inversion, useful especially in applications like ring couplers, mixers, doublers, etc.

Ultra-wideband CPW to CPW, vertical transitions with phase inverting nature have been designed, optimized and prototyped for the first time. The proposed transitions utilize two types of CPW to DSPSL transitions. A summarized design procedure for the transitions is discussed. The simplified equivalent circuit of the transition is a Π shaped, low pass LC network. Using standard photolithography process, transitions are prototyped on both FR4 and RO4003C substrates. Moreover, out of phase, vertical transitions are useful in the microwave applications like differential amplifiers, mixers, doublers etc.

A compact CPW Fed UWB Antipodal Vivaldi Antenna has been designed, optimized and prototyped on the cost effective substrate (FR4). The CPW fed AVA structures are very rare in literature. The gain and radiation pattern of the antenna are measured. The proposed antenna utilizes the CPW to DSPSL transition as feeding structure and elliptically tapered flares as radiators.

6.3 Suggestions for Future Work

CPW probe pads for device under tests (DUTs) always keep the demand for transitions from CPW in a high demand. The balanced (differential) nature of the DSPSL and its implementations, guarantee good common-mode noise immunity. The offsetted versions of the DSPSL is also ver popular now. In this scenario, new optimized and multi-functional transition structures between CPW and DSPSL can be explored.

The DSPSL crossover can be implemented using the back to back configuration of the CPW to DSPSL transitions. The CPW to CPW phase inverting vertical transitions together with DSPSL signal swap can be used in creating a lot of useful applications like filters, crossovers and ring couplers etc. Introduction of resonant structures in these transitions, easily result in frequency selective devices like CPW fed filters. A pair of inverting/non-inverting transitions can implement the ring coupler structures also. Finally the radiation characteristics of the proposed CPW fed UWB AVA can be improved by modifying the flared structures of the antenna or by the ground planes of the feeding CPW.

List of Publications

Journals:

1. **Nelson K. Jacob**, Lindo A. Ouseph, Chandroth K. Aanandan, Mohanan Pezholil and Kesavath Vasudevan, " *Broadband Vertical Transitions Between Double-Sided Parallel-Strip Line and Coplanar Waveguides*", Progress In Electromagnetics Research Letters, Vol. 75, 119-124, 2018.
2. Devassy Tony, Valiyaveetil P. Sarin, Neeraj K. Pushkaran, **Kokkadan J. Nelson**, Pezholil Mohanan, and Kesavath Vasudevan, " *Artificial Dielectric Superstrate Loaded Antenna for Enhanced Radiation Performance*", Progress In Electromagnetics Research M, Vol. 85, 185–194, 2019.
3. **Nelson K. J.**, Chandroth K. Aanandan, Mohanan Pezholil and Kesavath Vasudevan, " *Via-less Wideband Transitions Between Double-Sided Parallel-Strip Line and Coplanar Waveguides*", Progress In Electromagnetics Research Letters, Communicated.
4. **Nelson K. J.**, Chandroth K. Aanandan, Mohanan Pezholil and Kesavath Vasudevan, " *Coplanar Waveguide Fed Ultra-wideband Antipodal Vivaldi Antenna*", IET Microwaves, Antennas & Propagation, Communicated.

NELSON K. J.

Assistant Professor in Electronics and Communication Engineering
Government Engineering College Thrissur.

+91 9496240227
nelsonkj@gmail.com

Education

- **Department of Electronics, Cochin University of Science and Technology** Cochin
Ph.D.(Microwave Electronics) (Part-Time) 2009 -
– Thesis: Coplanar Waveguide to Double-Sided Parallel-Strip Line Transitions and Their Applications
- **Department of Electronics, Cochin University of Science and Technology** Cochin
M.Tech.(Electronics) 2006 - 2008
– Graduated with First Class with Distinction
- **Government Engineering College Thrissur (University of Calicut)** Thrissur
B.Tech.(Electronics and Communication Engineering) 2001 - 2005
– Graduated with First Class
- **St. Thomas College Thrissur (University of Calicut)** Thrissur
Pre-Degree (First Group) 1999 - 2001
– Graduated with First Class
- **St. Antony's High School, Pudukad** Thrissur
Secondary School Leaving Certificate (S.S.L.C.) 1999
– Graduated with First Class with Distinction

Work Experience

- **Assistant Professor** Technical Education (Government of Kerala)
Electronics and Communication Engineering 2009 -

Personal Details

- Age & Date of Birth : **35 & 16.04.1984**
- Permanent Address : **Kokkadan House, Chengaloor P. O., Thrissur, Kerala - 680312.**

References

- **Dr. K .Vasudevan,**
Emeritus Professor, Department of Electronics, Cochin University of Science and Technology, Cochin, Kerala - 682021.
email: vasudevankdr@gmail.com, Phone: +91 9447357328.
- **Dr. Jayan A. R.,**
Professor and Head, Department of Electronics and Communication Engineering, Government Engineering College Sreekrishnapuram, Palakad, Kerala - 678633.
email: arjayan71@gmail.com, Phone: +91 8129418002.

